Distributed Control of Multi-Vehicle Systems Using Modular Architectures

Vom Promotionsausschuss der
Technischen Universität Hamburg
zur Erlangung des akademischen Grades

Doktor der Naturwissenschaften (Dr. rer. nat.)

genehmigte Dissertation

von
Adwait Vinod Datar

aus
Mumbai, Indien

2023

Erster Gutachter:
Prof. Dr. Herbert Werner
Institut für Regelungstechnik
Technische Universität Hamburg

Zweiter Gutachter:
Prof. Dr. Peter J. Seiler
Electrical Engineering Computer Science
University of Michigan, Ann Arbor, USA

Dritter Gutachter:
Prof. Dr. rer. nat. Marko Lindner
Institut für Mathematik
Technische Universität Hamburg

Vorsitzender des Prüfungsauschusses:
Prof. Dr.-Ing. Robert Seifried
Institut für Mechanik und Meerestechnik
Technische Universität Hamburg

Tag der mündlichen Prüfung: 4. November 2022

Author: https://orcid.org/0000-0002-4085-9675
DOI: https://doi.org/10.15480/882.4763
ISBN: 978-3-8439-5238-5

To my Family

Acknowledgment

First and foremost, I wish to extend my sincere gratitude to my supervisor Prof. Herbert Werner for introducing me to the field of control and systems theory and for guiding me in my research journey. It has been a pleasure to explore, learn and conduct research under his guidance and his endless enthusiasm in the pursuit of getting to the bottom of complex concepts has been inspiring. I am especially grateful for the book seminars and countless discussions emerging out of these.

I would also like to express my gratitude to Prof. Peter Seiler and Prof. Marko Lindner for serving on my doctoral committee and Prof. Robert Seifried for chairing it. I would like to thank all my teachers and in particular, my high-school mathematics teacher, Mr. Pradeep Saraf, who introduced me to the joy of problem solving. Special thanks to all those professors who decided to make their teaching material available online and significantly shaped my academic journey. In this regard, I would like to especially thank Prof. Herbert Werner for deciding to upload his lecture material online and thanks to Patrick Göttsch for his support in organizing this.

I would like to thank my colleagues at ICS who made my PhD experience an unforgettable one. Thanks to Antonio, Furugh, Ann-Kathrin and Avi for being my earliest friends at ICS and a special thanks to Antonio for giving me company for all the last-minute midnight submissions and all the fun that came with it. Thanks Christine for tricking me to take up running and thank you Lennart, Philipp, Hamideh, Ahmed and Shuyuan for sharing all the coffee breaks. A shout out to Christian for the challenging puzzles and the innumerable interesting discussions on topics of control, mathematics and otherwise. Big thanks to Prima and Bindu for always being eager to help out and special thanks to Prima for all the delicious food. Thanks Pablo for all the random interesting discussions while sharing the office space. I would also like to thank Aly Attallah and Peter Paulsen for the joint collaboration which led to some of the results in my dissertation. Special thanks to Herwig Meyer, Klaus Baumgart and Dirk Baack for adding humor and creativity to all the PhD defense celebrations with their most creative hats. I would

also like to thank Uwe Jahns for always being willing to help out with all the computer issues. The invaluable support of Christine Kopf and Bettina Schrieber in all the administrative tasks cannot be overstated and I would like to sincerely thank them for their time and efforts.

I am especially grateful to Ira, Pablo, Christian, and Antonio for putting in a lot of time and effort for giving invaluable feedback that significantly improved the quality of my dissertation and special thanks to Julian for his honest advice and encouragement when preparing for the defense.

Finally, words cannot express the depth of my gratitude towards my family. I would like to thank my wife Uma for her unwavering support, understanding, patience and for being my best friend for almost half of my life. Special thanks to my brother Chinya for his ever present optimism and encouragement and offering his perspective from time to time. I cannot express nearly enough gratitude to my parents Aai, Baba and my entire extended family back home in India for their unconditional love and encouragement. Their continued support is invaluable and I extend my deepest gratitude towards them.

Summary

For problems involving cooperative control of multiple vehicle agents, it is commonly proposed to divide the problem into a study of networks of simplified vehicle models (*network dynamics*) and apply local tracking controllers on complex vehicles (*tracking dynamics*) such that these vehicles track the trajectories generated by simplified models. Building on this paradigm, two modular architectures are studied in this thesis.

The *coupled architecture* is studied first, where the *tracking dynamics* module is embedded inside the *network dynamics* module in a cascaded structure and agents share their outputs (positions and/or velocities) with neighboring agents. Non-convex flocking interaction potentials with additional forcing terms are proposed to address the source-seeking problem, where agents are required to locate the minimum of an external scalar field. The proposed dynamics are experimentally tested with small quadrotors and analyzed using dissipativity theory and integral quadratic constraints (IQCs). Stronger performance analysis results are obtained with the so-called Zames-Falb (ZF) α-IQCs when considering convex interaction potentials. A derivation of the general high order non-causal ZF α-IQCs along with a parameterization is given making all arguments in time-domain and therefore allowing straightforward extensions to linear parameter varying systems. Numerical examples and simulation studies involving quadrotor models and underwater robot models, among others, complement the theoretical results.

The *decoupled architecture* is studied thereafter, where the *tracking dynamics* module is connected in series with the *network dynamics* module such that agents share virtual outputs (generated by the simplified models) with neighboring agents while locally trying to follow these virtual trajectories. The induced l_2 to l_∞ norm is used to analyze the extent to which the decoupled architecture is reasonable. The obtained peak tracking-error either justifies the architecture or detects a possible collision. Finally, the focus is brought on *network dynamics* module by considering packet dropouts. A novel consensus protocol is proposed as a generalization of existing protocols and its benefits are demonstrated on a representative example.

Contents

Chapter 1

Introduction

The last few decades have witnessed a lot of work in the analysis and design of distributed control laws for groups of mobile robots undergoing specific coordination tasks. See [Chen and Ren, 2019], [Bullo et al., 2009], [Bullo, 2021], [Ren and Beard, 2008], [Mesbahi and Egerstedt, 2010] and the references therein for examples. A major portion of the literature typically assumes simple agent dynamics such as single or double integrator dynamics. When considering interconnections of higher order non-linear agent dynamics such as quadrotors, unicycle models or complex underwater robots, it is commonly proposed (for example in [Cortés and Egerstedt, 2017], [Ren and Beard, 2008], [Francis and Maggiore, 2016], [Fax and Murray, 2004], [de Campos et al., 2012]) to implement local tracking controllers on these complex vehicles such that they track the trajectories generated by the simplified first or second-order dynamics. The authors in [Cortés and Egerstedt, 2017] propose to design cooperative control algorithms for interconnected systems assuming single integrator agent dynamics and wrap local tracking controllers around these trajectories so that agents with high-order complex dynamics act like single integrators. This idea is further demonstrated for differentially flat systems [van Nieuwstadt et al., 1998] with a simple example of a kinematic unicycle in [Cortés and Egerstedt, 2017], without considering disturbances on the agents. Similar architectures with local tracking controllers have been proposed in [Francis and Maggiore, 2016]. For example, it is proposed that a bicycle model under high gain feedback control can be approximated by a unicycle, which can be feedback linearized to an integrator, thereby allowing (in principle) the application of first-order consensus protocols on these complex vehicle models. Such modular architectures have also been reported in [Ren and Beard, 2008, Fig. 8.5 and Fig. 8.6], where the control architecture is composed of a first-order consensus module, a formation keeping module and so on. A consensus loop in series with a decoupled local tracking control

loop is considered and the stability of the overall system is implied by the series connection of two input-to-state stable systems (see Section 8.3.4 in [Ren and Beard, 2008]). Such architectures with different degrees of coupling between physical agents are discussed but a quantitative measure which can act as a guideline for deciding on the architecture is absent in the literature. A decoupled architecture for extending the framework of flocking to general vehicle models is pursued in [Z. Li et al., 2011] where an $\mathcal{L}_1$ adaptive control technique is used to guarantee tracking performance with the caveat of having no bounds on the control input. Another closely related line of work is to use arguments from singular perturbation theory and time-scale separation as in [Awad et al., 2019], [Awad et al., 2015], where the tracking dynamics are assumed to be much faster than the consensus dynamics and vice-versa. A similar decoupled architecture in the continuous-time setting is considered in [de Campos et al., 2012] where stability analysis is presented without a discussion on the applicability of the decoupled architecture. In a discrete-time setting, [Fax and Murray, 2004], [Pilz et al., 2011] consider information flow filters that decouple information flow dynamics and local tracking dynamics and present a stability analysis. A comparison between two such architectures is presented in [Bartels and Werner, 2014].

One of the overarching goals of this work is to build on these ideas and

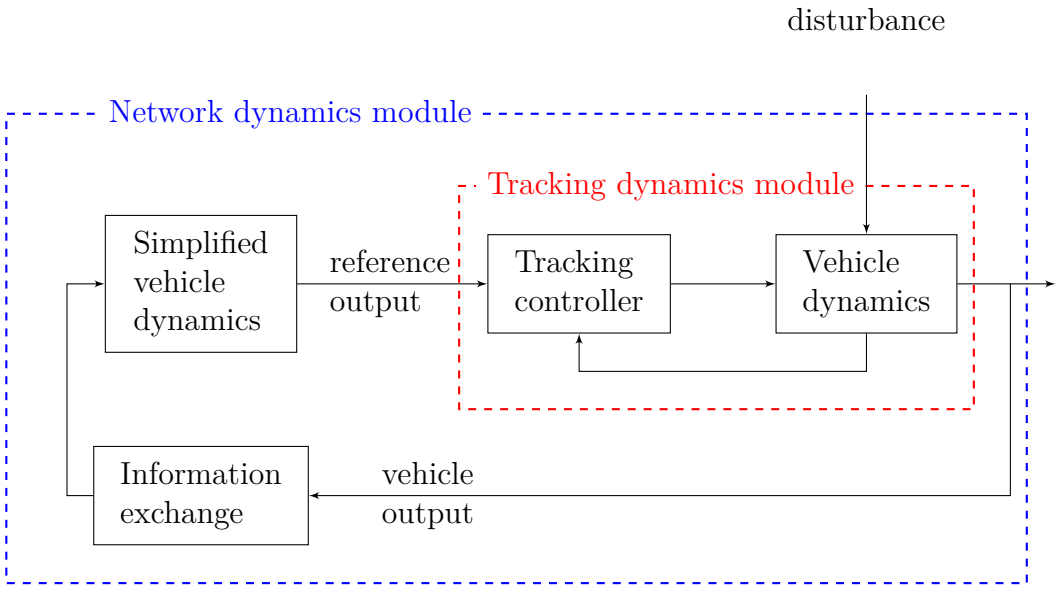

Figure 1.1: Coupled architecture where each vehicle agent shares true outputs with neighboring agents via the *Information exchange* block.

analyze such modular control architectures. Figures 1.1 and 1.2 show two such modular architectures considered in this work. The *Tracking dynamics module* consists of high-order, possibly non-linear *Vehicle dynamics* subject to local disturbances and a *Tracking controller* producing a desired closed-loop behavior. The *Network dynamics module* on the other hand consists of *Simplified vehicle dynamics* and an *Information exchange* block distributing information among neighboring agents in the network. Based on the type of architecture used, each agent either shares vehicle outputs with neighboring agents (see Fig. 1.1) or shares a virtual reference output generated by simplified dynamics (see Fig. 1.2). This is described by the different input signals going in to the *Information exchange* block.

The rationale behind such architectures is that if the tracking controllers are well tuned and are able to track the generated reference trajectories well, the output trajectories generated from the overall dynamics are *close* to the trajectories generated from the dynamics with simplified models which are well studied in the literature. Most of the work presented here can be seen as analyzing (whenever possible) and testing the validity of the this rationale for both architectures depicted in Fig. 1.1 and Fig. 1.2.

The decoupled architecture (as depicted in Fig. 1.2) considers a situation when only the references generated by the *Simplified vehicle dynamics*, the virtual reference outputs, are shared between different vehicles and the

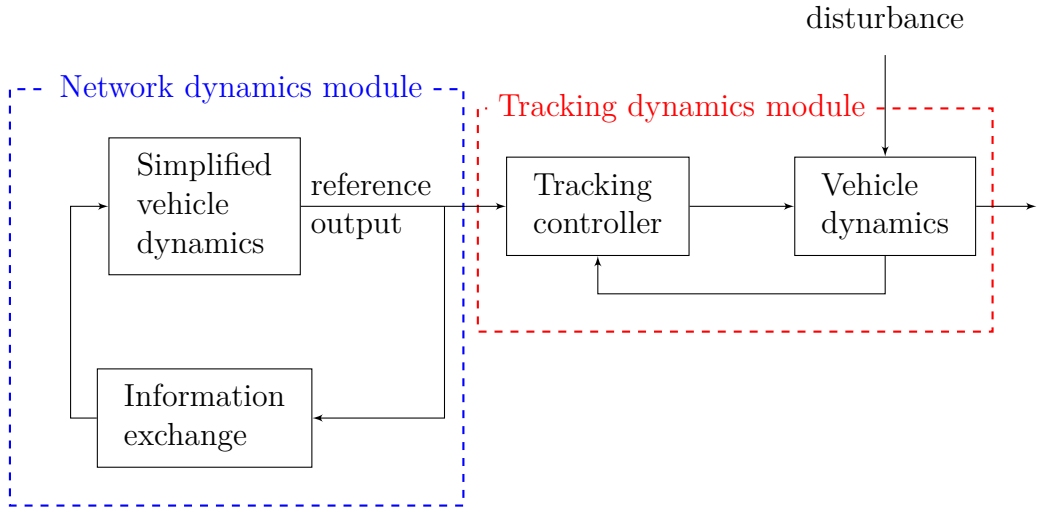

Figure 1.2: Decoupled architecture where each vehicle agent shares a virtual output generated by *Simplified vehicle dynamics* with neighboring agents via the *Information exchange* block.

true output trajectories are not shared. This architecture is favorable in scenarios involving large inter-agent distances where the disturbances need to be rejected locally at individual agents with no effects stemming from the disturbances being propagated throughout the network. Since all agents are oblivious to the true outputs (such as positions) of its neighboring vehicles, a natural question that arises is if one can bound the worst case (peak) tracking error at each vehicle and thereby provide bounds on the deviations of the vehicles' true outputs from the communicated one. This question is addressed in Chapter 4, where a quantitative measure is provided which takes into account the disturbances acting at each individual agent. Such a quantitative measure can assist in making the decision on the choice of architecture used and is absent in the current literature. As part of the study of the decoupled architecture, Chapter 5 focuses attention on the simplified first-order consensus dynamics (*Network dynamics module* from Fig. 1.2), where the network is considered to be non-ideal and involves packet dropouts. The more involved (and arguably more interesting) coupled architecture (as depicted in Fig. 1.1) considers the situation, where the true positions of the vehicles are shared with neighboring vehicles. Scenarios involving tightly coupled vehicle agents with small inter-vehicle distances necessitate the use of this architecture since even small disturbances could possibly cause a collision and the agents typically need to react to disturbances acting on neighboring agents. To consider a concrete scenario for the analysis of the coupled architecture, Chapter 2 and Chapter 3 focus attention on the specific problem of source-seeking.

With this short and general introduction to modular architectures considered in this work, the next two sections, viz., Section 1.1 and Section 1.2, introduce the specific problems considered in this work along with the most relevant literature, followed by a discussion on the adopted philosophy in Section 1.3 and a list of main contributions and an outline in Section 1.4.

1.1 Source-Seeking Dynamics Under a Coupled Architecture

One interesting application scenario of cooperative control of large groups of mobile robots is termed as the source-seeking problem and this forms the focal point for the work on coupled architecture considered here. This problem is abstracted from practical problems such as that of finding the source of an oil spill [Senga et al., 2007], [Aznar et al., 2014], the source of a gas leakage [Burgués et al., 2019] or the source of light [Duisterhof et al., 2021], etc. For

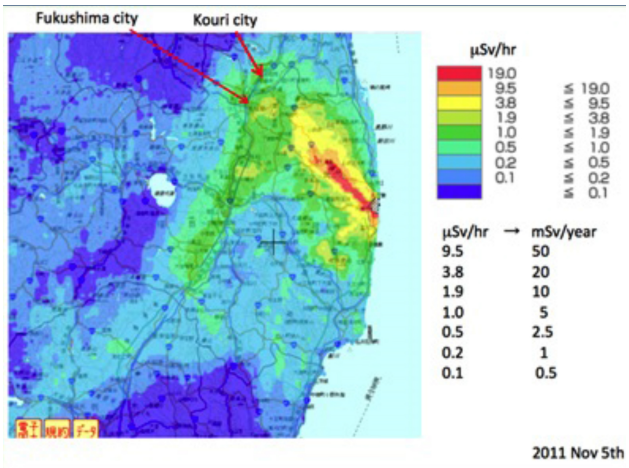

Figure 1.3: Radiation levels after the Fukushima disaster [Jeffrey Norris, 2012].

another concrete example, consider the Fukushima nuclear disaster of 2011 and the radiation levels depicted in Fig. 1.3. In such a scenario, in order to not put humans at risk, it would be desirable to deploy a fleet of robots with suitable sensors such that they cooperatively locate regions with highest radiation levels. For example, each robot could measure the radiation level at its respective location, communicate this with neighboring robots, estimate the gradient and move along the gradient to hopefully locate the source.

The abstract mathematical problem then relates to designing distributed control algorithms, that can be locally implemented on agents, that drive them to the minimum (or maximum based on convention) of an external scalar field (such as the radiation levels or luminosity). This needs to be achieved by cooperating with nearby agents but without the presence of a centralized control unit. Prior works addressing this problem include [Leonard and Fiorelli, 2001], which is based on the flocking framework developed in [Ogren et al., 2004], where a high fidelity simulation with the model of an underwater glider is used to demonstrate the approach. In [Angelico et al., 2021], the authors provide a gradient-free approach by using ideas from extremum-seeking control [Zhang et al., 2007] and provide some robot-in-loop experiments with an omni-wheel robot. Another gradient-free approach based on flocking is presented in [Turgeman et al., 2019], where experimental results were demonstrated with eight differential drive robots. A recent work dealing with quadrotors [Parker et al., 2019] uses ideas from particle swarm optimization and repulsive potential fields to deal with obstacle avoidance which is typically not included in the literature on particle

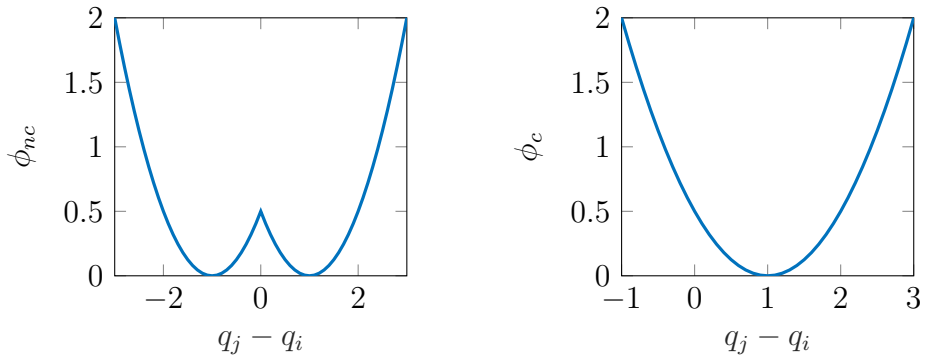

Figure 1.4: Non-convex pair-wise interaction potential $\phi_{nc} = \frac{1}{2}(|q_j - q_i| - 1)^2$ (left) and convex pair-wise interaction potential $\phi_c = \frac{1}{2}(q_j - q_i - 1)^2$ (right).

swarm optimization. An algorithm to seek light sources has been recently developed in [Duisterhof et al., 2021], whereas for localization of a gas source, an additional olfactory sensor was developed and tested in [Burgués et al., 2019]. Source-seeking with circular rotating formations is studied in [Moore and Canudas-de Wit, 2010], [Sepulchre et al., 2007] where the agents are required to continuously revolve around a virtual point to estimate the gradient at this point. Most of the literature on such source-seeking problems uses tools from extremum-seeking control [Khong et al., 2014], [Li et al., 2020], [Dürr et al., 2017], [Zhang et al., 2016], [Angelico et al., 2021]. One of the ideas in these works is to inject an oscillating signal in order to collect data for estimating the gradient of the external field. The approach taken in this work deviates from the above approach in the sense that the gradient (and the Hessian) is assumed to be cooperatively estimated by communicating with neighbors and collecting relevant measurement data from neighboring agents. This fairly intuitive idea is demonstrated in experiment under an artificially corrupted field measurement. Furthermore, in order to improve the estimated gradients, a cooperative control strategy (flocking/ formation control) is deployed so that the vehicles spread out uniformly, thereby improving the estimation. That being said, the aspects tied to gradient and Hessian estimation are not the focus in this work and are not considered in analysis but only tested in experiment, i.e., the theoretical results developed in this work assume the availability of the gradient. The only exception to this is Theorem 3.11 where a multiplicative noise in the gradient measurement is explicitly considered.

Two cooperative control mechanisms are studied in this thesis, viz., the flocking dynamics introduced by [Olfati-Saber, 2006] and formation control dynamics presented in [Fax and Murray, 2004]. Since the flocking frame-

work specifies the desired arrangement of agents based on distances (without directions), it models the interactions by a non-convex pairwise interaction potential such as the one shown in Fig. 1.4 (left) for agents i and j. Note that the desired arrangement of agents which corresponds to the minima of the interaction potential is achieved when $q_j = q_i \pm 1$. In contrast, the formation control dynamics specifies the desired arrangement of agents based on distances and directions which is modeled by a convex pair-wise interaction potential such as the one shown in Fig. 1.4 (right). Note that the desired arrangement of agents which corresponds to the minimum of the interaction potential is achieved when $q_j = q_i + 1$.

The analysis of the more involved flocking dynamics for general, possibly non-linear, vehicles specifically addressing the source-seeking problem is the main goal of Chapter 2. Chapter 2 uses the flocking framework developed in [Olfati-Saber, 2006] and proposes to add a forcing term that drives the flock towards the source. The forcing term is motivated from momentum methods in optimization [Alvarez et al., 2002], [Attouch and Redont, 2001]. The idea here is to modify the dynamics of typical methods such as steepest-descent or Newton by adding some memory (or momentum). It is known that this usually damps oscillations and accelerates the convergence. Motivated by the second-order continuous-time dynamics of Newton-type methods [Alvarez et al., 2002], a forcing term is defined that drives the flock of agents towards the source. In the spirit of the coupled architecture discussed in the previous section (see Fig. 1.1), fast velocity tracking controllers are wrapped around simplified double integrator velocities as suggested in [Cortés and Egerstedt, 2017]. This is analyzed in Section 2.1 first with double integrator agent dynamics and experimentally tested with an indoor quadrotor setup and reported in Section 2.1.3. The stability analysis, first presented for double integrator agents, is extended to general non-linear agents with a given input-output tracking performance in Section 2.2 and numerical simulations with a complex underwater vehicle model are presented in Section 2.2.3. Although the theoretical results are under the assumption of strictly convex fields and availability of gradients, experimental results (see Section 2.1.3) on non-convex fields with noisy measurements show that with a pre-filtering step, these protocols perform well in practice. All the theoretical results discussed above are presented in the framework of dissipativity [Scherer and Weiland, 2000], where an energy-like function, called a storage function, is sought which is used to show convergence of state trajectories to equilibria. For the results presented above, the storage functions are constructed based on physical intuition.

As a prelude to Chapter 3, a generalization of the stability analysis presented in Section 2.2.2 using the framework of integral quadratic constraints

(IQC/IQCs) [Megretski and Rantzer, 1997] is given in Section 2.3. The framework of IQCs is used for analyzing the stability of an interconnection of two systems; a linear and stable *nominal* system and a possibly non-linear *uncertain* system. The key idea is to capture the input-output properties of the uncertain system in the form of integral quadratic constraints and use these constraints to derive sufficient conditions on the nominal system that certify stability of the interconnection. See [Veenman et al., 2016], [Jönsson, 2001] for a tutorial. The results obtained from the so-called *hard*-IQCs [Megretski and Rantzer, 1997] can be interpreted with dissipativity-based arguments and vice-versa. This equivalence connects the results obtained in Chapter 2 which are based on dissipativity arguments to the results from Chapter 3 where *hard*-IQCs are used.

The standard formation control dynamics (an example of the coupled architecture) is extensively studied in the literature (see [Fax and Murray, 2004], [Bartels and Werner, 2014], [Gonzalez et al., 2015], [Hoffmann and Werner, 2017] for a few representative examples and [Chen and Ren, 2019] for an example survey). Source-seeking dynamics with interactions based on formation control is the focus of Chapter 3. Furthermore, convexity of the interaction potential emerging from formation control dynamics allows for analyzing exponential performance instead of merely stability. The main tool for analyzing robust performance of source-seeking dynamics under formation control interactions is the framework of IQCs.

The starting points for the theoretical work on IQCs presented here are [Lessard et al., 2016] and [Hu and Seiler, 2016] where the exponential versions of the IQCs are introduced for systems in discrete-time (ρ-IQCs) and in continuous-time (α-IQCs), respectively. Zames-Falb (ZF) α-IQCs with causal multipliers are introduced in [Hu and Seiler, 2016]. While [Zhang et al., 2019] extends [Lessard et al., 2016] to less conservative non-causal ZF multipliers in the discrete-time setting, [Freeman, 2018] presents the extension of [Hu and Seiler, 2016] to non-causal multipliers in the continuous-time setting. The theory developed in [Freeman, 2018] is in a very general setting of Bochner spaces and covers Lemma 3.12 in this work. Moreover, proof of [Freeman, 2018, Lemma 3] (which corresponds to Lemma 3.12 here) is not available and a proof, making all arguments in time-domain instead of frequency-domain, is given here building on ideas presented in a sidebar in [Scherer, 2022]. [Freeman, 2018] focuses on the derivation of the IQCs and does not consider parameterizations of the multiplier to arrive at a quasi-convex optimization problem for performance analysis. The present work extends these results by considering a parameterization proposed in [Veenman et al., 2016] adapted to the α-IQCs setting. Different multiplier factorizations are compared in [Zhang et al., 2019] which includes the discrete-time

analogue of the parameterization in [Veenman et al., 2016]. In the spirit of [Zhang et al., 2019] and [Freeman, 2018], which present examples showing the benefit of non-causal multipliers, an example of a continuous-time system with an integrator and an example of a linear parameter varying (LPV) system demonstrating the benefit of non-causal higher order multipliers over causal ones are presented. A closely related work is [Fazlyab et al., 2018], where causal and static multipliers are used to obtain non-exponential convergence rates when the dynamics are not exponentially stable. Finally, previous works (such as [Lessard et al., 2016], [Hu and Seiler, 2016] and [Freeman, 2018]) on the exponential version of IQCs present results for linear time invariant (LTI) systems. Since all arguments made here are with *hard*-IQCs in time-domain, it is rather straightforward to extend these results to LPV [Shamma and Cloutier, 1992] systems as it is done in [Pfifer and Seiler, 2015] for the standard IQCs. An example of such an extension to LPV systems is demonstrated in Theorem 3.4. This opens the doors for considering non-linear vehicle models with quasi-LPV representations. The framework developed here can be applied to extremum-seeking control problems [Michalowsky and Ebenbauer, 2016], or problems involving realtime-optimization [Nelson and Mallada, 2018]. Although the setup considered in [Nelson and Mallada, 2018] is similar to the one considered here (except for the LPV extension), the focus there is on designing an optimizer and obtaining conditions for optimality and stability with static $\alpha-$IQCs.

When considering formation control dynamics with a gradient-based forcing term, the recent work on the analysis of distributed optimization algorithms [Sundararajan et al., 2020] becomes relevant since the overall closed-loop dynamics emerging there are almost identical. Assuming one correctly translates the discrete-time results obtained in [Sundararajan et al., 2020] to a continuous-time setting, the first key hindrance in directly applying the ideas from [Sundararajan et al., 2020] is that the problem considered here allows for a subset of agents (instead of all agents) to have the gradient information, thereby making the dynamics heterogeneous in a sense. The requirement on the connectedness of the graph is also relaxed and instead existence of a path to at least one agent with gradient information is required. As a result, the decomposition approach used in [Sundararajan et al., 2020] to obtain a smaller linear matrix inequality (LMI/ LMIs) does not go through without modification. More importantly, since time-varying graphs are not considered here, dynamic multipliers can be used instead of the static multipliers used in [Sundararajan et al., 2020].

The monograph [Arcak et al., 2016] presents a dissipativity and IQC based compositional approach to analyzing stability and performance of an interconnected system by using properties of its sub-systems. Sparse LMIs

with a known structure are derived that can be efficiently solved with distributed optimization algorithms. In contrast, the results presented in this thesis derive LMIs that are independent of the network size and have a complexity corresponding to the analysis of a single sub-system. Furthermore, the interconnection structure is assumed to be uncertain. However, the results presented here have a similar essence of decomposing the overall system into dissipative subsystems interconnected through an uncertain operator characterized via a dissipation inequality or an integral quadratic constraint.

1.2 Formation Control Under a Decoupled Architecture

The goal of Chapter 4 is to analyze the decoupled architecture and understand the extent to which the decoupled architecture is reasonable in the context of a formation stabilization problem. Although [Z. Li et al., 2011] presents a decoupled architecture for flocking of higher order vehicle models, the technique proposes gain adaptation to ensure a guarantee on the tracking performance which may come at the cost of high control input. This is not addressed in [Z. Li et al., 2011]. Moreover, flocking dynamics are suitable when agents have small inter-agent distances and are tightly coupled. This tight coupling therefore necessitates that agents react to disturbances acting on neighboring agents to avoid collisions and therefore a decoupled architectures seems unreasonable for scenarios involving flocking dynamics. The decoupled architecture is hence studied in the context of formation stabilization with slightly higher inter-agent distances. The l_∞ norm (see Section 1.5.2 for the definition) is used as the performance measure of the local tracking performance. Based on the inter-agent distances of the simplified dynamics, this l_∞ norm of the tracking error can be used to either argue that the trajectories remain collision free or to decide on a coupled architecture in case a collision is possible. A very closely related problem of consensus of general non-linear vehicles modeled as quasi-LPV systems is considered in the continuous-time setting in [Hespe et al., 2020]. In contrast to [Hespe et al., 2020], a priori knowledge of the spectrum of the graph Laplacian is not required here. Instead, the recently developed results [Rantzer and Valcher, 2018], [Rantzer, 2015] on scalable analysis and control of positive systems are used as the first main ingredient in our analysis. As a second ingredient, a local input-output performance is used for the tracking dynamics to obtain one LMI condition per agent that guarantees the stability and performance of the local tracking feedback loops in the sense of the l_2 to l_∞ norm

(generalized H_2 norm [Scherer and Weiland, 2000], [Rotea, 1993]).

Chapter 5 focuses on consensus of first-order dynamics (*Network dynamics module* from Fig. 1.2) in the presence of packet dropouts. Consensus problems in networks with non-ideal communication have gained increasing attention in the last few decades [Fagnani and Zampieri, 2009], [Zhang and Tian, 2010], [Li et al., 2011], [Liu et al., 2011], [Münz et al., 2010], [Wu and Shi, 2012] and references in [Chen and Ren, 2019]. The kinds of imperfections include time delays, quantized communication and packet dropouts to name a few. These imperfections in communication render the fairly well understood consensus dynamics with ideal communications challenging to analyze and at the same time interesting.

There are two intuitive ways for an agent (say agent i) to act when a packet from a neighboring agent (say agent j) is dropped. In such a scenario, agent i can consider the link to be broken and thereby remove agent j from its neighbors for that instant. This can be interpreted as replacing the state of neighboring agent j by its own state. Alternatively, agent i can use the most recent information that was received from agent j. These two ways and their various interpretations have been studied mainly in distributed estimation and average consensus [Fagnani and Zampieri, 2009]. [Wang et al., 2010] compares these two ideas for the simplified case that when a packet is lost, the whole network loses a packet. A *Memory Weighted Protocol* is proposed in Chapter 5 which encompasses these two different approaches. The intuition behind the proposed protocol is that in case of a lost packet from agent j, agent i uses a convex combination of its own state and the most recent received information from agent j. The convex coefficients are free variables and can be tuned based on different network characteristics, agent dynamics etc. The sampling time is an important factor while designing communication protocols whenever communication is expensive or in general, when less frequent communication is preferred. However, there is a limit on the variation of this sampling time in order to maintain the guarantee on stability. Finding the least possible communication frequency/ maximum possible sampling time such that stability could still be certified is a central motivation behind the proposed protocol. An effective gain ϵ, called the *discrete gain*, is defined, which is the product of control gain K and sampling time T. It is shown that with the proposed protocol, the set of stabilizing values of the *discrete gain* is enlarged which allows less frequent communication. At the same time, the proposed protocol allows for selecting higher control gains which could be used to increase the convergence speed. A representative example showing the benefit of the proposed protocol is presented eventually.

1.3 Juggling Between Theory, Simulation and Experiment: Adopted Philosophy

The aim of this work is to make progress on open problems analytically in terms of theorems that can be proven under some assumptions, while not losing sight of the practical problem that motivates the analysis. This is done by studying an abstract (usually simplified) mathematical problem which has the same fundamental issues and properties as the original problem but removes the less relevant details. This approach makes the analysis possible (due to the simplifying assumptions) while increasing our understanding of some fundamental aspects of the original problem. At best, such an approach leads to an efficient methodology/algorithm which can be applied, not just on the simplified problem, but on the actual practical problem. In order to achieve this goal, this work juggles between theory and simulation (and sometimes experiments), each complementing the other. For example, consider the practical source-seeking problem of locating the source of an oil-spill with an underwater mobile robot. Realistic situations involve non-stationary scalar fields that are governed by partial differential equations [Aznar et al., 2014]. Furthermore, the control of underwater robotic agents such as the *HippoCampus* (see Appendix B.2) brings out other difficulties such as the non-holonomic constraint, state-estimation, etc. (see [Hackbarth et al., 2015], [Dücker et al., 2018b]). An abstraction of this complex problem focusing on source-seeking that is amenable to theoretical analysis considers a convex, stationary and smooth scalar field with locally stabilized vehicles driven along the gradient directions of the scalar field. First and foremost, the analysis illustrates pitfalls and situations, where even the abstracted problem fails to yield a solution, thereby demanding a different approach altogether. When the abstracted problem provides a solution, it may seem remote from the original practical problem, but it guides heuristic strategies that can then be tested on the original problem. The analysis is therefore typically followed by simulation studies involving situations closer to reality than the one treated in theory. Finally, experimental results further validate the approach. In some situations, simulations and experiments (successful or otherwise) trigger a further theoretical investigation as a means to explain the observations. This underlying philosophy is the basis and methodology for the results developed in this thesis.

1.4 Contributions and Outline

The key contributions of this work are summarized in the following list which also acts as an outline for the thesis together with a graph depicted in Fig. 1.5, where paths represent a recommendation on possible reading sequences and a general organization of chapters in this work.

1 An extension of flocking dynamics with additional forcing terms to address the source-seeking problem is proposed, analyzed and experimentally tested (see Section 2.1). Specifically, Theorem 2.1 and Corollary 2.2 present a standard dissipativity-based analysis of asymptotic stability for double integrator agents under strictly convex external fields by manually constructing storage functions. A practical implementation strategy is proposed in the form of Algorithm 2.1 and experimentally tested in an indoor experimental setup with 7 quadrotors under different virtual scalar fields artificially corrupted with measurement noise (see Section 2.1.3). These results (with slight variations) have been reported in [Datar et al., 2020].

2 Extension of flocking-based source-seeking dynamics to general, possibly non-linear, vehicle models under strictly convex external fields is proposed and analyzed in Section 2.2. Specifically, Theorem 2.3 proves asymptotic stability of the proposed dynamics using typical small-gain-type arguments and provides a qualitative understanding of the involved dynamics supporting the numerical simulations presented in Section 2.2.3 with a complex non-holonomic underwater robot model. These results (with slight variations) have been reported in [Attallah et al., 2020].

3 Theorems 2.1 and 2.3 are generalized by using the framework of IQCs to present a local analysis of asymptotic stability in Theorem 2.4. The sufficient condition here is presented in the form of an LMI (independent of network size) which automates the search for storage functions instead of prescribing them manually as in item 2. This analysis is applied on the model of a linearized quadrotor in Section 2.3.3. These results have been reported in [Datar et al., 2022, under review].

4 Moving from robust stability to robust performance analysis, source-seeking dynamics with LTI agents under uncertain strongly convex external fields and convex inter-agent interactions (typical formation control dynamics) with uncertain interconnections are analyzed in Theorem 3.10. Supporting this main result, Lemmata 3.7 and 3.8 characterize the equilibria of the source-seeking dynamics and Lemma 3.9

provides a decomposition result to obtain an LMI independent of the network size. Representative examples are provided in Section 3.3 that suggest that the obtained estimates can be tight. Finally, the analysis is extended to include multiplicative noise in the gradient measurement in Theorem 3.11 along with a numerical example with a quadrotor demonstrating the nominal performance versus noise robustness trade-off (see Section 3.5.1). These results have been reported in [Datar and Werner, 2022] and [Datar et al., 2022, under review]

5 As one of the critical ingredients for the main IQC result in Theorem 3.10, a derivation of the general non-causal ZF α-IQC along with an adaptation of a standard ZF parameterization to the α-IQC setting is given via Lemma 3.12 and Theorems 3.1 and 3.3. Lemma 3.12 is covered by [Freeman, 2018, Lemma 3] where the result is presented in a very general setting of Bochner spaces. Moreover, since the proof of [Freeman, 2018, Lemma 3] is unavailable, a proof is given here making arguments purely in time-domain to facilitate a seamless application to LPV systems (and possibly non-linear systems) as demonstrated in Theorem 3.4. This has been reported in [Datar and Werner, 2022] and [Datar et al., 2022, under review].

6 A scalable analysis of the decoupled architecture for heterogeneous networks is presented in the form of LMIs using the induced l_2 to l_∞ norm in Theorem 4.3 along with the corresponding controller synthesis LMIs in Theorem 4.5. Under bounded local disturbances, the analysis either validates the decoupled architecture by showing that the trajectories remain collision free as shown in the numerical example in Section 4.4 or demands a consideration of the coupled architecture by detecting possible collisions. These results have been reported in [Datar and Werner, 2021].

7 The problem of consensus under packet dropouts is considered in Chapter 5 and a novel memory-weighted consensus protocol based on two standard protocols from the literature is proposed in (5.5). The proposed protocol generalizes the two existing protocols. A representative example demonstrating situations where the proposed protocol outperforms the two existing protocols is given in Section 5.4. These results have been reported in [Datar et al., 2018]

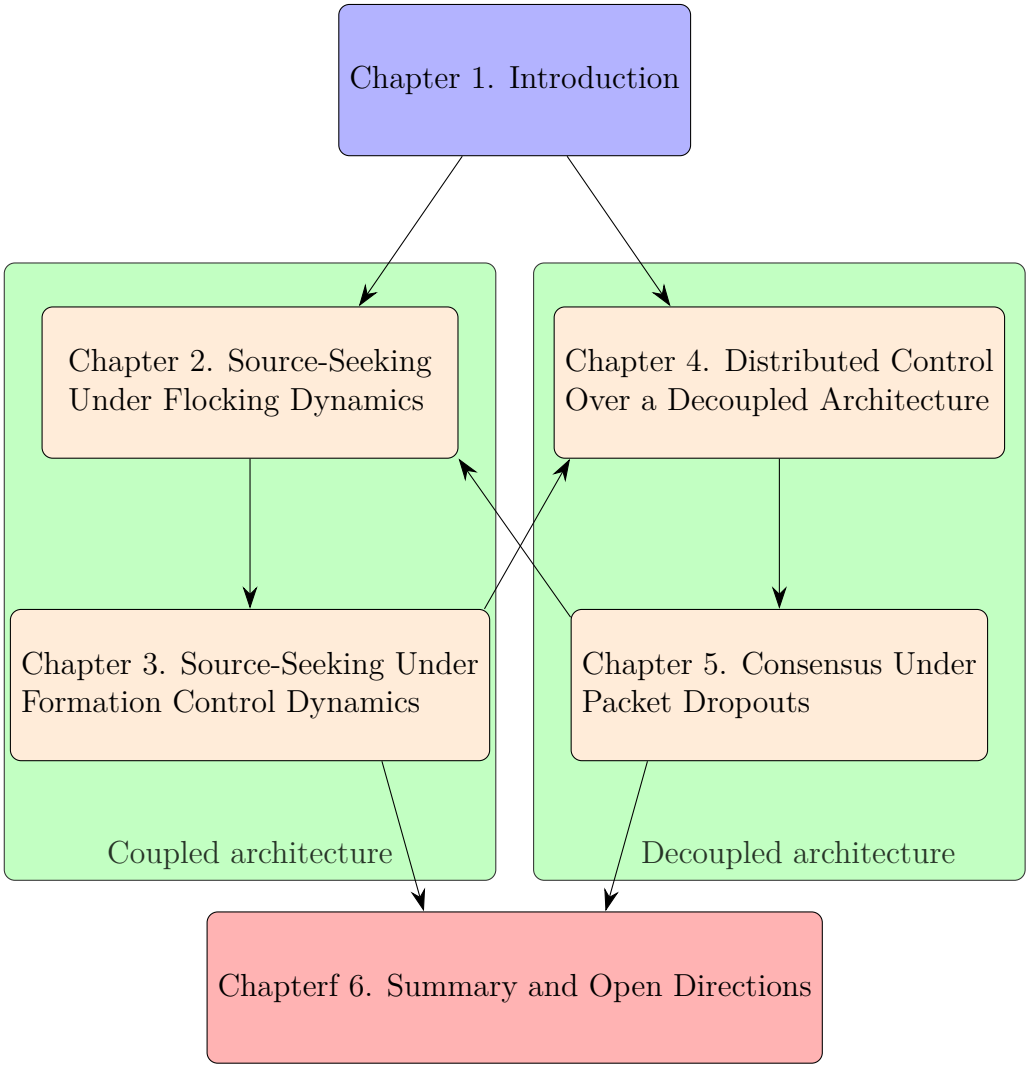

Figure 1.5: Flow graph with paths suggesting reading sequences and organization of the chapters.

1.4.1 Remarks on Existence and Uniqueness of Solutions

A majority of dynamical systems considered here are described by non-linear differential equations and an important aspect in their study is the existence and uniqueness of sufficiently smooth solutions [Logemann and Ryan, 2014]. Such aspects are not addressed in this work but instead, an approach adopted from [Scherer, 2022] is taken which sidelines these questions of existence and uniqueness.

The key idea is to derive sufficient conditions which imply that solutions to these non-linear differential equations, whenever they exist, satisfy some desirable property such as asymptotic convergence or exponential convergence to an equilibrium. For a concrete example, Theorem 3.4 derives sufficient conditions which imply that the solutions to the non-linear differential equations governed by (3.25), whenever they exist, satisfy a desirable property of exponential convergence with a specified rate α. There might exist multiple solutions, no solution or a unique solution but Theorem 3.4 neither requires the existence of unique solutions, nor proves it. In this spirit, the reader may substitute the phrase 'trajectories generated by the dynamics satisfy property X´ by 'sufficiently smooth solutions of the dynamics, whenever they exist, satisfy property X´.

On the same note, the property of well-posedness usually associated with the existence and uniqueness of solutions to feedback loops involving dynamical systems is not central in this work, i.e., well-posedness is neither required nor implied by the results considered here.

1.5 Notation

The common notation spanning multiple chapters is now discussed.

1.5.1 General Notation

Let $\mathbb{R}$ be the set of real numbers, $\mathbb{R}_+$ be the set of non-negative real numbers and $\mathbb{N}$ be the set of natural numbers including 0. The notation $X > (\geqslant) 0$ denotes that all entries of the matrix X are positive (non-negative) and X^T represents the transpose of matrix X. $\mathbb{S}^n$ denotes the set of symmetric real matrices of size n. For $X \in \mathbb{S}^n$, $X \succ (\succeq)\ 0$ means that X is positive definite (semi-definite), and $X \prec (\preceq)\ 0$ means that $-X$ is positive definite (semi-definite). For $X \in \mathbb{S}^n$, let $\lambda_{\max}(X)$ and $\lambda_{\min}(X)$ be the maximum and minimum eigenvalue of X, respectively. Let $\mathrm{cond}(X)$ denote the condition number of a matrix X and $\rho(M)$ denotes the spectral radius of an matrix M. For $x \in \mathbb{R}^n$, $\mathrm{diag}(x)$ is the diagonal matrix formed by placing the entries of x along the diagonal. Similarly, $\mathrm{blkdiag}(X_1, X_2, \cdots, X_N)$ is a block-diagonal matrix formed by placing the matrices X_1, X_2 and so on, as the diagonal blocks. For block matrices, $*$ is used to denote entries needed to make the matrix symmetric. Let $\mathbf{0}$ and $\mathbf{1}$ denote the column vectors or matrices of all zeroes and ones of appropriate sizes, respectively. Let I_d be the identity matrix of dimension d and the subscript d is suppressed when the dimension is clear from context. The i^{th} canonical basis vector (or i^{th} column of the

identity matrix) of appropriate size is denoted by e_i. For $x \in \mathbb{R}^n$, $||x||_p$ denotes the standard Euclidean p-norm and if the subscript p is unspecified as in $||x||$, it denotes the standard Euclidean 2 norm. The average of a vector is written as $\text{avg}(x) = \frac{1}{n}\mathbf{1}^T x$.

1.5.2 System Theoretic Notation

The notation $\left[\begin{array}{c|c} A & B \\ \hline C & D \end{array}\right]$ represents a continuous-time LTI system described by

$$\begin{aligned} \dot{x}(t) &= Ax(t) + Bu(t), \qquad x(0) = x_0, \\ y(t) &= Cx(t) + Du(t), \end{aligned} \tag{1.1}$$

where $x(t)$, $u(t)$ and $y(t)$ represent the state, input and output vector signals of appropriate dimension. The series interconnection of two LTI systems can be computed as

$$\left[\begin{array}{cc|c} A_1 & B_1C_2 & B_1D_2 \\ \mathbf{0} & A_2 & B_2 \\ \hline C_1 & D_1C_2 & D_1D_2 \end{array}\right] = \left[\begin{array}{c|c} A_1 & B_1 \\ \hline C_1 & D_1 \end{array}\right] \left[\begin{array}{c|c} A_2 & B_2 \\ \hline C_2 & D_2 \end{array}\right].$$

The notation for continuous-time LPV systems [Shamma and Cloutier, 1992] is analogous to the LTI case with the dependence on the scheduling parameter explicitly shown in state-space matrices. The series interconnection of an LTI system with constant matrices of appropriate size can be analogously computed as

$$T_1 \left[\begin{array}{c|c} A & B \\ \hline C & D \end{array}\right] T_2 = \left[\begin{array}{c|c} A & BT_2 \\ \hline T_1C & T_1DT_2 \end{array}\right].$$

The space of measurable functions $f : [0, T] \to \mathbb{R}^n$ which are square-integrable over $[0, T]$, i.e., $\int_0^T ||f(t)||^2 dt < \infty$ is denoted by $\mathcal{L}_2^n[0, T]$ where the super-script n is omitted when it is clear from context. The space of measurable functions $f : [0, \infty) \to \mathbb{R}^n$ which are square-integrable over $[0, T]$ for any finite $T < \infty$ is denoted by $\mathcal{L}_{2e}[0, \infty)$ where the super-script is omitted when it is clear from context. Let $\mathcal{L}_1(-\infty, \infty)$ denote the set of measurable functions $h : \mathbb{R} \to \mathbb{R}$, such that $\int_{-\infty}^{\infty} |h(t)|dt < \infty$. Let the convolution operation be denoted by $a(t) * b(t) = \int_0^t a(t - \tau)b(\tau)d\tau$. For any $q \in \mathcal{L}_{2e}[0, \infty)$, and a fixed $T \geqslant 0$, let the extension q_T defined on $(-\infty, \infty)$ be defined by

$$q_T(t) = \begin{cases} q(t), & \text{if } t \in [0, T], \\ \mathbf{0}, & \text{if } t \in \mathbb{R}\backslash[0, T]. \end{cases} \tag{1.2}$$

Remark 1.1. *Note that the word extension is used here to indicate an extension of the domain of the function from* $[0, \infty)$ *to* $(-\infty, \infty)$*. Borrowing convention from the robust-control literature, the sub-script* T *is used here to denote that this extension operation is also truncating the function on* (T, ∞)*, i.e., the extended function maps any inputs outside* $[0, T]$ *to zero.*

For a sequence of vectors $w = (w_1, w_2, \cdots)$, define the l_2 norm by $||w||_{l_2} = \sqrt{\sum_{k=0}^{\infty} ||w_k||_2^2}$. The space of real vector-valued signals w with $||w||_{l_2} < \infty$ is denoted by l_2. Similarly, define the l_1 norm by $||w||_{l_1} = \sum_{k=0}^{\infty} ||w_k||_2$ and the space of signals with finite l_1 norm be denoted by l_1. Let the l_∞ norm be defined by $||w||_{l_\infty} = \sup_k ||w_k||_2$.

1.5.3 Graph Theoretic Notation

The number of agents is denoted by N and $\mathcal{G} = (\mathcal{V}, \mathcal{E})$ denotes an undirected graph of order N with the set of nodes given by $\mathcal{V} = \{1, 2, \ldots, N\}$ and the set of edges $\mathcal{E} \subseteq \mathcal{V} \times \mathcal{V}$. Assume that $(i, j) \in \mathcal{E}$ if and only if $(j, i) \in \mathcal{E}$. The set of *informed* agents is denoted by $\mathcal{V}_l \subseteq \mathcal{V}$ which represents a subset of nodes with more information, such as the local gradient, and is used to differentiate them from other agents $\mathcal{V} \backslash \mathcal{V}_l$. A path between nodes i and j is a sequence of vertices $(v_1, v_2, \ldots, v_n)$ such that $v_1 = i$, $v_n = j$ and $(v_m, v_{m+1}) \in \mathcal{E}$ for all $m \in \{1, 2, \ldots, n-1\}$. The adjacency matrix $\mathcal{A}_d \in \{0, 1\}^{N \times N}$ is a matrix with the i, j^{th} entry $a_{ij} = 1 \iff (i, j) \in \mathcal{E}$. The set of neighbors of node i is denoted by $\mathcal{N}_i = \{j \in \mathcal{V} | (i, j) \in \mathcal{E}\}$. Let d_i be the degree of node i, i.e., the number of edges at that node and let $\mathcal{D} \in \mathbb{R}^{N \times N}$ be a diagonal matrix formed by the d_i's along the diagonal. The maximum degree $\max_i(d_i)$ is denoted by $d_{\max}$ and let $|\mathcal{E}|$ represent the total number of edges. Define the graph Laplacian matrix $\mathcal{L} \in \mathbb{S}^N$ as $\mathcal{L} = \mathcal{D} - \mathcal{A}_d$.

1.5.4 Notation Related to Kronecker Product

The Kronecker product is represented by $\otimes$. For convenience, let $\hat{X}$ denote the matrix $I_N \otimes X$ and let $X_{(d)}$ denote the matrix $X \otimes I_d$ for any matrix X. For an ordered set of vectors $(x_1, x_2, \ldots, x_N)$, let the vector formed by stacking these vectors be denoted by $x = \begin{bmatrix} x_1^T & x_2^T & \ldots & x_N^T \end{bmatrix}^T$. For any LTI system $G = \left[\begin{array}{c|c} A & B \\ \hline C & D \end{array}\right]$, the notation $G \otimes I$ represents an LTI system given by $\left[\begin{array}{c|c} A \otimes I & B \otimes I \\ \hline C \otimes I & D \otimes I \end{array}\right]$, whereas the notation $I \otimes G$ represents an LTI system given by $\left[\begin{array}{c|c} I \otimes A & I \otimes B \\ \hline I \otimes C & I \otimes D \end{array}\right]$.

1.5.5 Notation Relevant for Source-Seeking Problems

The source-seeking problem is considered in Chapter 2 and Chapter 3 and the notation relevant to it is discussed next. Consider N agents moving in $\mathbb{R}^d$ space (typically $d \in \{1, 2, 3\}$) and embedded in an external differentiable scalar field $\psi : \mathbb{R}^d \to \mathbb{R}$ which represents the spatial variation of a quantity of interest, such as the radioactivity in a disaster scenario. It is assumed that ψ is well-defined on $\mathbb{R}^d$, i.e., the domain of ψ is $\mathbb{R}^d$ and ψ is continuously differentiable on $\mathbb{R}^d$. The precise assumptions on ψ are stated more formally when presenting the main results. Informally, the scalar field is assumed to be strictly convex and sufficiently smooth and it is assumed that $q_* \in \mathbb{R}^d$ uniquely minimizes ψ, which is called the *source* of the field. At spatial position $q_i \in \mathbb{R}^d$ (of agent i), $\nabla\psi(q_i) \in \mathbb{R}^d$ and $\nabla^2\psi(q_i) \in \mathbb{R}^{d\times d}$ denote the gradient and Hessian evaluated at q_i, respectively. For a given configuration of positions of all agents $q = [q_1^T q_2^T \dots q_N^T]^T$, define $\Psi : \mathbb{R}^{Nd} \to \mathbb{R}$ by $\Psi(q) = \sum_{i=1}^N \psi(q_i)$. With this definition,

$$\nabla\Psi(q) = [\nabla\psi(q_1)^T \ \nabla\psi(q_2)^T \dots \nabla\psi(q_N)^T]^T,$$

$$\nabla^2\Psi(q) = \text{blkdiag}(\nabla^2\psi(q_1), \nabla^2\psi(q_2), \cdots, \nabla^2\psi(q_N)).$$

The notions of strict and strong convexity (see [Nesterov, 2004] for details) play a central role in the analysis and are reviewed next. A function $\psi : \mathbb{R}^d \to \mathbb{R}$ is strictly convex if for any $\theta \in (0, 1)$,

$$\psi(\theta y_1 + (1-\theta)y_2) < \theta\psi(y_1) + (1-\theta)\psi(y_2) \quad \forall y_1, y_2 \in \mathbb{R}^d, \ y_1 \neq y_2.$$

It is strongly convex with parameter $m_\psi > 0$ if for any y_1, $y_2 \in \mathbb{R}^d$,

$$m_\psi ||y_1 - y_2||^2 \leqslant (\nabla f(y_1) - \nabla f(y_2))^T (y_1 - y_2).$$

Note that the class of strongly convex functions is a subset of the class of strictly convex functions and an example of a strictly convex, but not strongly convex function is $\psi(y) = y^4$. More details can be found in [Nesterov, 2004]. Finally, the convex hull of a finite set of points $\{y_1, \cdots, y_N\}$ is the set $\{\sum_{i=1}^N \lambda_i y_i : \sum_{i=1}^N \lambda_i = 1, \ \lambda_i \geqslant \text{ for all } i\}$.

Chapter 2

Source-Seeking Under Flocking Dynamics: Stability Analysis and Experimental Results

This chapter focuses on the problem of source-seeking with a coupled architecture involving non-convex inter-agent interactions, typical from standard flocking dynamics [Olfati-Saber, 2006], [Leonard and Fiorelli, 2001], [Su et al., 2009] or with distance-based cooperative control [Oh et al., 2015], [Krick et al., 2008], [Dörfler and Francis, 2009]. Specifically, assuming double integrator agent dynamics, an extension of flocking dynamics [Olfati-Saber, 2006] with a forcing term is proposed in Section 2.1.1, analyzed in Section 2.1.2 and experimental results with an indoor quadrotor setup are reported in Section 2.1.3. An extension of the double integrator models involved in flocking to general vehicle models with local velocity controllers is considered in Section 2.2 with stability analysis given in Section 2.2.2 and simulation results in Section 2.2.3. As a prelude to Chapter 3, a generalization of the stability analysis presented in Section 2.2.2 using the framework of IQCs is given in Section 2.3. The key contributions of this chapter have been reported (with slight variations) in [Datar et al., 2020], [Attallah et al., 2020] and [Datar et al., 2022, under review].

2.1 Double Integrator Vehicle Models

This section assumes that vehicles can be modeled as double integrators and presents an extension of the flocking dynamics to address the source-seeking problem.

2.1.1 Problem Setup

Consider N agents living in a $d-$dimensional space and let $q_i,\ p_i \in \mathbb{R}^d$ denote their positions and velocities, respectively. Let $q,\ p \in \mathbb{R}^{Nd}$ be constructed by stacking q_i as $q = [q_1^T q_2^T \dots q_N^T]^T$ and similarly, $p = [p_1^T p_2^T \dots p_N^T]^T$. The inter-agent interaction potential function between agent i and j is denoted by $\phi(q_i, q_j)$ (see [Olfati-Saber, 2006], [Leonard and Fiorelli, 2001] and [Dörfler and Francis, 2009] for examples of interaction potentials) and the potential for the complete system is then denoted by $V(q) = \frac{1}{2}\sum_{i,j}\phi(q_i, q_j)$. To represent the spatial variation of a quantity of interest, let $\psi : \mathbb{R}^d \to \mathbb{R}$ be a sufficiently smooth scalar field. For the theoretical analysis, the scalar field is assumed to be strictly convex with the point $q_* \in \mathbb{R}^d$, called the *source*, uniquely minimizing ψ. Even though the theoretical analysis deals with a strictly convex and smooth field ψ with perfect gradient and Hessian measurements, experiments with non-convex fields and noisy measurements are presented in Section 2.1.3 demonstrating the applicability of the proposed approach to more general situations. Let $\nabla\psi$ and $\nabla^2\psi$ be the gradient and Hessian of ψ, respectively. As described in Section 1.5.5, let $\Psi : \mathbb{R}^{Nd} \to \mathbb{R}$ be defined by $\Psi(q) = \sum_i \psi(q_i)$ and let $\nabla\Psi$ and $\nabla^2\Psi$ be its gradient and Hessian, respectively.

The flocking dynamics as described in [Olfati-Saber, 2006] can be represented as

$$\begin{aligned} \dot{q} &= p, \\ \dot{p} &= -\nabla V(q) - (\mathcal{L}_{(d)}(q) + cI)p + f_\gamma \end{aligned} \tag{2.1}$$

with initial conditions $q(0)$ and $p(0)$, where $V(q)$ is the non-negative inter-agent interaction potential, $\mathcal{L}(q)$ is the state-dependent graph Laplacian, $\mathcal{L}_{(d)}(q) = \mathcal{L}(q) \otimes I_d$, $c \in \mathbb{R}$ is a positive friction coefficient and f_γ represents an external forcing term to drive the flock to a desired location. The state-dependent Laplacian matrix $\mathcal{L}(q)$ is calculated by defining a communication topology induced by the positions q where $(i, j) \in \mathcal{E}$ if and only if $||q_i - q_j|| \leqslant r_{\text{sensing}}$, where r_{sensing} is the interaction range. See [Olfati-Saber, 2006] for more details on flocking dynamics.

For the problem of minimizing a convex function $\psi(x)$, it has been shown in [Alvarez et al., 2002], that, with positive constants k_1 and k_2, the dynamics of the continuous-time analogue of the second-order Newton-type method with momentum are represented by

$$\begin{aligned} \dot{x} &= v, \\ \dot{v} &= -k_1\nabla^2\psi(x)v - k_2\nabla\psi(x) \end{aligned} \tag{2.2}$$

and $x(t)$ approaches the minimizer x^* of ψ asymptotically under some technical conditions. Refer to [Alvarez et al., 2002], [Wilson et al., 2021] for more details. Motivated by this idea and the known convergence results of the dynamics (2.2), let the forcing term in the flocking dynamics (2.1) be defined as

$$f_\gamma = -k_1 \nabla^2 \Psi(q) p - k_2 \nabla \Psi(q), \tag{2.3}$$

where $k_1 \geqslant 0$ and $k_2 > 0$ are tuning parameters. With the choice of f_γ as in (2.3), the closed-loop dynamics with initial conditions $q(0)$ and $p(0)$ can be written as

$$\begin{aligned} \dot{q} &= p, \\ \dot{p} &= -\nabla V(q) - (\mathcal{L}_{(d)}(q) + cI)p - k_1 \nabla^2 \Psi(q) p - k_2 \nabla \Psi(q). \end{aligned} \tag{2.4}$$

Note that the interconnection between the different agents is state-dependent and depends on the sensing radius r_{sensing} which is built into the inter-agent potential $\phi(q_i, q_j)$ and the state-dependent Laplacian $\mathcal{L}_{(d)}(q)$. For more details on this, the interested reader is referred to [Olfati-Saber, 2006].

Problem 2.1. *Derive sufficient conditions independent of the network size N under which the trajectories q and p generated by dynamics (2.4) remain bounded for all $t \geqslant 0$ and asymptotically converge to an equilibrium of the dynamics.*

2.1.2 Analysis

The interaction potential $V(q)$ has the form $V(q) = \frac{1}{2}\sum_{i,j} \phi(q_i, q_j)$, where $\phi(q_i, q_j)$ is a function only depending on $||q_i - q_j||$ [Olfati-Saber, 2006] and is therefore pair-wise symmetric, i.e., $\frac{\partial}{\partial q_i}\phi(q_i, q_j) = -\frac{\partial}{\partial q_j}\phi(q_i, q_j)$. This simply means that the net force along each pair of agents balances out and sums to 0. Similarly, the state-dependent graph Laplacian $\mathcal{L}(q)$ is symmetric if all agents have the same interaction range r_{sensing}. Therefore, the net force cancels out for every pair of agents and the force acting on the center of mass due to pair-wise interactions ($-\nabla V(q)$) and from velocity alignment ($-\mathcal{L}_{(d)}(q)p$) is zero (see [Olfati-Saber, 2006]). This is summarized in

$$\begin{aligned} (\mathbf{1}_N^T \otimes I_d) \cdot \nabla V(q) &= \mathbf{0} \quad \forall q \in \mathbb{R}^{Nd}, \\ (\mathbf{1}_N^T \otimes I_d)(\mathcal{L}(q) \otimes I_d) = (\mathbf{1}_N^T \mathcal{L}(q)) \otimes I_d &= \mathbf{0}. \end{aligned} \tag{2.5}$$

By defining the center of mass position and velocity as in [Olfati-Saber, 2006] by

$$\begin{aligned} q_c &= \frac{1}{N}(\mathbf{1}_N \otimes I_d)^T q, \\ p_c &= \frac{1}{N}(\mathbf{1}_N \otimes I_d)^T p, \end{aligned}$$

the translational dynamics of the center of mass with appropriate initial conditions can be derived from (2.4) and (2.5) as

$$\begin{aligned} \dot{q}_c &= p_c, \\ \dot{p}_c &= -cp_c - \frac{1}{N}(\mathbf{1}_N \otimes I_d)^T (k_1 \nabla^2 \Psi(q) p + k_2 \nabla \Psi(q)). \end{aligned} \tag{2.6}$$

Theorem 2.1 (Analysis for Problem 2.1)**.** *Let the flocking interaction potential $V : \mathbb{R}^{Nd} \to \mathbb{R}$ be a continuously differentiable function with a uniform lower bound $V_{\min}$, i.e., $V(q) \geqslant V_{\min}$ $\forall q$. Let all agents have the same interaction range r_{sensing}, i.e., the state-dependent graph Laplacian $\mathcal{L}(q)$ is symmetric for all q. For a twice continuously differentiable, strictly convex field $\psi : \mathbb{R}^d \to \mathbb{R}$ with a unique minimum at q_*, the flocking dynamics* (2.4) *with any $c > 0$, $k_2 > 0$ and $k_1 \geqslant 0$ are stable, i.e., the trajectories generated by these dynamics remain bounded for all $t \geqslant 0$. Moreover, for all initial conditions $(q(0), p(0))$, the trajectories converge asymptotically to the set*

$$\mathcal{W} := \{(q, 0) | \nabla V(q) + \nabla \Psi(q) = 0\}. \tag{2.7}$$

Additionally, if

1) *ψ is radially symmetric about the source q_*, i.e., it has the form $\psi(q) = \psi_r(||q - q_*||)$ for some function $\psi_r : \mathbb{R} \to \mathbb{R}$,*
2) *V is pairwise-symmetric, i.e., it has the form $V(q) = \frac{1}{2}\sum_{i,j} \phi(||q_i - q_j||)$ for some function $\phi : \mathbb{R} \to \mathbb{R}$,*

then the source q_* lies in the convex hull of equilibrium agent positions.

Proof. For the continuous-time dynamics (2.4), consider the energy-like nonnegative function $E : \mathbb{R} \to \mathbb{R}$ defined as

$$E(t) := V(q(t)) - V_{\min} + k_2(\Psi(q(t)) - \Psi(q_*)) + \frac{1}{2} p(t)^T p(t). \tag{2.8}$$

Differentiating $E(t)$ with respect to time,

$$\begin{aligned} \dot{E} &= (\nabla V(q) + k_2 \nabla \Psi(q))^T \dot{q} + p^T \dot{p} \\ &= -p^T (\mathcal{L}_{(d)}(q) + cI + k_1 \nabla^2 \Psi(q)) p \\ &\leqslant 0. \end{aligned}$$

The last inequality is obtained by using $\mathcal{L}(q) \geqslant 0$ and convexity of ψ which implies $\nabla^2 \Psi(q) \geqslant 0$ for all $q \in \mathbb{R}^{Nd}$. Thus, $E(t) \leqslant E(0)$ $\forall t \geqslant 0$. Finally note that strict convexity of ψ (and the existence of a unique minimizer q_*)

implies that ψ has bounded sub-level sets. Therefore, the trajectories remain bounded for all $t \geqslant 0$.

Moreover, $\dot{E} = 0$ if and only if $p = 0$. Hence, by using the LaSalle's invariance principle [Bullo, 2021, Theorem 14.7], the trajectories asymptotically converge to the the set $\mathcal{W}$ defined in (2.7).

Finally, if V is pairwise-symmetric, i.e., $V(q) = \frac{1}{2}\sum_{i,j}\phi(||q_i - q_j||)$ for some function $\phi : \mathbb{R} \to \mathbb{R}$ and the state-dependent graph Laplacian $\mathcal{L}(q)$ is symmetric, the discussion preceding this theorem shows that center of mass dynamics is governed by (2.6). Therefore, the equilibrium q must satisfy

$$\frac{1}{N}(\mathbf{1}_N \otimes I_d)^T \nabla\Psi(q) = 0. \tag{2.9}$$

Now let $\psi(q) = \psi_r(||q - q_*||)$, which implies that

$$\nabla\psi(q) = \begin{cases} \frac{\psi_r'(||q-q_*||)}{||q-q_*||}(q - q_*) & \text{if } q \neq q_* \\ 0 & \text{otherwise} \end{cases}$$

Plugging this into (2.9), we obtain

$$0 = \sum_{i, q_i \neq q_*} \frac{\psi_r'(||q_i - q_*||)}{||q_i - q_*||}(q_i - q_*). \tag{2.10}$$

Now assume that q_* does not belong to the convex hull of $\{q_i : i \in \mathcal{V}\}$. This implies that there is a separating hyperplane characterized by an $h \in \mathbb{R}^d$ and an offset $c_h \in \mathbb{R}$ such that $h^T q_i + c_h \geqslant 0$ for all $i \in \mathcal{V}_l$ and for some $\varepsilon \geqslant 0$, $h^T q_* + c_h = -\varepsilon < 0$. Multiplying both sides of equation (2.10) from the left by h^T, we get

$$\begin{aligned} 0 &= \sum_{i \in \mathcal{V}, q_i \neq q_*} \frac{\psi_r'(||q_i - q_*||)}{||q_i - q_*||} h^T(q_i - q_*) \\ &= \sum_{i \in \mathcal{V}, q_i \neq q_*} \frac{\psi_r'(||q_i - q_*||)}{||q_i - q_*||}((h^T q_i + c_h) - (h^T q_* + c_h)) \\ &= \sum_{i \in \mathcal{V}, q_i \neq q_*} \frac{\psi_r'(||q_i - q_*||)}{||q_i - q_*||}((h^T q_i + c_h) + \varepsilon) \end{aligned}$$

Now, strict convexity of ψ implies that for all $q \neq q_*$, $\psi(q_*) > \psi(q) + \nabla\psi(q)^T(q_* - q)$ which implies that $(q - q_*)^T\nabla\psi(q) > \psi(q) - \psi(q_*) > 0$. Therefore, for all $q \neq q_*$, $(q - q_*)^T\nabla\psi(q) = \psi_r'(||q - q_*||).||q - q_*|| > 0$. Putting this together, we have that for all $q \neq q_*$, $\psi_r'(||q - q_*||) > 0$ and each term inside the sum above is positive leading to a contradiction. Therefore,

there exists no hyperplane separating $\{q_i | i \in \mathcal{V}\}$ and q_* which implies that q_* is in the convex hull of $\{q_i | i \in \mathcal{V}\}$.

□

Another desirable property of the equilibrium for the case of quadratic fields is presented in the next corollary.

Corollary 2.2. *Assume that the field $\psi : \mathbb{R}^d \to \mathbb{R}$ is strictly convex, quadratic and has a unique minimum at q_*. The center of mass governed by dynamics* (2.6) *corresponding to the overall dynamics* (2.4) *converges asymptotically to the source, i.e., $\lim_{t\to\infty} q_c(t) = q_*$.*

Proof. Let $\psi(y) = \frac{1}{2} y^T H y + g^T y + c_0$ with $H \in \mathbb{R}^{d\times d}$ and $H \succ 0$ due to strict convexity. Thus, $q_* = -H^{-1}g$ is the unique minimizer of ψ. Characterization of the equilibrium $q_e = [q_{e_1}^T q_{e_2}^T \dots q_{e_N}^T]^T$ under given dynamics gives

$$\frac{1}{N}(\mathbf{1}_N \otimes I_m)^T \nabla\Psi(q_e) = \frac{1}{N}\sum_{i=1}^{N}(Hq_{e_i} + g) = H(\frac{1}{N}\sum_{i=1}^{N} q_{e_i}) + g = 0,$$

which implies $\frac{1}{N}\sum_{i=1}^{N} q_{e_i} = -H^{-1}g = q_*$. Finally, using Theorem 2.1 to imply asymptotic stability of the equilibrium, we get, $\lim_{t\to\infty} q_c(t) = q_*$. □

2.1.3 Experiments with Indoor Quadrotors

The ideas developed in the last section are tested in an indoor experimental platform with Crazyflie 2.1 (see Appendix A), the details of which are discussed next before presenting the experimental results.

Experimental Setup

The experiments were conducted on an open-source experimental platform from Bitcraze AB called the Crazyflie 2.1 along with an indoor positioning based on the Decawave DWM1000 chip called the Loco-positioning system. A peer-to-peer communication protocol, sufficient for the purposes of the experiment, was developed and deployed on the software along with a heuristic control mechanism to avoid clock drifts [Paulsen, 2018], [Paulsen, 2019]. For implementing the source-seeking Algorithm 2.1 (presented later in the current section), the analytic function ψ was stored on-board but only queried to get a corrupted field strength at the agent location. The position, velocity and the measured field values were broadcast to neighboring agents. More details are given in Appendix A.

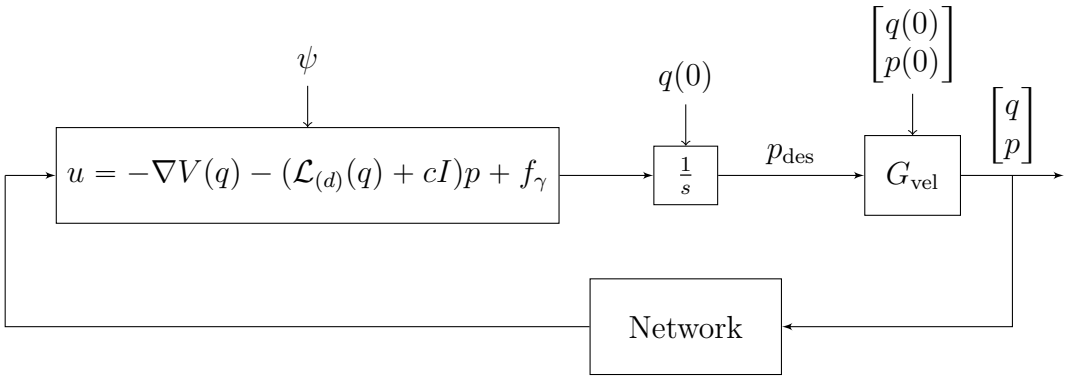

Figure 2.1: Control architecture representing the experimental implementation on quadrotors.

Control Architecture With a Local Velocity Controller

Initial experiments with Crazyflie 2.1 show that the onboard velocity controller shows satisfactory tracking performance for low frequency references [Paulsen, 2019]. This local velocity controller is used to track the desired velocities and these closed-loop dynamics are represented by G_{vel} with the desired velocity input p_{des}. A nested control architecture with a fast attitude controller and a relatively slow velocity controller (although faster than the flocking dynamics) wrapped around the attitude controller is used. Such a nested control architecture is standard in quadrotor control [Powers et al., 2015]. More specifically, a proportional-integral-derivative (PID) attitude controller runs at 500 Hz and an outer proportional-integral (PI) velocity controller runs at 100 Hz. Some preliminary tests on the velocity controller revealed that the tracking performance within the linear regime leads to a rise time of around half a second for reference steps in velocities and this makes a plausible case for modeling a quadrotor as a double integrator if the flocking dynamics are slow-enough. The output of G_{vel} is then the position and velocity vectors, q and p, respectively. This is shown in Fig. 2.1, where the computed flocking control input (force) is integrated to obtain desired velocity p_{des}, which is fed in to the velocity controller.

Gradient and Hessian Estimation Heuristic

In order to estimate the gradient and the Hessian locally at each agent, two dictionaries of 30 points each are maintained and each agent solves two least squares problems at each sampling time. For the gradient estimation, the

dictionary is updated locally by each agent by collecting measurements as it moves through space. The dictionary for the Hessian estimation is built and maintained by communication with neighbors. A new data point (locally measured or received from the neighbor) is only added to the dictionary if it is novel enough. A simple heuristic of adding a data point only if it is at least some fixed distance away from the last one collected from the same agent is used. Additionally, the Hessian is discarded if it is not positive definite.

For the experimental results, the local field measurement is artificially corrupted by five percent noise relative to the field strength (multiplicative noise). A formal analysis that explicitly considers multiplicative noise is presented later in Section 3.5. For a typical source-seeking experiment with a quadratic field ψ, Figure 2.2 shows histograms of errors in degrees between the estimated and the true gradient direction $\nabla\psi(q_i)$ (in orange) and between the estimated and true direction $k_1\nabla^2\psi(q_i) + k_2\nabla\psi(q_i)$ (in blue) for a typical agent. The data is collected over about 11-13 seconds at 50 Hz. It can be seen that the distribution of error angles (in degrees) for the direction $k_1\nabla^2\psi(q_i) + k_2\nabla\psi(q_i)$ is roughly centered about zero with most of the errors falling between -40 and 40 degrees which means that the estimated direction belongs to the same quadrant as the true direction. The errors for the gradient direction $\nabla\psi(q_i)$ show a spread out distribution. The areas under the histograms also represent the number of times each direction is used using the heuristic mentioned above. Because of the inertia of the agents, it can be seen that, some erroneous outliers at isolated time instances do not cause a significant problem (see Fig. 2.3, Fig. 2.4 and Fig. 2.5).

Implementation Algorithm

Algorithm 2.1 describes the key steps in the implementation code that runs on an arbitrary agent i. It is divided into five steps. At each execution time k, agent i starts by measuring the agent's own position q_i, velocity p_i and the field value at the current location $\psi(q_i)$ corrupted by some zero-mean white noise process η. This information is then exchanged with all neighbors j. A dictionary is maintained by collecting novel measurements (in the sense of distance) from neighbors and local measurements. Once the dictionary is full, the oldest measurements are replaced with new ones (the old measurements are discarded). Each agent then solves a linear least-squares problem based on local measurements to fit a plane and estimate the gradient g. Another least-squares problem to fit a paraboloid is then solved to estimate the Hessian at the current location. If the obtained Hessian is not positive semi-definite, it is discarded for this time step and only gradient information is used. Finally, the flocking force f_α is computed based on the

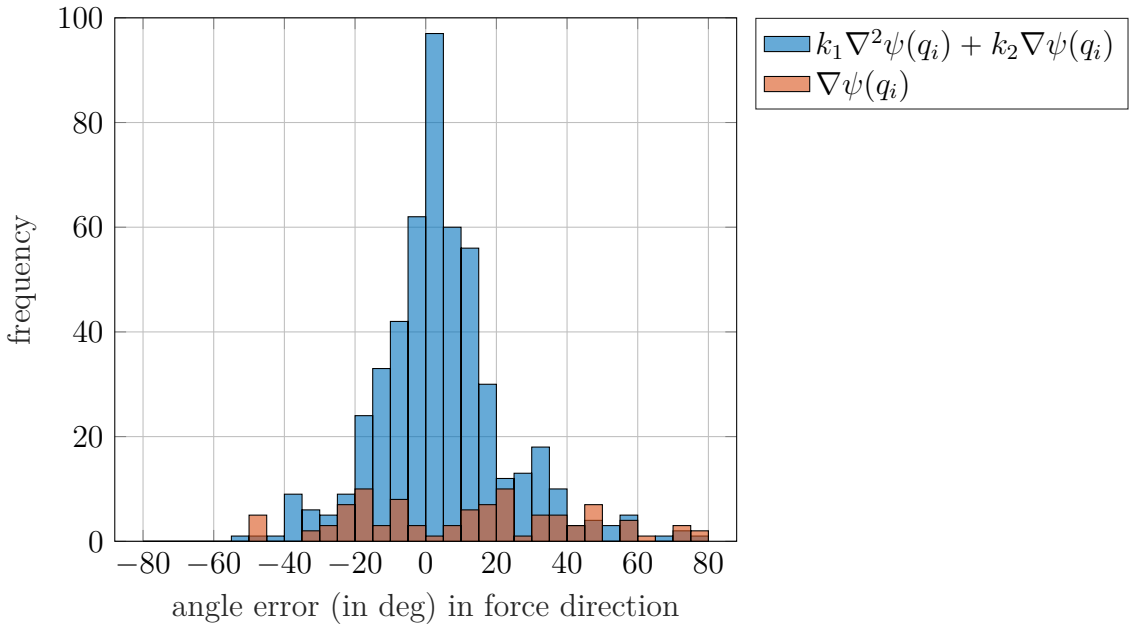

Figure 2.2: Histograms of angle errors (in degrees) between the true direction and estimated direction (with noisy field measurements and estimated gradients and Hessians).

positions and velocities of the neighbors. The net force u is then used to calculate the desired velocity p_{des} based on the sampling time T. This p_{des} is then passed on to the internal velocity controller as the desired velocity.

Experimental Results

The details on the experimental platform are discussed in the Appendix A. The results are now reported for a strictly convex field ψ_1, a non-convex field ψ_2 with a single minimum and a non-convex field with two minima ψ_3 given by

$$\begin{aligned}
\psi_1(q) &= (q - c_0)^T \begin{bmatrix} 1 & 0 \\ 0 & 2 \end{bmatrix} (q - c_0), \\
\psi_2(q) &= -\exp\left(-||(q - c_0)||^2\right), \\
\psi_3(q) &= -\exp\left(-||(q - c_1)||^2\right) - \exp\left((-||(q - c_2)||^2)\right),
\end{aligned} \tag{2.11}$$

where $c_0 = [2 \;\; 1.5]^T$, $c_1 = [3 \;\; 2]^T$ and $c_2 = [1 \;\; 1]^T$. The field strength measurement is corrupted by zero mean noise with an amplitude of five percent of the field strength. Figures 2.3, 2.4 and 2.5 show the flight trajectories

Algorithm 2.1 Runs on agent i at 20Hz

1: Initialize offline:
   - i Flocking parameters (see [Olfati-Saber, 2006]) such as equilibrium distance d, friction-coefficient c
   - ii k_1, k_2
   - iii $\forall j \in \mathcal{N}_i \cup \{i\}$, $\hat{q}_j = \{\}$

2: Measure:
   - i Measure q_i, p_i
   - ii Measure $\psi(q_i) \leftarrow \psi(q_i)+$ noise (corrupted)

3: Communicate:
   - i Broadcast $(q_i, p_i, \psi(q_i))$
   - ii Receive $(q_j, p_j, \psi(q_j))$ $\forall j \in \mathcal{N}_i$

4: Estimate:
   - i Estimate the gradient g by fitting a plane with locally measured data.
   - ii Update dictionary:
     if $\forall j \in \mathcal{N}_i \cup \{i\}$, $||q_j - \hat{q}_j|| > d$ **or** $\hat{q}_j = \{\}$,
     then: add $(q_j, \psi(q_j))$ to dictionary and $\hat{q}_j \leftarrow q_j$
   - iii Estimate the Hessian H by fitting a paraboloid on the dictionary data.

5: Compute:
   - i $f_\alpha \leftarrow -\partial V(q)/\partial q_i - cp_i - \sum_{j \in \mathcal{N}_i \cup i} \mathcal{L}_{ij} p_j$ (where $\mathcal{L}_{ij}$ is $(i,j)^{\text{th}}$ element of $\mathcal{L}$)
   - i $f_\gamma \leftarrow -k_2 g$
   - ii **if** $H > 0$, **then**: $f_\gamma \leftarrow f_\gamma - k_1 H p_i$
   - iii $u \leftarrow f_\alpha + f_\gamma$
   - iv Calculate $p_{\text{des}} \leftarrow p_i + T \cdot u$ (where T is the sampling time)

6: Pass p_{des} to the velocity tracking controller (100 Hz)
7: Repeat (go to step 2)

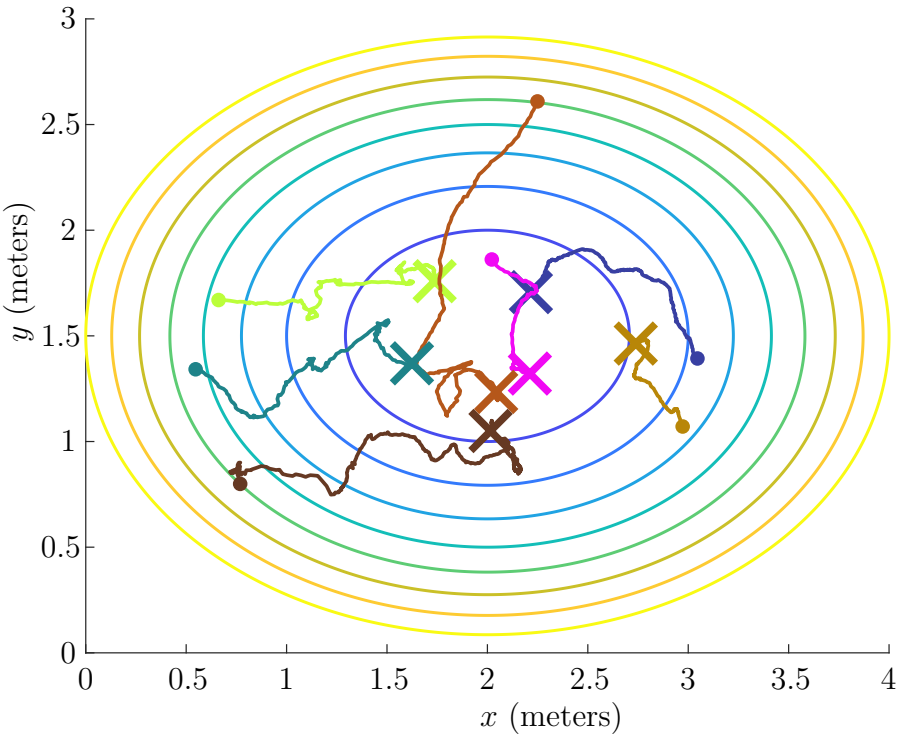

Figure 2.3: Experimental results: Trajectories of 7 agents for ψ_1 as defined in (2.11). The solid dot marker shows the initial position and the X marker shows the end position. https://www.tuhh.de/ics/institute/people/personal-pages/adwait-datar/source-seeking-experimental-videos.html

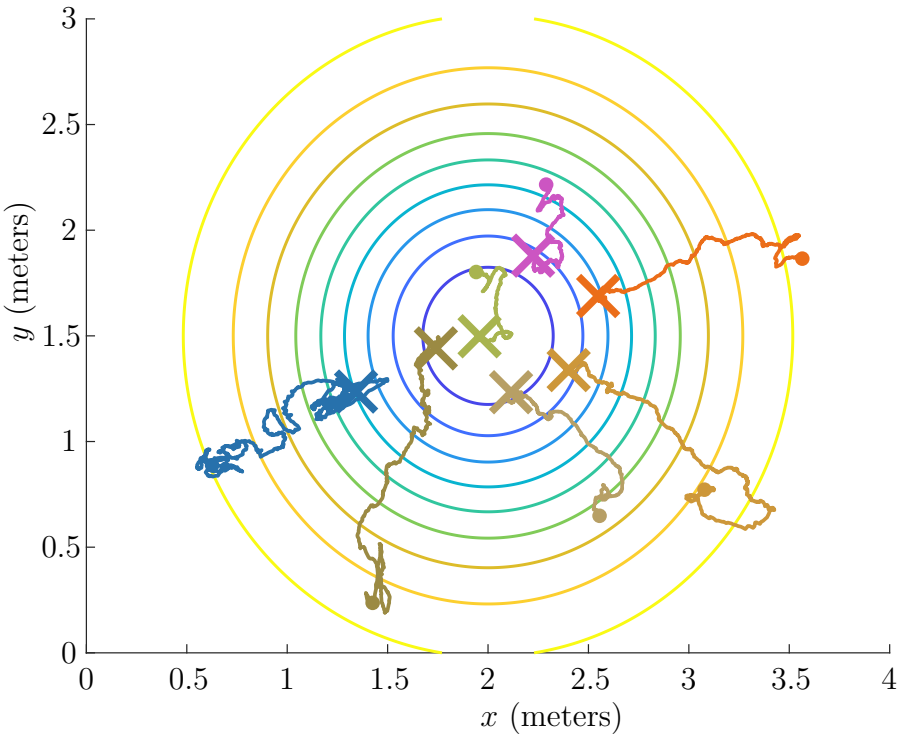

Figure 2.4: Experimental results: Trajectories of 7 agents for ψ_2 as defined in (2.11). The solid dot marker shows the initial position and the X marker shows the end position. https://www.tuhh.de/ics/institute/people/personal-pages/adwait-datar/source-seeking-experimental-videos.html

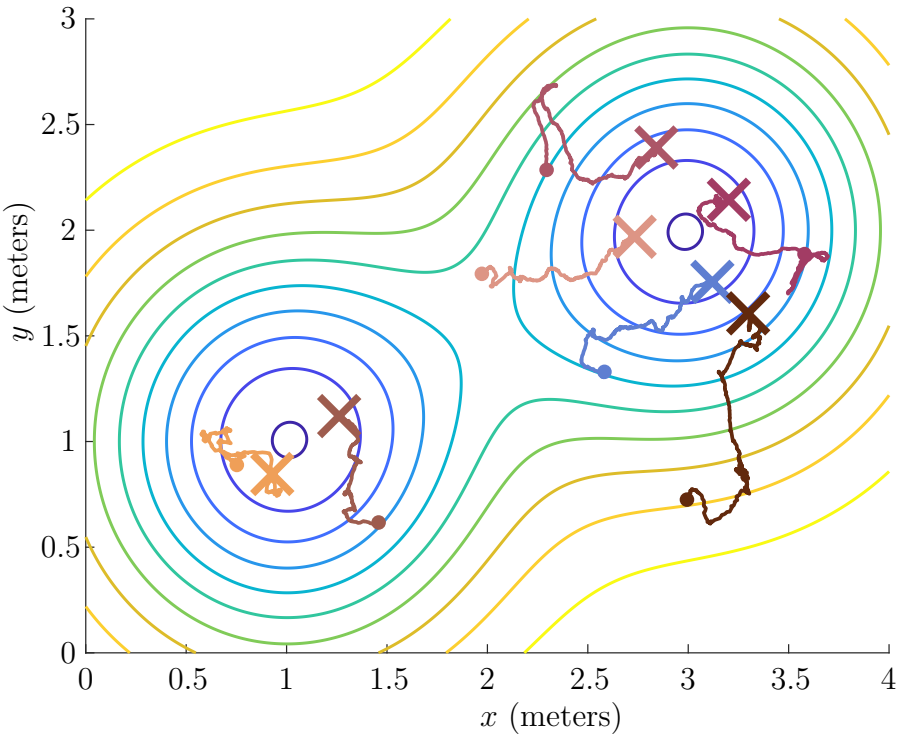

Figure 2.5: Experimental results: Trajectories of 7 agents for ψ_3 as defined in (2.11). The solid dot marker shows the initial position and the X marker shows the end position. https://www.tuhh.de/ics/institute/people/personal-pages/adwait-datar/source-seeking-experimental-videos.html

of 7 Crazyflie quadrotors for these fields. The solid dot marker shows the initial position and the X marker shows the end position. It can be seen that the agents locate the source in all cases. For ψ_3, both minima are located by two disconnected groups of agents based on their initial conditions. Note that interconnection graph between the agents for these experiments is state-dependent and therefore time-varying and not displayed in the above figures.

2.2 Extension to General Vehicle Models

The theoretical results so far assumed that the vehicles can be modeled as double integrators. Drawing motivation from successful experimental results with quadrotors, this section provides a theoretical analysis by explicitly including general vehicle models with local tracking controllers in the dynamics.

2.2.1 Problem Setup

It is assumed that a local tracking controller is designed such that the closed-loop system takes as input, the desired position q and the desired velocity p and outputs the position y and velocity v of the vehicle. This can be modeled by closed-loop non-linear dynamics of the form

$$\begin{aligned} \dot{x} &= f(x, \begin{bmatrix} q \\ p \end{bmatrix}), \qquad x(0) = x_0, \\ \begin{bmatrix} y \\ v \end{bmatrix} &= g(x) \end{aligned}$$

for suitable functions f and g. Let $G^{x_0}_{\text{veh}}$ denote the operator that models this closed-loop system and maps trajectories $\begin{bmatrix} q^T & p^T \end{bmatrix}^T$ into trajectories $\begin{bmatrix} y^T & v^T \end{bmatrix}^T$. The overall dynamics (with $k_1 = k_2 = 1$ for simplicity) can be represented as in Fig. 2.6 and are governed by

$$\begin{aligned} \dot{q} &= p, \\ \dot{p} &= -\nabla V(y) - (\mathcal{L}_{(d)}(y) + cI - \nabla^2 \Psi(y))v - \nabla \Psi(y), \\ \begin{bmatrix} y \\ v \end{bmatrix} &= G^{x_0}_{\text{veh}}(\begin{bmatrix} q \\ p \end{bmatrix}) \end{aligned} \tag{2.12}$$

with initial conditions $q(0)$ and $p(0)$. Observe that if $G^{x_0}_{\text{veh}}$ is an identity map, these dynamics reduce to dynamics (2.4) which have been analyzed in Theorem 2.1.

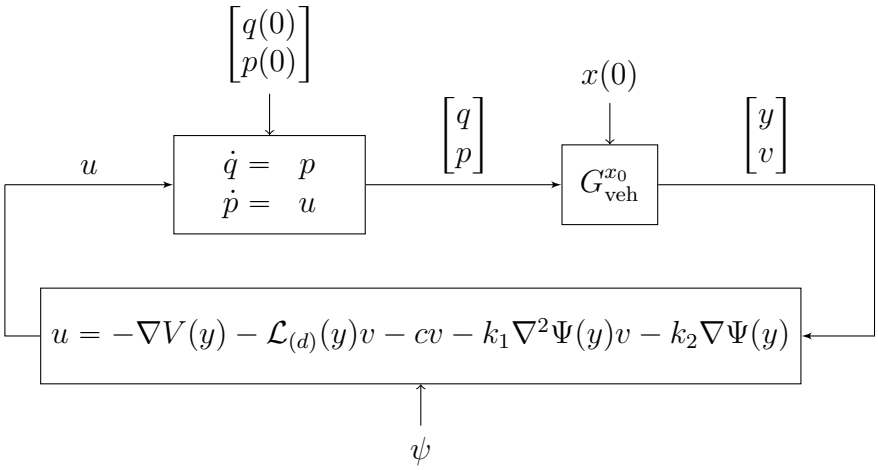

Figure 2.6: Control architecture with a general vehicle dynamics block represented by $G^{x_0}_{\text{veh}}$.

Problem 2.2. *Derive sufficient conditions independent of the network size N under which trajectories q, p, y and v generated by the dynamics* (2.12) *remain bounded for all $t \geqslant 0$ and asymptotically converge to an equilibrium of the dynamics.*

2.2.2 Analysis

The following assumptions on the external scalar field ψ, the interaction potential V and the state-dependent graph are required for the stability analysis presented thereafter.

Assumption 2.1. *The scalar field $\psi : \mathbb{R}^d \to \mathbb{R}$ is twice continuously differentiable, strictly convex, has a unique minimum at q_* and satisfies the Lipschitz condition*

$$||\nabla\psi(q_i) - \nabla\psi(q_j)|| \leqslant L_\psi||q_i - q_j|| \quad \forall q_i, q_j \in \mathbb{R}^d \tag{2.13}$$

with a non-negative constant L_ψ.

Assumption 2.2. *The flocking interaction potential $V : \mathbb{R}^{Nd} \to \mathbb{R}$ is continuously differentiable, has a uniform lower bound $V_{\min}$, i.e., $V(q) \geqslant V_{\min}$ $\forall q$ and satisfies the Lipschitz condition*

$$||\nabla V(q) - \nabla V(\tilde{q})|| \leqslant L_V||q - \tilde{q}|| \quad \forall q, \tilde{q} \in \mathbb{R}^{Nd} \tag{2.14}$$

with a non-negative constant L_V.

Assumption 2.3. *The state-dependent graph Laplacian $\mathcal{L}(y(t))$ is symmetric and uniformly bounded by L_λ for any feasible trajectory $y(t)$ under the dynamics* (2.12)*, i.e., $||\mathcal{L}(y(t))|| = \lambda_{\max}(\mathcal{L}(y(t))) \leqslant L_\lambda$ for all $t \geqslant 0$.*

Note that Assumption 2.1 implies $||\nabla\Psi(q) - \nabla\Psi(\tilde{q})|| \leqslant L_\psi||q - \tilde{q}||$ and $\nabla^2\Psi(q) \leqslant L_\psi$ for all $q, \tilde{q} \in \mathbb{R}^{Nd}$ and can be seen as a bound on the curvature of the field. Assumption 2.3 can be verified in practice by looking at the maximum number of possible neighbors (maximum degree $d_{\max}$) and bounding $\lambda_{\max}(\mathcal{L}(y(t))) \leqslant 2d_{\max}$.

Remark 2.1. *This chapter focuses on stability analysis under strictly convex fields ψ and non-convex interactions V. Performance analysis under convex interactions V of the form $(q-r)^T\mathcal{L}_{(d)}(q-r)$ and strongly convex fields ψ is deferred to Chapter 3, where a guaranteed exponential convergence rate can be verified with an LMI via ZF α-IQCs. A local version of the following result within the framework of IQCs is presented later in Section 2.3.*

Theorem 2.3 (Analysis for Problem 2.2)**.** *Let Assumptions 2.1, 2.2 and 2.3 hold. Further assume that a local tracking controller has been designed at each agent i to achieve a closed-loop $\mathcal{L}_2$ tracking performance described by*

$$\int_0^T \left(\frac{1}{\gamma_q^2}||q_i(t) - y_i(t)||^2 + \frac{1}{\gamma_p^2}||p_i(t) - v_i(t)||^2\right) dt \leqslant \int_0^T ||p_i(t)||^2 dt \tag{2.15}$$

for all $T \geqslant 0$ with $\gamma_p < 1$ and $c > \frac{1}{1-\gamma_p}\left((\gamma_q + \gamma_p)L_\psi + \gamma_q L_V + \gamma_p L_\lambda\right)$. Then, the dynamics (2.12) *are stable, i.e., the trajectories generated by these dynamics remain bounded for $t \geqslant 0$. Moreover, trajectories q and y converge asymptotically to the set $\mathcal{W} := \{q|\nabla V(q) + \nabla\Psi(q) = 0\}$ and trajectories p and v converge to* 0*.*

Proof. Let $W(y) = V(y) + \Psi(y)$ and $H(y) = \mathcal{L}_{(d)}(y) + cI + \nabla^2\Psi(y)$. The dynamics described in (2.12) can then be represented as

$$\begin{aligned} \dot{q} &= p, \\ \dot{p} &= -\nabla W(y) - H(y)v, \\ \begin{bmatrix} y \\ v \end{bmatrix} &= G_{\text{veh}}(\begin{bmatrix} q \\ p \end{bmatrix}). \end{aligned} \tag{2.16}$$

Let the local tracking error be defined by

$$\begin{aligned} e_q &= q - y, \\ e_p &= p - v. \end{aligned} \tag{2.17}$$

With these error variables,

$$\begin{aligned} \dot{q} &= p, \\ \dot{p} &= -\nabla W(q) - H(y)p + d, \end{aligned} \tag{2.18}$$

where

$$d = \nabla W(q) - \nabla W(q - e_q) + H(y)e_p. \tag{2.19}$$

Since

$$||e_q||^2 = ||q - y||^2 = \sum_{i=1}^{N} ||q_i - y_i||^2$$

and

$$||e_p||^2 = ||p - v||^2 = \sum_{i=1}^{N} ||p_i - v_i||^2,$$

(2.15) implies

$$\int_0^T \left(\frac{1}{\gamma_q^2} ||e_q(t)||^2 + \frac{1}{\gamma_p^2} ||e_p(t)||^2 \right) dt \leqslant \int_0^T ||p(t)||^2 dt. \tag{2.20}$$

Assumptions 2.1, 2.2 and 2.3 along with the triangle inequality can be used to obtain the following bounds on $||\nabla W(q) - \nabla W(q - e_q)||$ and $||He_p||$.

$$\begin{aligned} ||\nabla W(q) - \nabla W(q - e_q)|| &= ||\nabla V(q) - \nabla V(q - e_q) + \nabla \Psi(q) - \nabla \Psi(q - e_q)|| \\ &\leqslant ||\nabla V(q) - \nabla V(q - e_q)|| \\ &\qquad + ||\nabla \Psi(q) - \nabla \Psi(q - e_q)|| \\ &\leqslant L_V ||e_q|| + L_\psi ||e_q|| \\ &= (L_V + L_\psi)||e_q||. \\ ||H(y)e_p|| &= ||\mathcal{L}_{(d)}(y)e_p + \nabla^2 \Psi(y)e_p + ce_p|| \\ &\leqslant ||\mathcal{L}_{(d)}(y)e_p|| + ||\nabla^2 \Psi(y)e_p|| + c||e_p|| \\ &\leqslant (||\mathcal{L}(y)|| + L_\psi + c)||e_p|| \\ &\leqslant (L_\lambda + L_\psi + c)||e_p||. \end{aligned}$$

With $\kappa_1 = L_V + L_\psi$ and $\kappa_2 = L_\lambda + L_\psi + c$, $d(t)$ can be bounded for all $t \geqslant 0$ as $||d(t)|| \leqslant \kappa_1 ||e_q(t)|| + \kappa_2 ||e_p(t)||$ which implies $||d(t)||^2 \leqslant \kappa_1^2 ||e_q(t)||^2 + \kappa_2^2 ||e_p(t)||^2 + 2\kappa_1 \kappa_2 ||e_q(t)|| ||e_p(t)||$. Integrating both sides from 0 to T and

using (2.20) along with Cauchy-Schwartz inequality for $\mathcal{L}_2[0,T]$,

$$\begin{aligned}
\int_0^T ||d(t)||^2 dt &\leqslant \int_0^T \left(\kappa_1^2||e_q(t)||^2 + \kappa_2^2||e_p(t)||^2 + 2\kappa_1\kappa_2||e_q(t)|| \cdot ||e_p(t)||\right) dt \\
&\leqslant \int_0^T (\kappa_1^2\gamma_q^2 + \kappa_2^2\gamma_p^2)||p(t)||^2 dt + \int_0^T 2\kappa_1\kappa_2||e_q(t)|| \cdot ||e_p(t)|| dt \\
&\leqslant (\kappa_1^2\gamma_q^2 + \kappa_2^2\gamma_p^2) \int_0^T ||p(t)||^2 dt \\
&\qquad + 2\kappa_1\kappa_2 \sqrt{\int_0^T ||e_q(t)||^2 dt} \sqrt{\int_0^T ||e_p(t)||^2 dt} \\
&\leqslant (\kappa_1^2\gamma_q^2 + \kappa_2^2\gamma_p^2) \int_0^T ||p(t)||^2 dt \\
&\qquad + 2\kappa_1\kappa_2 \sqrt{\gamma_q^2 \int_0^T ||p(t)||^2 dt} \sqrt{\gamma_p^2 \int_0^T ||p(t)||^2 dt} \\
&\leqslant (\kappa_1\gamma_q + \kappa_2\gamma_p + 2\kappa_1\kappa_2\gamma_q\gamma_p) \int_0^T ||p(t)||^2 dt.
\end{aligned}$$

Therefore, $\int_0^T ||d(t)||^2 dt \leqslant (\kappa_1\gamma_q + \kappa_2\gamma_p)^2 \int_0^T ||p(t)||^2 dt$. Now, consider the energy function $E : \mathbb{R}_+ \to \mathbb{R}$ defined by

$$E(t) := W(q(t)) + \frac{1}{2} p(t)^T p(t) \tag{2.21}$$

Differentiating with respect to time (and suppressing the notation for showing the dependence on time), we get,

$$\begin{aligned}
\dot{E} &= \nabla W(q)^T p + \dot{p}^T p \\
&= \nabla W(q)^T p - \nabla W(q)^T p - p^T H(y) p + d^T p \\
&= -p^T \left(\mathcal{L}_{(d)}(y) + cI + \nabla^2 \Psi(y)\right) p + d^T p \\
&\leqslant -c||p||^2 + d^T p.
\end{aligned}$$

Integrating on both sides, and using Cauchy-Schwartz inequality for $\mathcal{L}_2[0,T]$,

the following holds $\forall T > 0$:

$$\begin{aligned} E(T) &\leqslant E(0) - c\int_0^T ||p(t)||^2 dt + \int_0^T d(t)^T p(t) dt \\ &\leqslant E(0) - c\int_0^T ||p(t)||^2 dt + \sqrt{\int_0^T ||d(t)||^2 dt}\sqrt{\int_0^T ||p(t)||^2 dt} \\ &\leqslant E(0) - c\int_0^T ||p(t)||^2 dt + (\kappa_1\gamma_q + \kappa_2\gamma_p)\int_0^T ||p(t)||^2 dt \\ &\leqslant E(0) - (c - (\kappa_1\gamma_q + \kappa_2\gamma_p))\int_0^T ||p(t)||^2 dt. \end{aligned}$$

Noting that $\gamma_p < 1$ and $c > \frac{1}{1-\gamma_p}\left((\gamma_q + \gamma_p)L_\psi + \gamma_q L_V + \gamma_p L_\lambda\right)$ implies $(c - (\kappa_1\gamma_q + \kappa_2\gamma_p)) > 0$, we get,

$$V_{\min} + \Psi(q(T)) \leqslant V(q(T)) + \Psi(q(T)) + \frac{1}{2}||p(T)||^2 = E(T) \leqslant E(0) \quad (2.22)$$

for all $T \geqslant 0$ and therefore, $\Psi(q(T)) \leqslant E(0) - V_{\min}$. Strict convexity of ψ implies that of Ψ and this, together with the existence of a minimizer implies that Ψ has bounded sub-level sets which implies that q stays bounded. Furthermore, since the inequality,

$$E(T) + (c - (\kappa_1\gamma_q + \kappa_2\gamma_p))\int_0^T ||p(t)||^2 dt \leqslant E(0)$$

holds for any $T \geqslant 0$, we get $\int_0^\infty ||p(t)||^2 dt < \infty$ which implies (using (2.20))

$$\int_0^\infty ||e_q(t)||^2 dt < \infty$$

and

$$\int_0^\infty ||e_p(t)||^2 dt < \infty.$$

Therefore, whenever smooth solutions (uniformly continuous) $q(t)$, $p(t)$, $y(t)$, $v(t)$ to the dynamics (2.12) exist, we have that $\lim_{t\to\infty} v(t) = \lim_{t\to\infty} p(t) = 0$ and $\lim_{t\to\infty} y(t) = \lim_{t\to\infty} q(t)$. Finally, due to an integral invariance principle [Byrnes and Martin, 1995], the trajectories q and y converge to the set $\mathcal{W}$ defined in the statement of Theorem 2.3. □

Remark 2.2. *Theorem 2.3 gives a qualitative understanding of the stability of flocking dynamics. Observe that when G_{veh} is the identity operator, γ_q*

and γ_p can be chosen arbitrarily small and Theorem 2.3 reduces to Theorem 2.1. This means that as γ_q and γ_p approach 0, i.e., as the local tracking performance improves, the condition on the damping constant reduces to $c > 0$. In other words, the poorer the local tracking performance, the higher the damping should be and the slower the reference trajectories p and q should evolve to accommodate for poor tracking.

Remark 2.3. *Note that Theorem 2.3 does not consider internal dynamics of the plant G_{veh} and asks only for an input-output performance prescribed by* (2.15).

2.2.3 Simulation Studies

Theorem 2.3 prompts for the following heuristic strategy for designing a distributed controller for possibly non-linear vehicles in order to address the source-seeking problem.

- Start by designing a local tracking controller for different vehicle models with any method of choice such that the tracking performance (ideally measured by an induced $\mathcal{L}_2$ norm) is optimized.
- Design a suitable interaction potential satisfying Assumption 2.2 (see e.g. [Olfati-Saber, 2006] which provides an interaction potential satisfying the assumption).
- Theorem 2.3 suggests that if the tracking performance in the sense of the induced $\mathcal{L}_2$ norm is good enough and the damping coefficient c is chosen large enough, asymptotic stability is guaranteed for external fields satisfying Assumption 2.1. Starting from a large value, c can thus be tuned to obtain reasonable performance.

This heuristic strategy is next demonstrated on a non-linear, non-holonomic underwater robot model of the *HippoCampus* [Hackbarth et al., 2015]. Details on the vehicle model and the design of local tracking controller are deferred to Appendix B. In what follows, it is assumed that a local tracking controller has been designed and the closed-loop vehicle dynamics are now tested in a source-seeking scenario with the architecture described in Fig. 2.6. Consider three underwater robots embedded in a quadratic field given by

$$\psi_{\text{quadratic}}(y) = \frac{1}{2}||(y-\mu)||^2, \tag{2.23}$$

where μ is the minimizer (source). Furthermore, consider the inter-agent interaction potential typically found in the literature on distance-based control

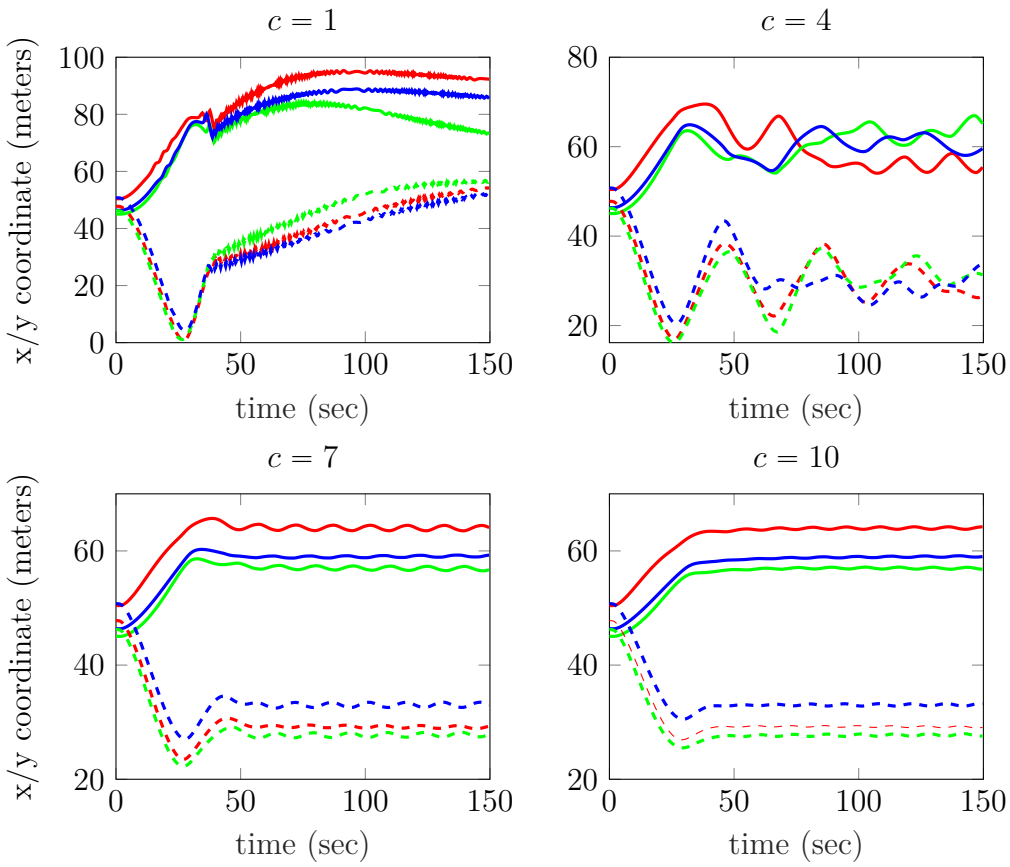

Figure 2.7: Three *HippoCampus* agents under quadratic interaction V_f flocking towards the source of a quadratic external field $\psi_{\text{quadratic}}$ (solid lines: x-coordinate and dashed lines: y-coordinate) for different values of c.

[Oh et al., 2015], [Krick et al., 2008], [Dörfler and Francis, 2009]) be described by

$$V_f(y) = \sum_{(i,j)} \frac{1}{2}(||y_i - y_j||_\sigma - d)^2, \tag{2.24}$$

where the sigma-norm is a function defined in [Olfati-Saber, 2006] by $||y||_\sigma = \sqrt{1 + ||y||^2} - 1$ and can be interpreted as a smoothed differentiable version of the usual euclidean 2-norm[1]. Simulation trajectories with different values of c are shown in Fig. 2.7 shows. As can be seen from Fig. 2.7 the trajectories converge to an equilibrium if c is large enough. Note that although Theorem 2.3 cannot be readily applied since the assumptions cannot be a priori verified, the simulation results agree qualitatively with the theoretical result in

[1]Note that this is not a valid norm.

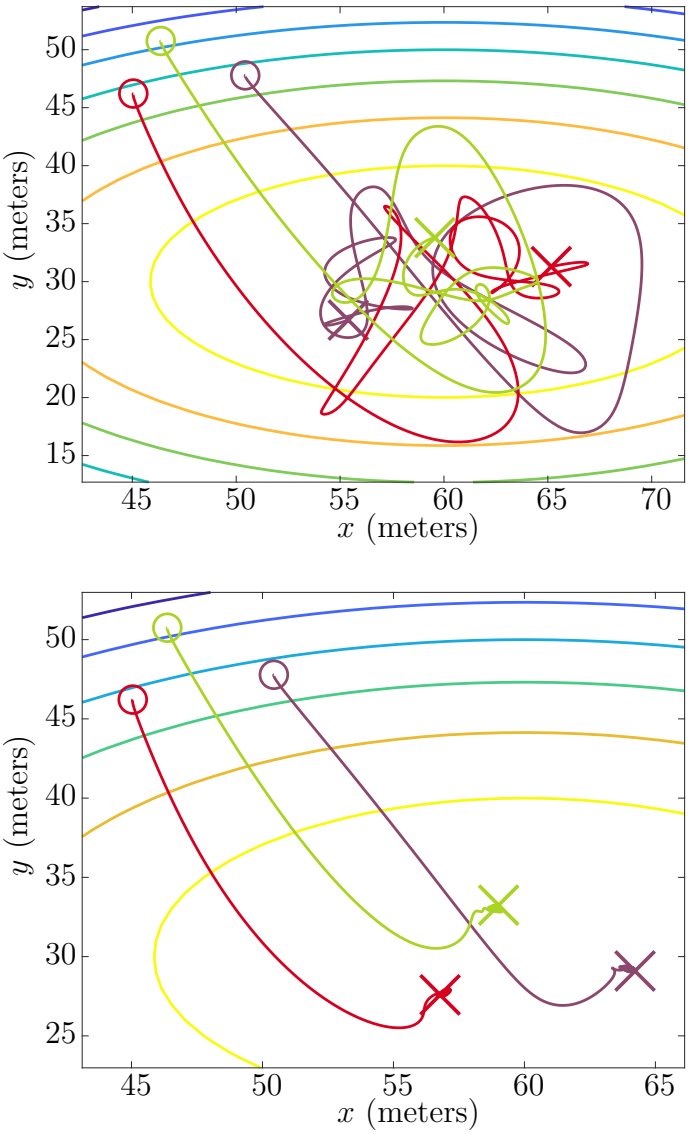

Figure 2.8: Flocking trajectories for $c = 4$ (top) and $c = 10$ (bottom) with 3 *HippoCampus* agents under quadratic interaction V_f flocking towards the source of a quadratic external field $\psi_{\text{quadratic}}$. The hollow circle marker shows the initial position and the X marker shows the end position (time= 150 sec).

the sense that if c is large enough, the dynamics are asymptotically stable. Figure 2.8 shows the trajectories and the contour lines of the external scalar field for two different values of c.

The experiment is now repeated with the same interaction potential but

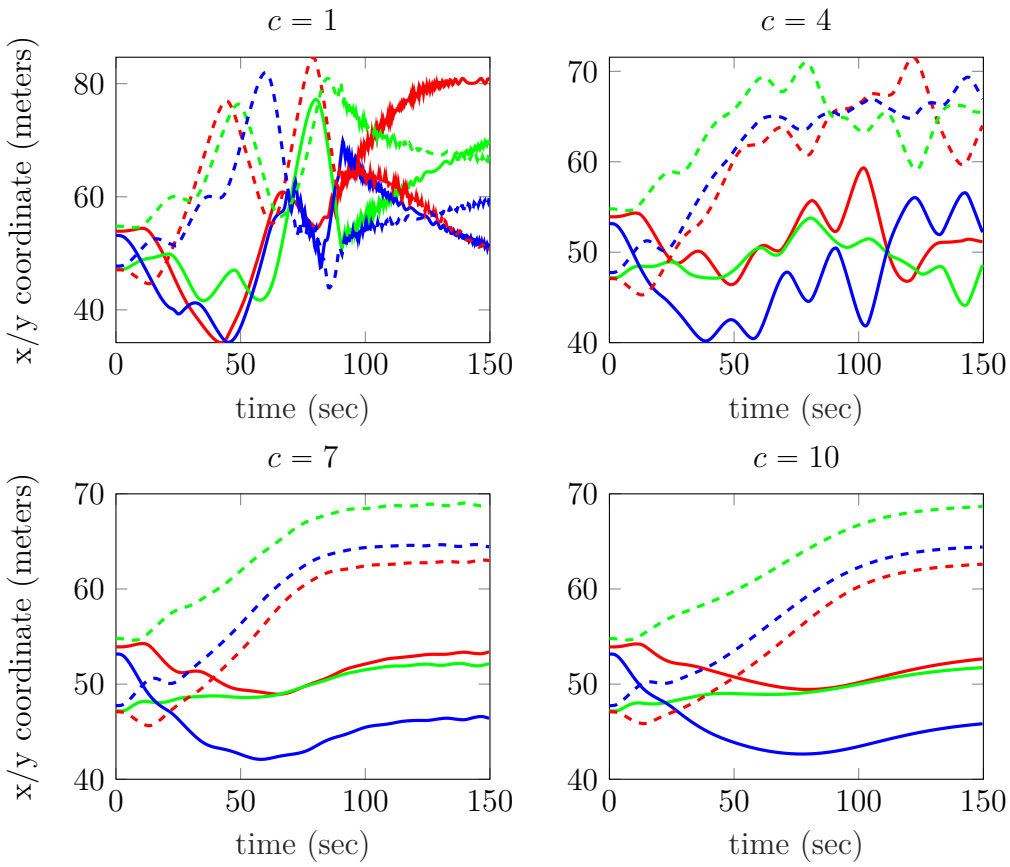

Figure 2.9: Three *HippoCampus* agents under quadratic interaction V_f flocking towards the source of an external field ψ_{exp} (solid lines: x-coordinate and dashed lines: y-coordinate) for different values of c.

an external field which is a sum of multivariate Gaussian fields given by

$$\psi_{\text{exp}}(y) = -50 \sum_{i=1}^{5} e^{-5||(y-\mu_i)||^2}, \tag{2.25}$$

where μ_i are the minimizers/centers of individual fields that are added together. Figure 2.9 shows simulation trajectories with different values of c.

As can be seen from Fig. 2.9, the trajectories for $c = 1$ and $c = 4$ do not seem to converge, whereas with $c = 7$ or higher, the trajectories converge to an equilibrium. Note that although Theorem 2.3 is not applicable here since the external field is even non-convex, the simulation results agree qualitatively with the theoretical result in the sense that if c is large enough, the dynamics are asymptotically stable. This is because, global convexity is not

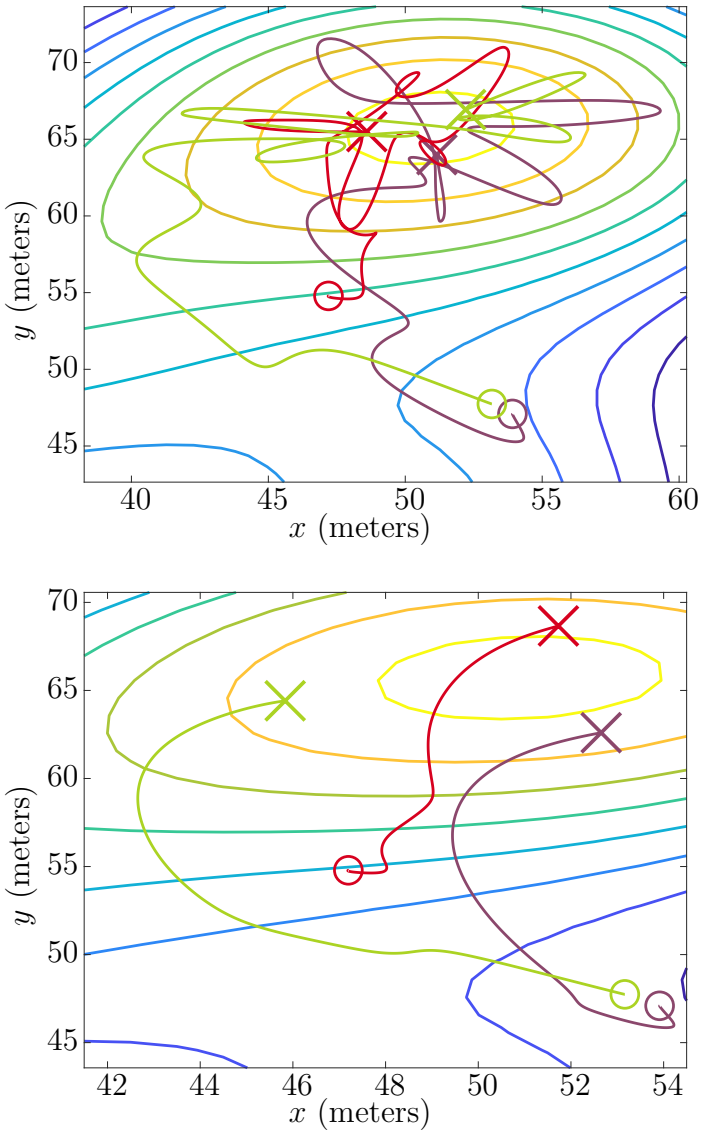

Figure 2.10: Flocking trajectories for $c = 4$ (top) and $c = 10$ (bottom) with 3 *HippoCampus* agents under quadratic interaction V_f flocking towards the source of an external field ψ_{exp}. The hollow circle marker shows the initial position and the X marker shows the end position (time=150 sec).

a critical assumption when showing asymptotic stability and this assumption is removed later in Theorem 2.4. Figure 2.10 shows the trajectories and the contour lines of the external scalar field for two different values of c. Finally, repeating the above simulation with the interaction potential proposed in

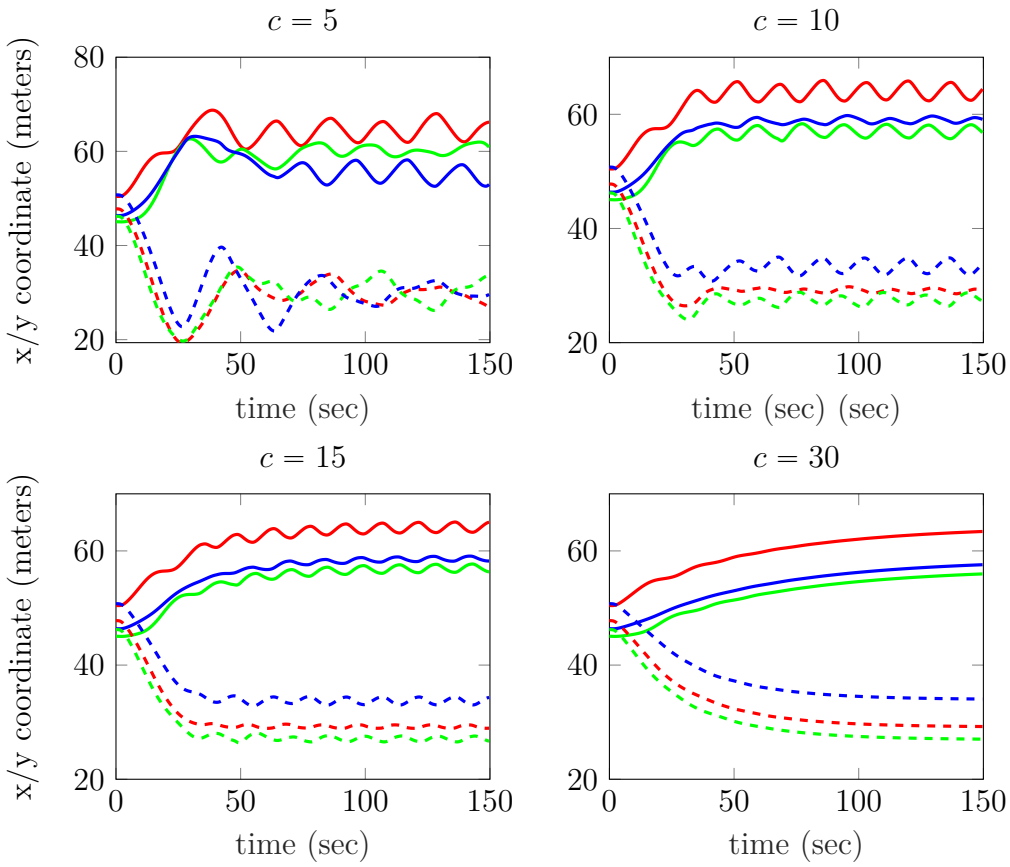

Figure 2.11: Three *HippoCampus* agents flocking with Olfati-Saber interaction field under external quadratic field $\psi_{\text{quadratic}}$ (solid lines: x-coordinate and dashed lines: y-coordinate) for different values of c.

[Olfati-Saber, 2006] produces Fig. 2.11 and leads to the same qualitative observations and conclusions as before.

More systematic controller synthesis procedures are possible by using techniques from LPV systems theory. For example, a controller minimizing the induced $\mathcal{L}_2$ norm can be synthesized with LMIs which also provides an estimate of γ_q and γ_p. An upper-bound on L_λ can be obtained using an estimate on the maximum-degree of agents as $\lambda_{\max}(\mathcal{L}(y(t))) \leqslant 2d_{\max}$. These estimates can go into the choice for c based on Theorem 2.3 to produce an *a priori* guarantee on asymptotic stability for all interaction fields and external fields satisfying Assumptions 2.1 and 2.2, respectively. Results along these lines are reported in [Attallah et al., 2020] and [Attallah and Werner, 2022].

2.3 Local Analysis with IQCs

As a prelude to the Chapter 3, the framework of IQCs is next deployed for the stability analysis of flocking dynamics to extend the earlier results in several ways such that the results of this section can be seen as a generalization of the results from the last section. To elaborate on this, Theorem 2.3 can be seen as an application of the incremental small-gain theorem [Scherer and Weiland, 2000] and the analysis of this section can be seen as a generalization in the same sense as IQC analysis can be seen as a generalization of the small-gain theorem. Concretely, (2.13) from Assumption 2.1 (for instance) can be equivalently written as

$$\begin{bmatrix} q_i - q_j \\ \nabla\psi(q_i) - \nabla\psi(q_j) \end{bmatrix}^T \begin{bmatrix} L_\psi^2 & 0 \\ 0 & -I \end{bmatrix} \begin{bmatrix} q_i - q_j \\ \nabla\psi(q_i) - \nabla\psi(q_j) \end{bmatrix} \geqslant 0 \quad \forall q_i, q_j \in \mathbb{R}^d.$$

The upcoming analysis replaces the central matrix with a general matrix M that encodes the assumption. Furthermore, instead of requesting an a priori induced $\mathcal{L}_2$ gain for the local controllers as in Theorem 2.3, an LMI that is independent of the size of the network N is given that verifies stability. Finally, the result is presented as a local result such that the above condition is required to hold only on a set $\mathcal{S} \subseteq \mathbb{R}^d$.

That being said, in order to simplify the discussion, the vehicle agents are assumed to be governed by LTI dynamics and each agent is assumed to share (by sensing or communication) only the positions of neighboring vehicles. Extension to LPV vehicle dynamics is possible along the same lines as in Section 3.2.3 and extensions to include velocity alignment are also possible in a rather straightforward manner.

2.3.1 Problem Setup

Assume that a local tracking controller has been designed and the closed-loop dynamics of the i^{th} vehicle agent with desired reference position $q_i(t)$, desired reference velocity $p_i(t)$ can be described for a given initial condition $x_i(0)$ by

$$\begin{aligned} \dot{x}_i(t) &= Ax_i(t) + \begin{bmatrix} B_q & B_p \end{bmatrix} \begin{bmatrix} q_i(t) \\ p_i(t) \end{bmatrix}, \\ y_i(t) &= Cx_i(t), \end{aligned} \tag{2.26}$$

where $y_i(t)$ is the position output of agent i. These closed-loop vehicle dynamics are augmented, as shown in Fig. 2.12, by the second-order dynamics,

$$\begin{aligned} \dot{q}_i(t) &= p_i(t), \\ \dot{p}_i(t) &= -k_d \cdot p_i(t) - k_p \cdot u_i(t), \end{aligned} \tag{2.27}$$

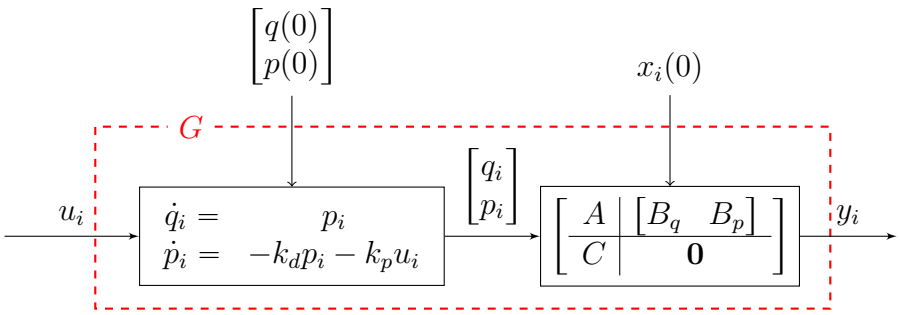

Figure 2.12: Local control architecture on agent i.

where $u_i(t) \in \mathbb{R}^d$ denotes external input, $q_i(0) = Cx_i(0)$, $p_i(0) = 0$ such that $q_i(t)$ and $p_i(t)$ are fed as inputs to dynamics (2.26).

Remark 2.4. *The main motivation behind introducing these second order dynamics is two fold. On one hand, these dynamics can be thought of as a crude approximation of the vehicle model that provides smooth trajectories to the higher order complex vehicle dynamics. Intuitively, if the vehicle is able to track these generated trajectories well enough, i.e., $y_i \approx q_i$, then from the simple dissipativity analysis for double integrator agents that was presented earlier, one can expect a stable behavior. This argument is made rigorous in this section and an LMI is derived as a sufficient condition for stability. Secondly, these augmented dynamics provide us with simple interpretable tuning knobs, specifically the damping co-efficient k_d, which can be used to slow-down or speed up the vehicle dynamics.*

The overall dynamics with state $\eta_i = \begin{bmatrix} x_i^T & q_i^T & p_i^T \end{bmatrix}^T$ and suitable initial condition $\eta_i(0)$ can be represented by

$$\begin{aligned} \dot{\eta}_i(t) &= A_G \eta_i(t) + B_G u_i(t), \\ y_i(t) &= C_G \eta_i(t), \end{aligned} \tag{2.28}$$

where

$$\left[\begin{array}{c|c} A_G & B_G \\ \hline C_G & D_G \end{array}\right] = \left[\begin{array}{ccc|c} A & B_q & B_p & \mathbf{0} \\ \mathbf{0} & \mathbf{0} & I_d & \mathbf{0} \\ \mathbf{0} & \mathbf{0} & -k_d I_d & -k_p I_d \\ \hline C & \mathbf{0} & \mathbf{0} & \mathbf{0} \end{array}\right].$$

Let $V : \mathbb{R}^{Nd} \to \mathbb{R}$ denote the interaction potential (typically non-convex) among agents (such as the one introduced in [Olfati-Saber, 2006]). It was so-far assumed that all agents have access to the gradient of the scalar field ψ

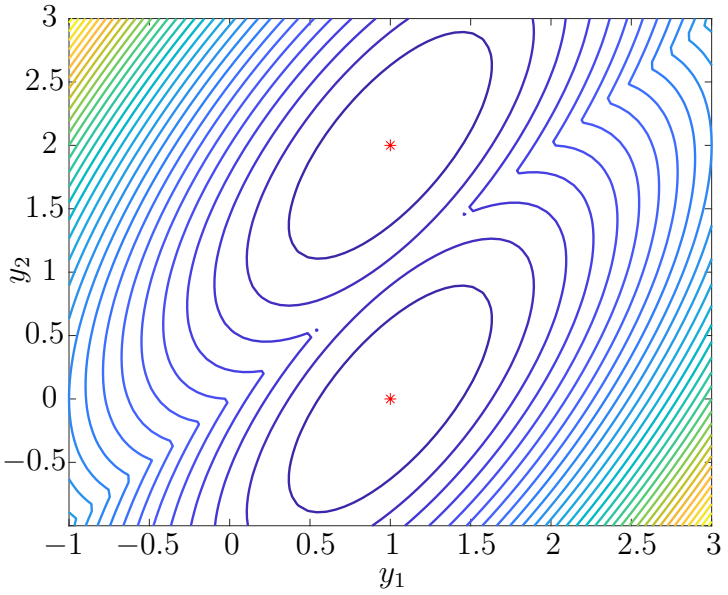

Figure 2.13: Contour plot of an example $f_{nc}(y) = \frac{1}{2}(|y_1 - y_2| - 1)^2 + \frac{1}{2}(y_1 - 1)^2$ with $N = 2$ and $d = 1$, where minimizers $[1\ 0]^T$ and $[1\ 2]^T$ are denoted by red stars.

evaluated at their respective locations. This assumption is now relaxed. Let $\mathcal{V}_l$ denote the subset of agents (called informed agents) that have access to the gradient at their respective positions. Define a function $f_{nc} : \mathbb{R}^{Nd} \to \mathbb{R}$ as follows[2].

Definition 2.1. *For a given interaction potential V, the set of informed agents $\mathcal{V}_l$ and a scalar field ψ, define a function $f_{nc} : \mathbb{R}^{Nd} \to \mathbb{R}$ by*

$$f_{nc}(y) = V(y) + \sum_{i \in \mathcal{V}_l} \psi(y_i). \tag{2.29}$$

A contour plot of an example $f_{nc}(y) = \frac{1}{2}(|y_1 - y_2| - 1)^2 + \frac{1}{2}(y_1 - 1)^2$ with $N = 2$, $d = 1$ is depicted in Fig. 2.13. Note that since agent 1 is the informed agent, the desired arrangements which correspond to the minima of f_{nc} are $y = [1 \quad 0]^T$ and $y = [1 \quad 2]^T$, i.e., the informed agent at the source and the agent 2 at a distance of 1 unit from the informed agent in either direction.

Using the notation described in Section 1.5.4, flocking dynamics with gradient-based forcing terms on the informed agents with initial condition

[2]subscript stands for non-convex in contrast to a convex function f_c defined later in Chapter 3

$\eta(0)$ can be described by

$$\begin{aligned} \dot{\eta}(t) &= \hat{A}_G \eta(t) + \hat{B}_G u(t), \\ y(t) &= \hat{C}_G \eta(t), \\ u(t) &= \nabla f_{nc}(y(t)). \end{aligned} \tag{2.30}$$

Problem 2.3. *Derive sufficient conditions independent of the network size N under which the state trajectories generated by the dynamics* (2.30) *remain bounded for all $t \geqslant 0$ and y converges asymptotically to a local minimizer of f_{nc}.*

2.3.2 Analysis

Before presenting the main analysis results, the dynamics described in (2.30) are transformed into a suitable form in two steps. First, an additional input and output channel is introduced to represent the dynamics (2.30) in an equivalent form as

$$\begin{aligned} \begin{bmatrix} \dot{\eta}(t) \\ q(t) \\ q(t) - y(t) \end{bmatrix} &= \begin{bmatrix} \hat{A}_G & \hat{B}_G & -\hat{B}_G \\ \hat{C}_1 & \mathbf{0} & \mathbf{0} \\ \hat{C}_2 & \mathbf{0} & \mathbf{0} \end{bmatrix} \begin{bmatrix} \eta(t) \\ d_1(t) \\ d_2(t) \end{bmatrix}, \\ d_1(t) &= \nabla f_{nc}(q(t)), \\ d_2(t) &= \nabla f_{nc}(q(t)) - \nabla f_{nc}(y(t)), \end{aligned} \tag{2.31}$$

where $C_1 = \begin{bmatrix} \mathbf{0} & I & \mathbf{0} \end{bmatrix}$ and $C_2 = \begin{bmatrix} -C & I & \mathbf{0} \end{bmatrix}$. As the second step, the the state vector $\eta = [\eta_1^T \ \cdots \ \eta_N^T]^T = [x_1^T \ q_1^T \ p_1^T \ \cdots x_N^T \ q_N^T \ p_N^T]^T$ is permuted to obtain dynamics in the new variable $\bar{\eta} = [x_1^T \ \cdots \ x_N^T \ q_1^T \ \cdots \ q_N^T \ p_1^T \ \cdots \ p_N^T]^T = [x^T \ q^T \ p^T]^T$ via a similarity transformation to obtain

$$\begin{aligned} \begin{bmatrix} \dot{\bar{\eta}}(t) \\ q(t) \\ q(t) - y(t) \end{bmatrix} &= \begin{bmatrix} \mathcal{A}_G & \mathcal{B}_G & -\mathcal{B}_G \\ \mathcal{C}_{G1} & \mathbf{0} & \mathbf{0} \\ \mathcal{C}_{G2} & \mathbf{0} & \mathbf{0} \end{bmatrix} \begin{bmatrix} \bar{\eta}(t) \\ d_1(t) \\ d_2(t) \end{bmatrix}, \\ d_1(t) &= \nabla f_{nc}(q(t)), \\ d_2(t) &= \nabla f_{nc}(q(t)) - \nabla f_{nc}(y(t)), \end{aligned} \tag{2.32}$$

where

$$\left[\begin{array}{c|cc} \mathcal{A}_G & \mathcal{B}_G & -\mathcal{B}_G \\ \hline \mathcal{C}_{G1} & \mathbf{0} & \mathbf{0} \\ \mathcal{C}_{G2} & \mathbf{0} & \mathbf{0} \end{array}\right] = \left[\begin{array}{ccc|cc} \hat{A} & \hat{B}_q & \hat{B}_p & \mathbf{0} & \mathbf{0} \\ \mathbf{0} & \mathbf{0} & I_{Nd} & \mathbf{0} & \mathbf{0} \\ \mathbf{0} & \mathbf{0} & -k_d I_{Nd} & -k_p I_{Nd} & k_p I_{Nd} \\ \hline \mathbf{0} & I_{Nd} & \mathbf{0} & \mathbf{0} & \mathbf{0} \\ -\hat{C} & I_{Nd} & \mathbf{0} & \mathbf{0} & \mathbf{0} \end{array}\right].$$

Assumption 2.4. *The function $f_{nc} : \mathbb{R}^{Nd} \to \mathbb{R}$ and an open set $\mathcal{S}$ containing a local minimizer y_* of f_{nc} satisfy the following conditions:*

1) f_{nc} is differentiable on $\mathcal{S}$.

2) $y_* \in \mathcal{S}$ is a local minimizer of f_{nc} on $\mathcal{S}$, i.e., $\nabla f_{nc}(y_*) = 0$ and

$$f_{nc}(y) \geqslant f_{nc}(y_*) = f_{\min} \quad \forall y \in \mathcal{S}.$$

3) For a given symmetric matrix M_{10}, and for all $y \in \mathcal{S}$,

$$\begin{bmatrix} y - y_* \\ \nabla f_{nc}(y) \end{bmatrix}^T (M_{10} \otimes I_{Nd}) \begin{bmatrix} y - y_* \\ \nabla f_{nc}(y) \end{bmatrix} \geqslant 0.$$

4) For a given symmetric matrix M_{20} and for all $x, y \in \mathcal{S}$,

$$\begin{bmatrix} x - y \\ \nabla f_{nc}(x) - \nabla f_{nc}(y) \end{bmatrix}^T (M_{20} \otimes I_{Nd}) \begin{bmatrix} x - y \\ \nabla f_{nc}(x) - \nabla f_{nc}(y) \end{bmatrix} \geqslant 0.$$

5) There exist constants c_1 and c_2 such that

$$\mathcal{S}_0 = \{y + e | (f_{nc}(y) - f_{\min}) \leqslant c_1, ||e||^2 \leqslant c_2\}$$

is bounded and contained in $\mathcal{S}$.

Remark 2.5. *The knowledge about f_{nc} needs to be captured via a suitable selection of matrices M_{10} and M_{20} in Assumption 2.4 items 3) and 4). See [Fazlyab et al., 2018, Section 6.2] for a few examples. If global properties of f_{nc} are known, one can set $\mathcal{S} = \mathbb{R}^{Nd}$. Since this section attempts to provide a local result, Assumption 2.4 item 5) is required to ensure an invariance property for set $\mathcal{S}$ such that trajectories do not exit this set to regions of $\mathbb{R}^{Nd}$ where properties of f_{nc} are not known.*

An additional assumption on the vehicle dynamics is made which states that the local tracking controller is stabilizing and has zero steady state error for step position references.

Assumption 2.5. *The vehicle dynamics* (2.26) *are such that every eigenvalue of the matrix A has strictly negative real part and $-CA^{-1}B_q = I$.*

For given matrices A, B_q and symmetric matrix variables R and Q, construct $\mathcal{X}_0$ with a block 3×3 partition as

$$\mathcal{X}_0 = R + \begin{bmatrix} I \\ B_q^T A^{-T} \\ \mathbf{0} \end{bmatrix} Q \begin{bmatrix} I & A^{-1}B_q & \mathbf{0} \end{bmatrix} + \begin{bmatrix} \mathbf{0} & \mathbf{0} & \mathbf{0} \\ \mathbf{0} & \mathbf{0} & \mathbf{0} \\ \mathbf{0} & \mathbf{0} & I_d \end{bmatrix} = \begin{bmatrix} \mathcal{X}_{11} & \mathcal{X}_{12} & \mathcal{X}_{13} \\ \mathcal{X}_{21} & \mathcal{X}_{22} & \mathcal{X}_{23} \\ \mathcal{X}_{31} & \mathcal{X}_{32} & \mathcal{X}_{33} \end{bmatrix}.$$

Now, let $x_* = -A^{-1}B_q y_*$, $q_* = y_*$, $p_* = 0$ and define the storage function

$$V_s(x,q,p) = (*)\begin{bmatrix} \hat{\mathcal{X}}_{11} & \hat{\mathcal{X}}_{12} & \hat{\mathcal{X}}_{13} \\ \hat{\mathcal{X}}_{21} & \hat{\mathcal{X}}_{22} & \hat{\mathcal{X}}_{23} \\ \hat{\mathcal{X}}_{31} & \hat{\mathcal{X}}_{32} & \hat{\mathcal{X}}_{33} \end{bmatrix}\begin{bmatrix} x - x_* \\ q - q_* \\ p - p_* \end{bmatrix} + 2\mu(f_{nc}(q) - f_{\min}), \quad (2.33)$$

Finally, let

$$\left[\begin{array}{c|c} \mathcal{A}_0 & \mathcal{B}_0 \\ \hline \mathcal{C}_{10} & \mathcal{D}_{10} \\ \mathcal{C}_{20} & \mathcal{D}_{20} \end{array}\right] = \left[\begin{array}{c|cc} A_G & B_G & -B_G \\ \hline C_1 & \mathbf{0} & \mathbf{0} \\ \mathbf{0} & I & \mathbf{0} \\ C_2 & \mathbf{0} & \mathbf{0} \\ \mathbf{0} & \mathbf{0} & I \end{array}\right]. \quad (2.34)$$

The analysis is based on the following chain of arguments. A non-negative energy function is defined based on the storage function as $E(t) := V_s(x(t), q(t), p(t))$ and it is shown that if this energy is bounded below some prescribed value, the state is bounded and the output belongs to the subset $\mathcal{S}_0$ of $\mathcal{S}$. An LMI is then derived which implies that if the output is in the set $\mathcal{S}$, the energy function is non-increasing. If the initial conditions are such that the initial energy is small enough and initial output starts in $\mathcal{S}_0$, a forward invariance of set $\mathcal{S}_0$ and thus boundedness of state and output trajectories is established. The convergence of trajectories is then implied with the help of the LaSalle's invariance principle. This is made precise in the following theorem and it's proof.

Theorem 2.4 (Analysis for Problem 2.3)**.** *Let $f_{nc} : \mathbb{R}^{Nd} \to \mathbb{R}$ and an open set $\mathcal{S} \subseteq \mathbb{R}^{Nd}$ satisfy Assumption 2.4 and let the vehicle dynamics* (2.26) *satisfy Assumption 2.5. If there exist $R \succeq 0$, $Q \succ 0$, $\mu > 0$, $\lambda_1 \geqslant 0$, $\lambda_2 \geqslant 0$ and $\varepsilon > 0$ such that*

$$\mathcal{Z} = \begin{bmatrix} \mathcal{A}_0^T\mathcal{X}_0 + \mathcal{X}_0\mathcal{A}_0 & \mathcal{X}_0\mathcal{B}_0 \\ \mathcal{B}_0^T\mathcal{X}_0 & \mathbf{0} \end{bmatrix} + \begin{bmatrix} \mathbf{0} & \mathbf{0} & \mathbf{0} & \mathbf{0} & \mathbf{0} \\ \mathbf{0} & \mathbf{0} & \mathbf{0} & \mathbf{0} & \mathbf{0} \\ \mathbf{0} & \mathbf{0} & \varepsilon I_d & \mu I_d & \mathbf{0} \\ \mathbf{0} & \mathbf{0} & \mu I_d & \mathbf{0} & \mathbf{0} \\ \mathbf{0} & \mathbf{0} & \mathbf{0} & \mathbf{0} & \mathbf{0} \end{bmatrix}$$
$$+ \sum_{i=1}^{2}(*)(\lambda_i M_{i0} \otimes I_d)\begin{bmatrix} \mathcal{C}_{i0} & \mathcal{D}_{i0} \end{bmatrix} \preceq 0 \quad (2.35)$$

and if the initial conditions x_0, q_0, p_0 are such that

$$V_s(x_0, q_0, p_0) \leqslant \min\{2c_1\mu, \frac{c_2\lambda_{\min}(Q)}{||C||^2}\}, \quad (2.36)$$

where c_1 and c_2 are constants involved in Assumption 2.4 item 5), then the state trajectory η generated by the dynamics (2.30) *remains bounded for all $t \geqslant 0$ and $y(t)$ converges to the set $\{y_* \in \mathcal{S} | \nabla f_{nc}(y_*) = 0\}$.*

Proof. With V_s as defined in (2.33), define a function $E : \mathbb{R} \to \mathbb{R}$ as

$$\begin{aligned} E(t) &= V_s(x(t), q(t), p(t)) \\ &\geqslant (x(t) + \hat{A}^{-1}\hat{B}_q q(t))^T \hat{Q}(x(t) + \hat{A}^{-1}\hat{B}_q q(t)) + 2\mu(f_{nc}(q(t)) - f_{\min}). \end{aligned}$$

Note that if $E(t) \leqslant V_s(x_0, q_0, p_0)$, then

$$\begin{aligned} f_{nc}(q(t)) - f_{\min} &\leqslant \frac{V_s(x_0, q_0, p_0)}{2\mu} \leqslant c_1 \text{ and} \\ ||y(t) - q(t)||^2 &= ||\hat{C}(x(t) + \hat{A}^{-1}\hat{B}_q q(t))||^2 \\ &\leqslant ||C||^2 \cdot ||x(t) + \hat{A}^{-1}\hat{B}_q q(t)||^2 \\ &\leqslant \frac{||C||^2 V_s(x_0, q_0, p_0)}{\lambda_{\min}(Q)} \leqslant c_2. \end{aligned} \tag{2.37}$$

This together with the fact that $\mathcal{S}_0$ is bounded and contained in $\mathcal{S}$ (Assumption 2.4 item 5)) implies that $q(t), y(t)$ are bounded and contained in $\mathcal{S}$ if $E(t) \leqslant V_s(x_0, q_0, p_0)$.

Now, let

$$\left[\begin{array}{c|c} \mathcal{A} & \mathcal{B} \\ \hline \mathcal{C}_1 & \mathcal{D}_1 \\ \mathcal{C}_2 & \mathcal{D}_2 \end{array}\right] = \left[\begin{array}{c|cc} \mathcal{A}_G & \mathcal{B}_G & -\mathcal{B}_G \\ \hline \mathcal{C}_{G1} & \mathbf{0} & \mathbf{0} \\ \mathbf{0} & I_{Nd} & \mathbf{0} \\ \mathcal{C}_{G2} & \mathbf{0} & \mathbf{0} \\ \mathbf{0} & \mathbf{0} & I_{Nd} \end{array}\right].$$

Using the structure of the mutipliers $(M_{10} \otimes I_{Nd})$ and $(M_{20} \otimes I_{Nd})$, it can be shown that if there exist $R \succeq 0$, $Q \succ 0$, $\mu > 0$, $\lambda_1 \geqslant 0$, $\lambda_2 \geqslant 0$ such that $\mathcal{Z}$ defined in (2.35) is negative semi-definite, then

$$\mathcal{X} = \begin{bmatrix} \hat{\mathcal{X}}_{11} & \hat{\mathcal{X}}_{12} & \hat{\mathcal{X}}_{13} \\ \hat{\mathcal{X}}_{21} & \hat{\mathcal{X}}_{22} & \hat{\mathcal{X}}_{23} \\ \hat{\mathcal{X}}_{31} & \hat{\mathcal{X}}_{32} & \hat{\mathcal{X}}_{33} \end{bmatrix}$$

is positive semi-definite and implies

$$\begin{aligned} \mathcal{Y} = \begin{bmatrix} \mathcal{A}^T\mathcal{X} + \mathcal{X}\mathcal{A} & \mathcal{X}\mathcal{B} \\ \mathcal{B}^T\mathcal{X} & \mathbf{0} \end{bmatrix} + \begin{bmatrix} \mathbf{0} & \mathbf{0} & \mathbf{0} & \mathbf{0} & \mathbf{0} \\ \mathbf{0} & \mathbf{0} & \mathbf{0} & \mathbf{0} & \mathbf{0} \\ \mathbf{0} & \mathbf{0} & \varepsilon I_{Nd} & \mu I_{Nd} & \mathbf{0} \\ \mathbf{0} & \mathbf{0} & \mu I_{Nd} & \mathbf{0} & \mathbf{0} \\ \mathbf{0} & \mathbf{0} & \mathbf{0} & \mathbf{0} & \mathbf{0} \end{bmatrix} \\ + \sum_{i=1}^{2} (*)(\lambda_i M_{i0} \otimes I_{Nd}) \begin{bmatrix} \mathcal{C}_i & \mathcal{D}_i \end{bmatrix} \preceq 0. \end{aligned} \tag{2.38}$$

This can be seen by observing that $\mathcal{Y}$ and $\mathcal{Z}$ are block 5×5 matrices with $\mathcal{Y}_{ij} = I_N \otimes \mathcal{Z}_{ij}$ for $i, j \in \{1, \cdots, 5\}$. Hence, there exists a permutation matrix such that $T^T \mathcal{Y} T = I_N \otimes \mathcal{Z}$.

Differentiating $E(t)$ with respect to t and using $\mathcal{Y} \preceq 0$, we get

$$\dot{E} + \varepsilon ||p||^2 + (*) \begin{bmatrix} \lambda_1 M_{10} \otimes I_{Nd} & \mathbf{0} \\ \mathbf{0} & \lambda_2 M_{20} \otimes I_{Nd} \end{bmatrix} \begin{bmatrix} q - q_* \\ \nabla f(q) \\ q - y \\ \nabla f_{nc}(q) - \nabla f_{nc}(y) \end{bmatrix} \leqslant 0$$

for all $t \geqslant 0$. Using Assumption 2.4, observe that if $q(t)$, $y(t)$ are in $\mathcal{S}$, then $\dot{E}(t) \leqslant 0$. Altogether, if $E(t) \leqslant V(q_0, q_0, p_0)$, then $q(t), y(t) \in \mathcal{S}_0 \subseteq \mathcal{S}$ which implies $\dot{E}(t) \leqslant 0$ and finally $E(t+s) \leqslant E(t) \leqslant V(x_0, q_0, p_0)$ for all $s \geqslant 0$. In other words, $\mathcal{S}_0$ is an invariant set. Finally, observe that q_0, y_0 are in $\mathcal{S}_0$ and hence $\dot{E}(t) \leqslant -\varepsilon ||p(t)||^2$ for all $t \geqslant 0$. Applying LaSalle's invariance principle, the trajectory $\bar{\eta}(t)$ converges to the set $\{\begin{bmatrix}(-\hat{A}^{-1}\hat{B}_q y_*)^T & y_*^T & 0\end{bmatrix}^T | \nabla f_{nc}(y_*) = 0, y_* \in \mathcal{S}\}$ and since $-\hat{C}\hat{A}^{-1}\hat{B}_q = I$, $y(t)$ converges to the set $\{y_* \in \mathcal{S} | \nabla f_{nc}(y_*) = 0\}$. □

Remark 2.6. *Note that the sufficient condition* (2.35) *contains model matrices appearing in the dynamics of a single agent and is independent of the size of the network N.*

Corollary 2.5. *Let f_{nc}, $\mathcal{S} = \mathbb{R}^{Nd}$ satisfy Assumption 2.4 and assume that the vehicle dynamics* (2.26) *satisfy Assumption 2.5. Additionally, let f_{nc} be proper, i.e., $\{q | f_{nc}(q) \leqslant c\}$ is compact for all $c \in \mathbb{R}$ [Bullo, 2021]. If there exist $R \succeq 0$, $Q \succ 0$, $\mu > 0$, $\lambda_1 \geqslant 0$, $\lambda_2 \geqslant 0$ such that $\mathcal{Z}$ defined in* (2.35) *is negative semi-definite, then, for any initial condition, the state trajectory η under dynamics* (2.30) *remains bounded for all $t \geqslant 0$ and $y(t)$ converges to the set $\{y_* | \nabla f_{nc}(y_*) = 0\}$.*

Proof. Since f_{nc} is proper and $\mathcal{S} = \mathbb{R}^{Nd}$, the set $\mathcal{S}_0$ is bounded and contained in $\mathcal{S}$ for any c_1, c_2. Therefore, the requirement on the initial condition is satisfied. Applying Theorem 2.4 with the above observation gives the result. □

Remark 2.7. *Theorem 2.4 and Corollary 2.5 are presented under general assumptions on f_{nc} without specifying the M_{10} and M_{20}. Examples considered later specialize to $M_{10} = M_{20} = \begin{bmatrix} L^2 & 0 \\ 0 & -1 \end{bmatrix}$.*

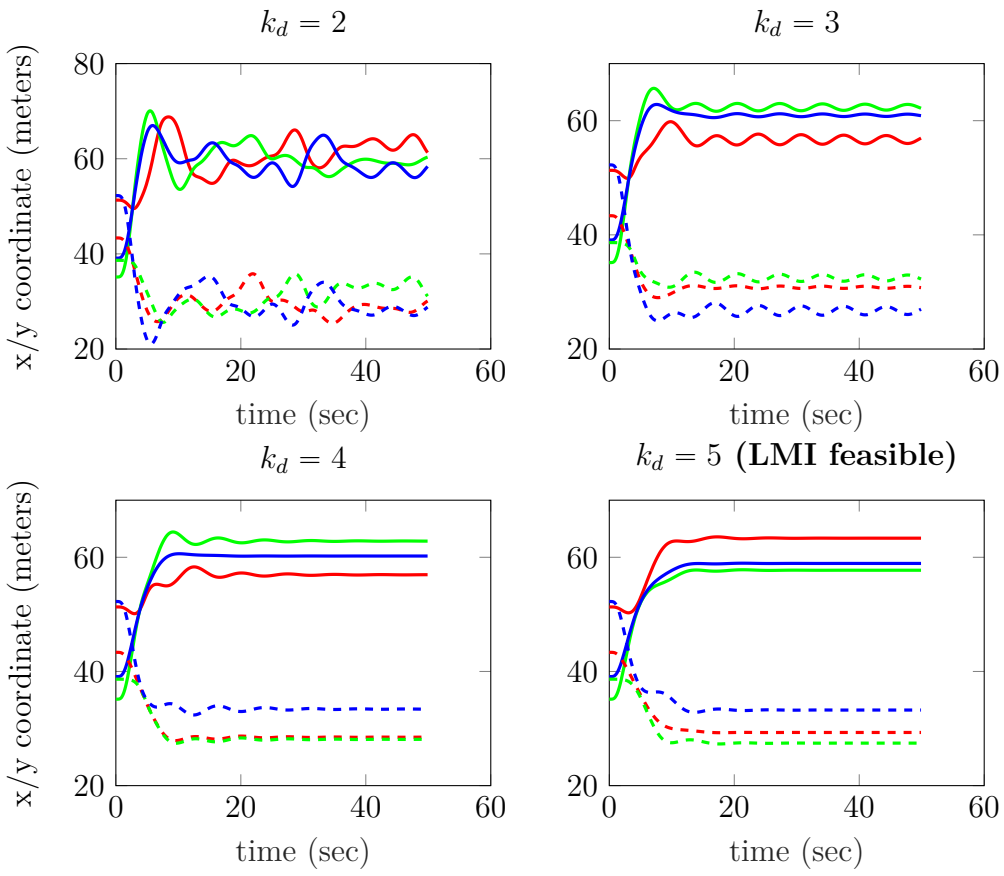

Figure 2.14: Flocking trajectories (solid lines: x-coordinate and dashed line: y coordinate) for different values of k_d with 3 quadrotor agents under quadratic interaction and quadratic external field with source located at (60,30).

2.3.3 Numerical Example

Consider a linearized quadrotor model with a linear quadratic regulator (LQR)-based state-feedback controller tuned for zero steady-state error when tracking step references in position (see Appendix B.1 for details). As discussed in Section 2.3.1, let this closed-loop system be represented by state-space realization (2.26) and augment it with dynamics (2.27) to obtain the system G. Now consider three quadrotors embedded in a strongly convex scalar field ψ with the minimizer at $y_{\text{opt}} = [60\ 30]^T$ and satisfying $\nabla^2\psi(y) \preceq I$ for all $y \in \mathbb{R}^d$. The interaction between the agents is mod-

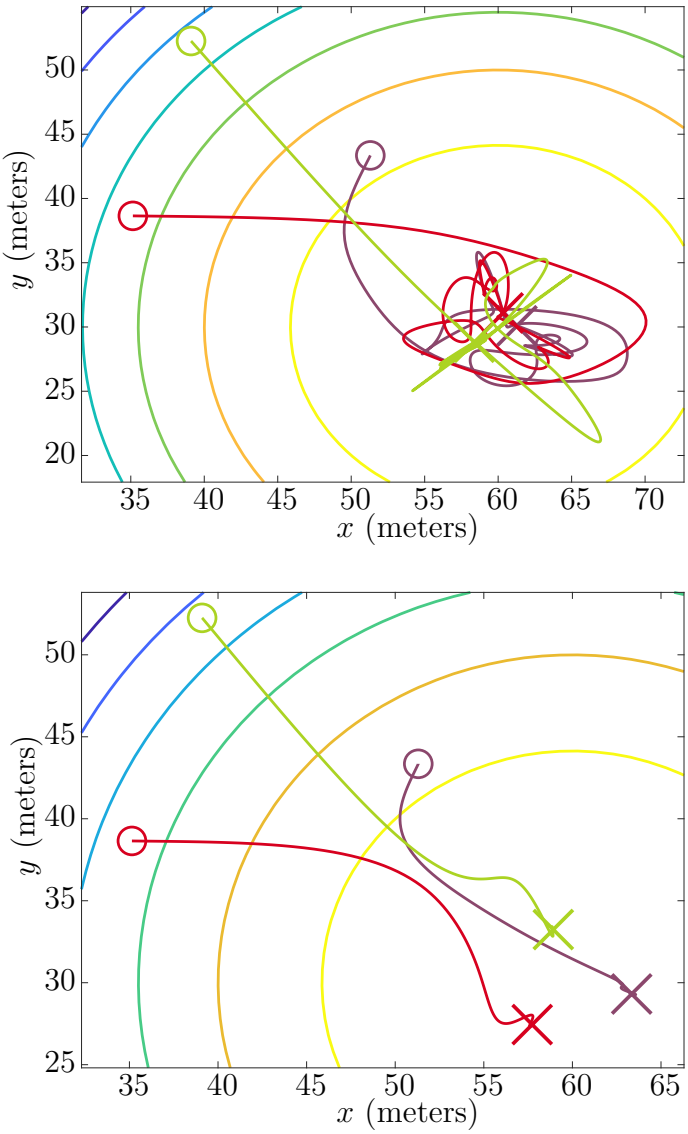

Figure 2.15: Flocking trajectories for $k_d = 2$ (top) and $k_d = 5$ (bottom) with 3 LTI quadrotors under quadratic interactions and external quadratic field. The hollow circle marker shows the initial position and the X marker shows the end position (time=50 sec).

eled with non-convex flocking interaction potential of the form

$$V_f(y) = \sum_{(i,j)} k\frac{1}{2}(||y_i - y_j||_\sigma - d)^2, \tag{2.39}$$

where k is uncertain with $0 \leqslant k \leqslant 1$. Further assume that at least one agent has access to the gradient. With these assumptions, it is easy to see that f_{nc} (see Definition 2.1) is proper since ψ is strongly convex, V_f is non-negative and agents that are not informed agents, if any, are connected to the informed agent at all times. Furthermore, it can be shown that

$$\nabla^2 f_{nc}(y) = \nabla^2 V_f(y) + \nabla^2 \left(\sum_{i \in \mathcal{V}_l} \psi(y_i) \right) \leq 2I + I = 3I,$$

which implies f_{nc} satisfies Assumption 2.4 with $\mathcal{S} = \mathbb{R}^{Nd}$ and

$$M_{10} = M_{20} = \begin{bmatrix} 9I & 0 \\ 0 & -I \end{bmatrix}.$$

Furthermore, the local LQR-based controller is designed to satisfy Assumption 2.5. Therefore, applying Corollary 2.5, a sufficient condition for stability of the overall dynamics is the satisfaction of $\mathcal{Z} \preceq 0$. For this example, $R = \mathbf{0}$ and $\lambda_2 = 0$ are fixed, although that is not required in general. With these choices, T_1 can be analytically computed such that $T_1^T \mathcal{Z} T_1 = 0$ and compute T_2 (by Gram-Schmidt orthogonalization) such that $T = [T_1 \; T_2]$ is an orthonormal matrix. Finally, impose $T_2^T \mathcal{Z} T_2 \prec 0$ which implies $\mathcal{Z} \preceq 0$. Considering k_d as the tuning gains, numerical studies verify that $\mathcal{Z} \preceq 0$ for $k_d \geqslant 4.8$. Figure 2.14 shows trajectories with different values of k_d for $\psi(z) = \frac{1}{2}||z - y_{\text{opt}}||^2$ and $k = 1$. Figure 2.15 shows the trajectories and the contour lines of the external scalar field for two different values of k_d. As can be seen from Fig. 2.14 and Fig. 2.15, the trajectories for $k_d \leqslant 3$ do not seem to converge, whereas with $k_d = 4$, the trajectories converge in spite of the fact that $\mathcal{Z}$ is not negative semi-definite showing a possible conservatism in the sufficient condition. However, this example demonstrates a possible way to tune the gains for maintaining stability of flocking dynamics. More elaborate local results with multiple minima and complex interaction fields are obtainable with Theorem 2.4 and is deferred to future work.

Chapter 3

Source-Seeking Under Formation Control Dynamics: Performance Analysis with Dynamic IQCs

The overarching goal of this chapter is to extend the stability analysis of source-seeking dynamics considered in Chapter 2 to performance analysis and estimate the exponential convergence rate. This goal is reached at the cost of some additional assumptions on the interaction field and the external scalar field. The main tool is the framework of integral quadratic constraints with dynamic Zames-Falb multipliers, well known from the literature on robust control theory. The main difficulty in analyzing the problem with interaction potentials of Chapter 2 via ZF IQCs is the non-convexity of the flocking-based interaction potentials. The focus of this chapter is therefore set on the convex interaction potentials of the form $\frac{1}{2}(y-r)^T(\mathcal{L}\otimes I_d)(y-r)$, common in the literature on formation control. Furthermore, since the goal is to estimate the exponential convergence rate, the external scalar field is now additionally assumed to be strongly convex, instead of just strictly convex as in Chapter 2. Specifically, the external scalar field $\psi : \mathbb{R}^d \to \mathbb{R}$ is now restricted to the class $\mathcal{S}(m_\psi, L_\psi)$ of continuously differentiable functions which are strongly convex with parameter m_ψ, and have Lipschitz gradients with parameter L_ψ for given constants $0 < m_\psi \leqslant L_\psi$, i.e., $\forall y_1, y_2 \in \mathbb{R}^d$,

$$m_\psi ||y_1 - y_2||^2 \leqslant (\nabla f(y_1) - \nabla f(y_2))^T (y_1 - y_2) \leqslant L_\psi ||y_1 - y_2||^2.$$

The key contributions of this chapter have been reported in [Datar and Werner, 2022] and [Datar et al., 2022, under review] and the outline of this chapter is as follows. After discussing the problem setup in Section 3.1, the

main theoretical results are presented in Section 3.2 followed by numerical examples in Section 3.3 and 3.4. Finally, results showing a trade-off between nominal performance and robustness against gradient measurement noise are presented in Section 3.5.

3.1 Problem Setup

Consider again a source-seeking scenario where N vehicle agents moving in $\mathbb{R}^d$ space (typically $d \in \{1, 2, 3\}$) are embedded in an external differentiable scalar field $\psi : \mathbb{R}^d \to \mathbb{R}$ satisfying the following assumption.

Assumption 3.1. *The scalar field $\psi : \mathbb{R}^d \to \mathbb{R}$ is a continuously differentiable function that is strongly convex with parameter m_ψ and has Lipschitz gradients with parameter L_ψ, i.e., $\psi \in \mathcal{S}(m_\psi, L_\psi)$ and let y_{opt} minimize ψ, i.e., $\psi(y) \geqslant \psi(y_{\text{opt}})\, \forall y \in \mathbb{R}^d$.*

The interconnections between the vehicle agents are modeled with an undirected graph $\mathcal{G} = (\mathcal{V}, \mathcal{E})$ such that each vertex $i \in \mathcal{V}$ represents a vehicle and vehicles i and j communicate if and only if $(i, j) \in \mathcal{E}$. It is assumed that a non-empty subset $\mathcal{V}_l \subseteq \mathcal{V}$ of informed agents (agents with additional information) have access to the local gradient $\nabla\psi$ evaluated at their respective positions. The dynamics of the these informed agents can therefore be augmented with a forcing term in the direction of the negative gradient that drives them towards the source. The following assumption on the connectivity of the graph is made, the necessity of which is discussed later in Lemma 3.6.

Assumption 3.2. *For every node $i \in \mathcal{V}$, there is a node $j \in \mathcal{V}_l$ such that $\mathcal{G}$ contains a path from i to j.*

For convenience, the details of the architecture discussed in the previous chapter is repeated next. Since this chapter deals primarily with analysis (compared to controller synthesis), it is assumed that a local tracking controller has been designed and identical to the setup in Section 2.3.1, the closed-loop dynamics of the i^{th} vehicle agent with desired reference position $q_i(t)$, desired reference velocity $p_i(t)$, internal state $x_i(t)$ and position output $y_i(t)$ can be described for a given initial condition $x_i(0)$ by

$$\begin{aligned} \dot{x}_i(t) &= Ax_i(t) + \begin{bmatrix} B_q & B_p \end{bmatrix} \begin{bmatrix} q_i(t) \\ p_i(t) \end{bmatrix}, \\ y_i(t) &= Cx_i(t). \end{aligned} \tag{3.1}$$

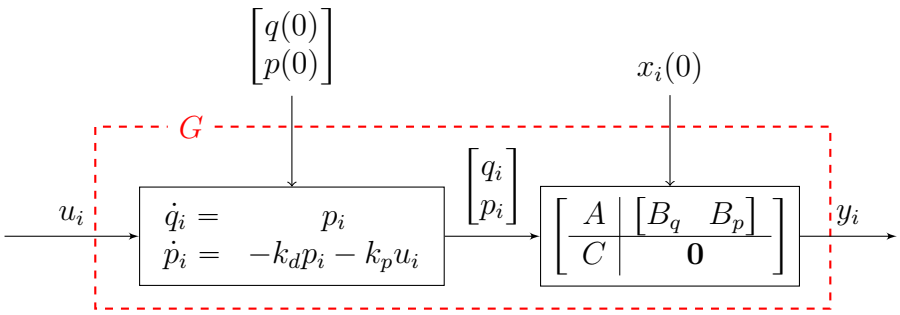

Figure 3.1: Local control architecture on agent i.

These closed-loop vehicle dynamics are augmented by the second-order dynamics,

$$\begin{aligned} \dot{q}_i(t) &= p_i(t), \\ \dot{p}_i(t) &= -k_d \cdot p_i(t) - k_p \cdot u_i(t), \end{aligned} \tag{3.2}$$

where $u_i(t) \in \mathbb{R}^d$ denotes external input, $q_i(0) = Cx_i(0)$, $p_i(0) = 0$ such that $q_i(t)$ and $p_i(t)$ are fed as inputs to dynamics (3.1). The motivation behind the augmented dynamics is discussed in Remark 2.4. The overall dynamics with state $\eta_i = \begin{bmatrix} x_i^T & q_i^T & p_i^T \end{bmatrix}^T$ and suitable initial condition $\eta_i(0)$ can be depicted as in Fig. 3.1 and represented by

$$\begin{aligned} \dot{\eta}_i(t) &= A_G \eta_i(t) + B_G u_i(t), \\ y_i(t) &= C_G \eta_i(t), \end{aligned} \tag{3.3}$$

where

$$G = \left[\begin{array}{c|c} A_G & B_G \\ \hline C_G & D_G \end{array}\right] = \left[\begin{array}{ccc|c} A & B_q & B_p & \mathbf{0} \\ \mathbf{0} & \mathbf{0} & I_d & \mathbf{0} \\ \mathbf{0} & \mathbf{0} & -k_d I_d & -k_p I_d \\ \hline C & \mathbf{0} & \mathbf{0} & \mathbf{0} \end{array}\right].$$

With the notation introduced in Section 1.5, let $\eta(t)$, $u(t)$ and $y(t)$ be obtained by stacking the states, inputs and outputs of the agents, respectively. The full system can be described by

$$\begin{aligned} \dot{\eta}(t) &= \hat{A}_G \eta(t) + \hat{B}_G u(t), \qquad \eta(0) = \eta_0, \\ y(t) &= \hat{C}_G \eta(t). \end{aligned} \tag{3.4}$$

Defining u_ψ by stacking up

$$u_{\psi_i}(t) = \begin{cases} \nabla\psi(y_i(t)), & \text{if } i \in \mathcal{V}_l, \\ 0 & \text{otherwise}, \end{cases} \tag{3.5}$$

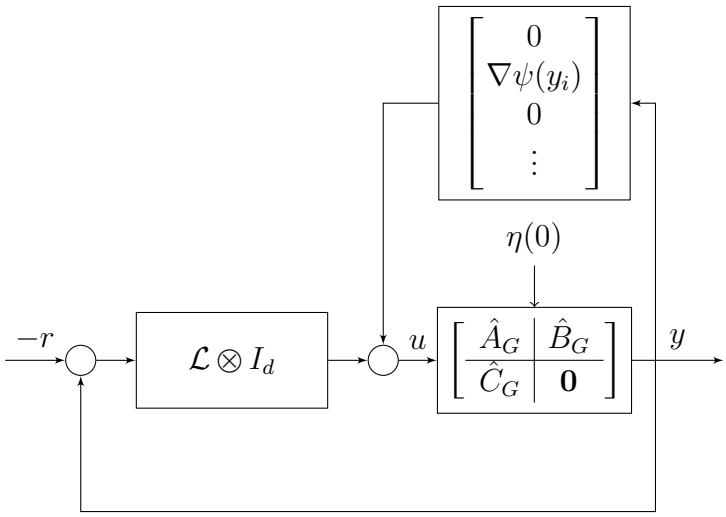

Figure 3.2: Control architecture under formation control dynamics.

standard formation control dynamics [Fax and Murray, 2004] with the formation reference r and an additional forcing term on the informed agents as depicted in Fig. 3.2 can be represented by

$$u = \mathcal{L}_{(d)}(y - r) + u_\psi. \tag{3.6}$$

The overall closed-loop system is now described by

$$\begin{aligned} \dot{\eta}(t) &= \hat{A}_G\eta(t) + \hat{B}_G u(t), \qquad \eta(0) = \eta_0, \\ y(t) &= \hat{C}_G\eta(t), \\ u(t) &= \mathcal{L}_{(d)}(y - r) + u_\psi. \end{aligned} \tag{3.7}$$

In order to pose the analysis of dynamics (3.7) as a standard robust control problem with the scalar field and communication graph modeled as an uncertainty, define a function $f_c : \mathbb{R}^{Nd} \to \mathbb{R}$ as follows.

Definition 3.1. *For a given graph $\mathcal{G}$ of order N (with its corresponding Laplacian $\mathcal{L}$), the set of informed agents $\mathcal{V}_l$, a scalar field ψ and a given formation reference vector $r \in \mathbb{R}^{Nd}$, define a function $f_c : \mathbb{R}^{Nd} \to \mathbb{R}$ by*

$$f_c(y) = \frac{1}{2}(y - r)^T(\mathcal{L} \otimes I_d)(y - r) + \sum_{i \in \mathcal{V}_l} \psi(y_i). \tag{3.8}$$

Consider an example with 2 connected agents living on $\mathbb{R}$, i.e., $d = 1$ and $\mathcal{L} = \begin{bmatrix} 1 & -1 \\ -1 & 1 \end{bmatrix}$. Let the first agent be an informed agent, i.e., $\mathcal{V}_l = \{1\}$

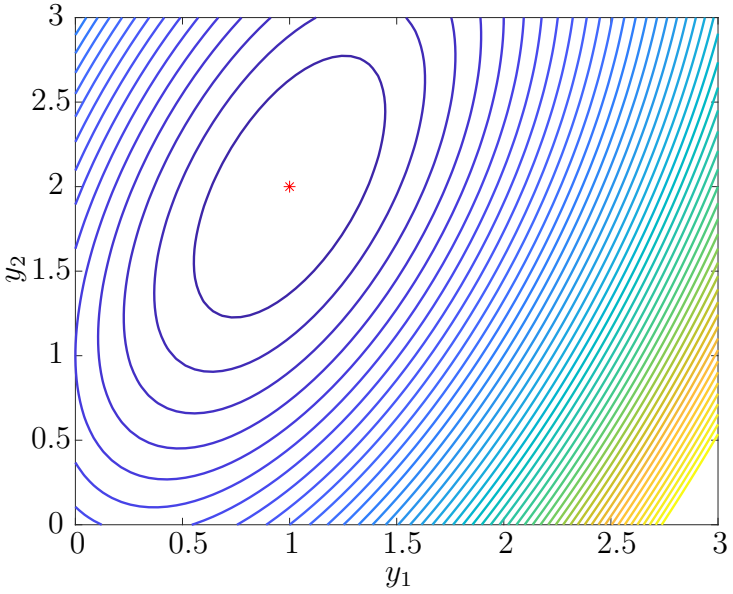

Figure 3.3: Contour plot of an example $f_c(y) = \frac{1}{2}(y_1 - y_2 - 1)^2 + \frac{1}{2}(y_1 - 1)^2$ with $N = 2$ and $d = 1$, where minimizer $[1\ 2]^T$ is denoted by red star.

and the desired formation specified by $r = [0 \quad 1]^T$. Finally, let the external scalar field be given by $\psi(y) = \frac{1}{2}(y-1)^2$. For this example setup, f_c can be computed as

$$\begin{aligned} f_c(y) &= \frac{1}{2}(y-r)^T(\mathcal{L}\otimes I_d)(y-r) + \sum_{i\in\mathcal{V}_l}\psi(y_i) \\ &= \frac{1}{2}\begin{bmatrix} y_1 & y_2 - 1\end{bmatrix}\begin{bmatrix} 1 & -1 \\ -1 & 1\end{bmatrix}\begin{bmatrix} y_1 \\ y_2 - 1\end{bmatrix} + \frac{1}{2}(y_1-1)^2 \\ &= \frac{1}{2}(y_1 - y_2 - 1)^2 + \frac{1}{2}(y_1-1)^2 \end{aligned}$$

and is depicted in Fig. 3.3. Note that since agent 1 is the informed agent, the desired arrangement corresponding to the minimum of f_c is $y = [1 \quad 2]^T$.

Observe that $u(t) = \nabla f_c(y(t))$. So the overall dynamics can be described by

$$\begin{aligned} \dot{\eta}(t) &= \hat{A}_G\eta(t) + \hat{B}_G u(t), \qquad \eta(0) = \eta_0, \\ y(t) &= \hat{C}_G\eta(t), \\ u(t) &= \nabla f_c(y(t)). \end{aligned} \tag{3.9}$$

Problem 3.1. *Assuming ψ, $\mathcal{G}$ and $\mathcal{V}_l$ satisfy Assumptions 3.1 and 3.2, characterize the equilibria of dynamics* (3.9) *and derive sufficient conditions independent of the network size N under which the state trajectories generated by the dynamics* (3.9) *remain bounded for all $t \geqslant 0$ and y converges exponentially with a rate α to the minimizer y_* of f_c, i.e., $\exists \kappa \geqslant 0$ such that $||y(t) - y_*(t)|| \leqslant \kappa e^{-\alpha t}$ holds for all $t \geqslant 0$.*

Note that the formation control law uses a convex interaction field $\frac{1}{2}(y - r)^T(\mathcal{L} \otimes I_d)(y - r)$ whereas flocking interaction potentials are typically non-convex as they are based on distance.

3.2 Robust Performance Analysis

Problem 3.1 can be posed as a standard robust control problem described by

$$\begin{aligned} \dot{\eta}(t) &= \hat{A}_G \eta(t) + \hat{B}_G u(t), \qquad \eta(0) = \eta_0, \\ y(t) &= \hat{C}_G \eta(t), \\ u(t) &= \Delta(y(t)). \end{aligned} \tag{3.10}$$

The operator Δ (∇f_c for Problem 3.1) is not explicitly known but is only assumed to belong to a set $\mathbf{\Delta}$ which characterizes our knowledge about the uncertainty in the model. The first step in carrying out an IQC analysis involves using the knowledge of the set $\mathbf{\Delta}$ to derive properties of the input and output signals u and y in the form of integral inequalities. These integral inequalities, specified by a given matrix P and a given LTI system

$$\Pi = \left[\begin{array}{c|c} A_\Pi & B_\Pi \\ \hline C_\Pi & D_\Pi \end{array}\right]$$

typically take the form

$$\int_0^T e^{2\alpha t} z(t)^T (P \otimes I) z(t) dt \geqslant 0 \quad \forall T \geqslant 0, \tag{3.11}$$

where $z(t)$ is given by

$$z(t) = \int_0^t C_\Pi e^{A_\Pi (t-\tau)} B_\Pi \begin{bmatrix} y(\tau) \\ u(\tau) \end{bmatrix} d\tau + D_\Pi \begin{bmatrix} y(t) \\ u(t) \end{bmatrix}.$$

One aims to derive properties which exactly characterize the set $\mathbf{\Delta}$. For Problem 3.1, we use the ZF α-IQCs.

The analysis for Problem 3.1 is first presented by postulating that $f_c \in \mathcal{S}(m, L)$ in Sections 3.2.1, 3.2.2 and 3.2.3 followed by a study of properties of f_c (including conditions ensuring $f_c \in \mathcal{S}(m, L)$) in Sections 3.2.4 and 3.2.5.

3.2.1 ZF α-IQC Parameterization

This section is devoted to deriving properties between the signals u and y related by the map $u = \nabla f(y)$ where f is an arbitrary function in $\mathcal{S}(m, L)$ and y_* minimizes f such that $\nabla f(y_*) = 0$. The standard (non-exponential) ZF IQCs have been well studied. The main contribution of this section is to give a purely time-domain derivation of the general non-causal higher order ZF α-IQCs with a modification of the parameterization from [Veenman et al., 2016] adapted to the α-IQC setting. A discussion on closely related literature is given in Section 1.1.

To simplify the discussion, the properties between the deviation signals $\tilde{y} = y - y_*$ and $\tilde{u} = u - u_* = \nabla f(y) - \nabla f(y_*) = \nabla f(y) = \nabla f(\tilde{y} + y_*)$ are derived instead of the signals u and y. It is convenient to derive properties of some new signals (defined below) related to the input and output signals $\tilde{u}$ and $\tilde{y}$. For constants m, L and for any $\tilde{u}, \tilde{y} \in \mathcal{L}_{2e}[0, \infty)$, define for $t \in [0, \infty)$,

$$\begin{aligned} p(t) &= \tilde{u}(t) - m\tilde{y}(t), \\ q(t) &= L\tilde{y}(t) - \tilde{u}(t). \end{aligned} \tag{3.12}$$

It can be shown just from basic convexity properties (for example using Proposition 5 from [Lessard et al., 2016]) that if $f \in \mathcal{S}(m, L)$, then $p(t)^T q(t) \geqslant 0$ for all $t \geqslant 0$ which implies that $\int_0^T e^{2\alpha t} p(t)^T q(t) dt \geqslant 0$ for any $T \geqslant 0$ and any $\alpha \in \mathbb{R}$. This corresponds to the well-known sector condition involved in the circle criterion [Scherer, 2022]. The aim of this section is to derive more general properties which include the sector condition mentioned above in order to better characterize the class of functions $f \in \mathcal{S}(m, L)$.

Let $h \in \mathcal{L}_1(-\infty, \infty)$ such that

$$h(s) \geqslant 0 \quad \forall s \in \mathbb{R} \text{ and } \int_{-\infty}^{\infty} h(s) ds \leqslant H, \tag{3.13}$$

for some $H \in \mathbb{R}$ and define signals w_1 and w_2 as shown in Fig. 3.4 by

$$\begin{aligned} w_1(t) &= \int_0^t e^{-2\alpha(t-\tau)} h(t-\tau) q(\tau) d\tau, \\ w_2(t) &= \int_0^t e^{-2\alpha(t-\tau)} h(-(t-\tau)) p(\tau) d\tau. \end{aligned} \tag{3.14}$$

Theorem 3.1. *Let h satisfying* (3.13) *be fixed and let $\alpha \geqslant 0$. Let $\tilde{u}, \tilde{y} \in \mathcal{L}_{2e}[0, \infty)$ be related by $\tilde{u} = \nabla f(\tilde{y} + y_*)$, where $f \in \mathcal{S}(m, L)$ and y_* minimizes f. Then, the signals defined in* (3.12) *and* (3.14) *satisfy*

$$\int_0^T e^{2\alpha t} \left(H p(t)^T q(t) - p(t)^T w_1(t) - q(t)^T w_2(t) \right) dt \geqslant 0, \tag{3.15}$$

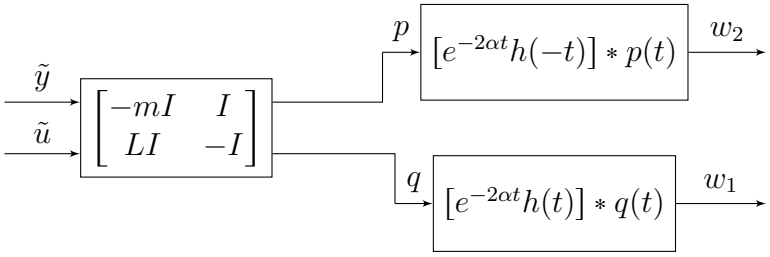

Figure 3.4: Signal definitions for p, q, w_1, w_2.

$\forall T \geqslant 0$.

Proof. With the signal definitions (3.14), an appropriate change of integration variable, signal extension as defined in (1.2) and Fubini's theorem, we obtain,

$$\begin{aligned}
\int_0^T e^{2\alpha t} p(t)^T w_1(t) dt &= \int_0^T e^{2\alpha t} p(t)^T \left(\int_0^t e^{-2\alpha(t-\tau)} h(t-\tau) q(\tau) d\tau \right) dt \\
&= \int_0^T \int_{s=0}^t e^{2\alpha(t-s)} p(t)^T h(s) q(t-s) ds dt \\
&= \int_0^T \int_{s=0}^\infty e^{2\alpha(t-s)} p(t)^T h(s) q_T(t-s) ds dt \\
&= \int_{s=0}^\infty h(s) \left(\int_0^T e^{2\alpha(t-s)} p(t)^T q_T(t-s) dt \right) ds. \qquad (3.16)
\end{aligned}$$

Similarly,

$$\int_0^T e^{2\alpha t} q(t)^T w_2(t) dt = \int_{s=-\infty}^0 h(s) \left(\int_{\tau=0}^T e^{2\alpha\tau} p(\tau)^T q_T(\tau - s) d\tau \right) ds. \qquad (3.17)$$

Putting (3.16) and (3.17) together and using a Lemma 3.12 (proven in Section 3.6),

$$\begin{aligned}
&\int_0^T e^{2\alpha t} (p(t)^T w_1(t) + q(t)^T w_2(t)) dt \\
&= \int_{s=-\infty}^\infty h(s) \left(\int_0^T e^{2\alpha t} \min\{1, e^{-2\alpha s}\} p(t)^T q_T(t-s) dt \right) ds \\
&\leqslant \int_{s=-\infty}^\infty h(s) \left(\int_0^T e^{2\alpha t} p(t)^T q(t) dt \right) ds \\
&\leqslant \int_0^T H e^{2\alpha t} p(t)^T q(t) dt,
\end{aligned}$$

where the first inequality follows from Lemma 3.12 and $h(t) \geqslant 0$ and the second inequality follows from (3.13).

Note that the asymmetry of the function $\beta(s) = \min\{1, e^{-2\alpha s}\}$ about the point time $s = 0$ arises effectively from the asymmetry generated by the factor $e^{2\alpha t}$ in the integrand of the α-IQC formulation. This factor is absent in the standard non-exponential versions of the the ZF IQC. Also note that this asymmetry is present in the exponential ZF IQCs presented in [Freeman, 2018]. □

Remark 3.1. *A factor of $2H$ is typically found in the literature instead of the factor H in the first term of the inequality* (3.15)*. This is because h is typically assumed to be symmetric about $t = 0$, i.e., $h(t) = h(-t)$ and a bound of the form $\int_0^\infty h(s)ds \leqslant H$ is assumed (instead of the upper-bound in* (3.13)*) which implies $\int_{-\infty}^{\infty} h(s)ds = \int_{-\infty}^{0} h(s)ds + \int_0^\infty h(s)ds \leqslant 2H$.*

Note that if $h(t) = 0$ for all t, (which implies $w_1(t) = 0$ and $w_2(t) = 0$ for all t), one can pick $H = 1$ to obtain $\int_0^T e^{2\alpha t} p(t)^T q(t)dt \geqslant 0$, the sector IQC involved in the circle criterion, discussed before the theorem. Theorem 3.1 thus produces a larger set of IQCs depending on the choice of h. The parameterization of h in the following discussion proceeds along the lines of [Veenman et al., 2016] (with the same notation). Observe that w_1 and w_2 defined in (3.14) can be seen as the outputs of fictitious LTI systems with impulse responses $e^{-2\alpha(t-\tau)}h(t-\tau)$ and $e^{-2\alpha(t-\tau)}h(-(t-\tau))$ and excited by inputs q and p, respectively. Consider a fictitious LTI systems of order ν (to be chosen) as follows. Let

$$A_\nu = \begin{bmatrix} \lambda & 0 & \dots & 0 \\ 1 & \lambda & \ddots & 0 \\ 0 & \ddots & \ddots & 0 \\ \vdots & 0 & 1 & \lambda \end{bmatrix}, B_\nu = \begin{bmatrix} 1 \\ 0 \\ \vdots \\ 0 \end{bmatrix}. \tag{3.18}$$

Choosing the λ appropriately is an open-problem as noted in [Veenman et al., 2016] and for all numerical experiments in this thesis, λ is set to -1 and the multiplier order ν is chosen from the set $\{1, 2, \cdots, 5\}$ with most applications showing good results already with first order multipliers, i.e., $\nu = 1$ (see Section 3.3). Due to this small size, the numerical conditioning issues typically associated with these Jordon blocks are not observed. Let

$$Q_\nu(t) = e^{A_\nu t} B_\nu = e^{\lambda t} R_\nu^2 \begin{bmatrix} 1 & t & \dots & t^{\nu-1} \end{bmatrix}^T,$$

where

$$R_\nu = \operatorname{diag}\left(\frac{1}{\sqrt{0!}}, \frac{1}{\sqrt{1!}}, \cdots, \frac{1}{(\sqrt{\nu-1})!}\right).$$

Parameterize h by variables $P_1 \in \mathbb{R}^{1\times\nu}$ and $P_3 \in \mathbb{R}^{1\times\nu}$ as

$$h(t) = \begin{cases} P_1 Q_\nu(-t) & \text{if } t < 0, \\ P_3 Q_\nu(t) & \text{if } t \geqslant 0. \end{cases} \tag{3.19}$$

Let $\tilde{\pi}_\nu(s) = \begin{bmatrix} 1 & \frac{s}{(s-\lambda)^{\nu-1}} & \cdots & \frac{s^{\nu-1}}{(s-\lambda)^{\nu-1}} \end{bmatrix}^T$ and let $\left[\begin{array}{c|c} \tilde{A}_\nu & \tilde{B}_\nu \\ \hline \tilde{C}_\nu & \tilde{D}_\nu \end{array}\right]$ be a state-space realization of $\tilde{\pi}_\nu$. It has been shown in [Veenman et al., 2016] that if H, P_1, P_3 are such that

$$H + (P_1 + P_3)A_\nu^{-1}B_\nu \geqslant 0 \tag{3.20}$$

and $\exists \mathcal{X}_1, \mathcal{X}_3 \in \mathbb{S}^{\nu-1}$ such that for $i = \{1, 3\}$,

$$(*)\begin{bmatrix} \mathbf{0} & \mathcal{X}_i & \mathbf{0} \\ \mathcal{X}_i & \mathbf{0} & \mathbf{0} \\ \mathbf{0} & \mathbf{0} & \operatorname{diag}(P_i) \end{bmatrix}\begin{bmatrix} I & \mathbf{0} \\ \tilde{A}_\nu & \tilde{B}_\nu \\ R_\nu \tilde{C}_\nu & R_\nu \tilde{D}_\nu \end{bmatrix} \succ 0, \tag{3.21}$$

then, h defined in (3.19) satisfies (3.13). Thus, every element in the set

$$\mathbb{P} = \left\{ \begin{bmatrix} \mathbf{0} & \mathbf{0} & H & -P_3 \\ \mathbf{0} & \mathbf{0} & -P_1^T & \mathbf{0} \\ * & * & \mathbf{0} & \mathbf{0} \\ * & * & \mathbf{0} & \mathbf{0} \end{bmatrix} | H, P_1, P_3 \text{ satisfy (3.20) and (3.21)} \right\}.$$

corresponds to an h satisfying (3.13).

Now, let $A_\nu^\alpha = A_\nu - 2\alpha I$, $Q_\nu^\alpha(t) = e^{-2\alpha t}Q_\nu(t)$ and $\pi = \left[\begin{array}{c|c} A_\nu^\alpha & B_\nu \\ \hline 0 & 1 \\ I_\nu & \mathbf{0} \end{array}\right]$. With

$$\pi_{m,L} = \begin{bmatrix} \pi & 0 \\ 0 & \pi \end{bmatrix}\begin{bmatrix} -m & 1 \\ L & -1 \end{bmatrix} = \left[\begin{array}{cc|cc} A_\nu^\alpha & \mathbf{0} & -mB_\nu & B_\nu \\ \mathbf{0} & A_\nu^\alpha & LB_\nu & -B_\nu \\ \hline \mathbf{0} & \mathbf{0} & -m & 1 \\ I_\nu & \mathbf{0} & \mathbf{0} & \mathbf{0} \\ \mathbf{0} & \mathbf{0} & L & -1 \\ \mathbf{0} & I_\nu & \mathbf{0} & \mathbf{0} \end{array}\right],$$

let $\Pi_0 = \pi_{m,L} \otimes I_d$ and $\Pi = \left[\begin{array}{c|c} A_\Pi & B_\Pi \\ \hline C_\Pi & D_\Pi \end{array}\right] = \pi_{m,L} \otimes I_{Nd}$. As shown in Fig. 3.5, let us define for any $\tilde{u}, \tilde{y} \in \mathcal{L}_{2e}[0, \infty)$,

$$\tilde{z}(t) = \int_0^t C_\Pi e^{A_\Pi(t-\tau)} B_\Pi \begin{bmatrix} \tilde{y}(\tau) \\ \tilde{u}(\tau) \end{bmatrix} d\tau + D_\Pi \begin{bmatrix} \tilde{y}(t) \\ \tilde{u}(t) \end{bmatrix}. \tag{3.22}$$

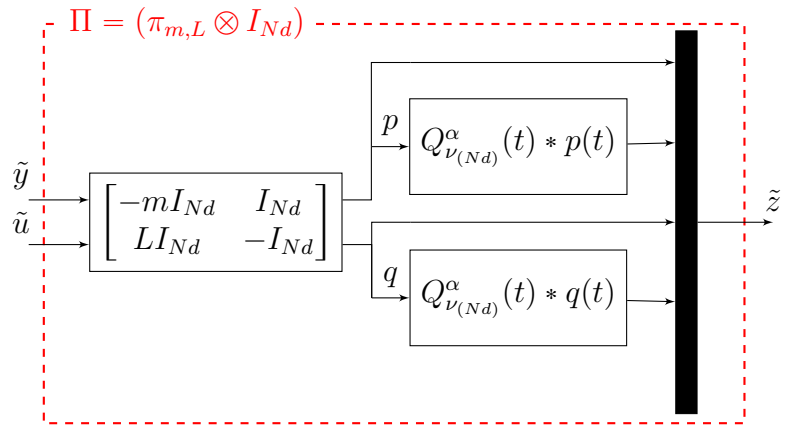

Figure 3.5: Structure of $\Pi = (\pi_{m,L} \otimes I_{Nd})$.

Theorem 3.2. *Let $\tilde{u}, \tilde{y} \in \mathcal{L}_{2e}[0, \infty)$ be related by $\tilde{u} = \nabla f(\tilde{y} + y_*)$, where $f \in \mathcal{S}(m, L)$ and y_* minimizes f. Then, for any $\alpha \geqslant 0$, the signal $\tilde{z}$ as defined in (3.22) satisfies*

$$\int_0^T e^{2\alpha t} \tilde{z}^T(t)(P \otimes I)\tilde{z}(t)dt \geqslant 0 \quad \forall P \in \mathbb{P}, \forall T \geqslant 0. \tag{3.23}$$

Proof. From the state-space realization of Π (shown in Fig. 3.5), the signal definitions (3.12), (3.14) and (3.19) and the block structure of matrices $P \in \mathbb{P}$, we get,

$$\tilde{z}^T(t)(P \otimes I)\tilde{z}(t) = 2(Hp(t)^T q(t) - p(t)^T w_1(t) - q(t)^T w_2(t)),$$

which can be used together with Theorem 3.1 to finish the proof.

□

Remark 3.2. *In the classical robust control literature, the transfer function $\hat{\Pi}^*(P \otimes I)\hat{\Pi}$ is the called general non-causal ZF multiplier, where $\hat{\Pi}$ is the transfer function corresponding to the LTI system Π, P is a matrix belonging to $\mathbb{P}$ and the superscript $*$ represents complex conjugate transpose. When enforcing $P_1 = \mathbf{0}$ ($P_3 = \mathbf{0}$), the multiplier is called causal (anti-causal) ZF multiplier and when enforcing $P_1 = \mathbf{0}$ and $P_3 = \mathbf{0}$, one ends up with static multipliers which correspond to the well-known circle-criterion (CC) [Scherer, 2022]. The conservatism in these specializations is investigated in Section 3.3. Since all the arguments made here are in time-domain, the transfer function $\hat{\Pi}^*(P \otimes I)\hat{\Pi}$ does not appear at any point in this thesis. The order ν of the LTI system π is called the order of the ZF multiplier.*

Remark 3.3. *Extension of these results to cases when the map from $\tilde{y}$ to $\tilde{u}$ is additionally known to be odd is possible along the same lines but is not pursued here.*

3.2.2 Analysis for LTI Systems

Finally, applying the standard IQC machinery, the analysis result is presented next which leads to a computational procedure for obtaining convergence rate estimates. Let $\left[\begin{array}{c|c} \mathcal{A} & \mathcal{B} \\ \hline \mathcal{C} & \mathcal{D} \end{array}\right] = (\pi_{m,L} \otimes I_{Nd}) \begin{bmatrix} I_N \otimes G \\ I_{Nd} \end{bmatrix}$. The following theorem from [Hu and Seiler, 2016] adapted to the current setting gives the performance analysis condition, the proof of which follows along the lines of the proof of Theorem 3.4.

Theorem 3.3 (adapted from [Hu and Seiler, 2016])**.** *If $\exists \mathcal{X} \succ 0, P \in \mathbb{P}$ such that*

$$\begin{bmatrix} \mathcal{A}^T\mathcal{X} + \mathcal{X}\mathcal{A} + 2\alpha\mathcal{X} & \mathcal{X}\mathcal{B} \\ \mathcal{B}^T\mathcal{X} & \mathbf{0} \end{bmatrix} + \begin{bmatrix} \mathcal{C}^T \\ \mathcal{D}^T \end{bmatrix} P_{(Nd)}(*) \preceq 0, \tag{3.24}$$

then, state trajectories generated by the dynamics (3.9) *with any $f_c \in \mathcal{S}(m, L)$ remain bounded and the output trajectory y converges exponentially to the minimizer y_* of f_c with rate α, i.e., $\exists \kappa \geqslant 0$ such that $||y(t) - y_*(t)|| \leqslant \kappa e^{-\alpha t}$ holds for all $t \geqslant 0$.*

Remark 3.4. *Note that* (3.24) *is not linear in α and $\mathcal{X}$ due to the product $\alpha\mathcal{X}$. It falls into the class of quasi-convex optimization problems which can be solved efficiently using a bisection over α as commonly suggested in the literature such as in [Lessard et al., 2016].*

Remark 3.5. *Note that for large networks, i.e., when N is large, the LMI* (3.24) *becomes computationally intractable. However, it can be decomposed into a smaller LMI independent of N as described in Section 3.2.6.*

3.2.3 Analysis for LPV Systems

Extensions of the results obtained in the previous section to LPV systems is straightforward and one such extension is demonstrated next when $N = 1$. Instead of the LTI system G, let $G(\rho)$ denote an LPV system with n_ρ scheduling parameters [Shamma and Cloutier, 1992], where, for a compact set $\mathcal{P} \subseteq \mathbb{R}^{n_\rho}$, the function $\rho : [0, \infty) \to \mathcal{P}$ captures the time-dependence of the model parameters. Assume that the system $G(\rho)$ still has the same structure as depicted in Fig. 3.1 with the difference being that the matrices

A, B_q, B_p, C may be parameter dependent. The overall dynamics can be represented by

$$\begin{aligned} \dot{\eta}(t) &= A_G(\rho(t))\eta(t) + B_G(\rho(t))u(t), \qquad \eta(0) = \eta_0, \\ y(t) &= C_G(\rho(t))\eta(t), \\ u(t) &= \nabla\psi(y(t)), \end{aligned} \tag{3.25}$$

where $\eta \in \mathbb{R}^{n_\eta}$ is the state vector and $\rho : [0, \infty) \to \mathcal{P}$ is an arbitrary scheduling trajectory. If the rate of parameter variation $\dot{\rho}$ is bounded and this bound is known, it could be included by considering parameter-dependent Lyapunov functions (see [Scherer and Weiland, 2000] for details), but this case is not treated here.

Let the series interconnection of the LTI system $(\pi_{m,L} \otimes I_d)$ and the LPV system $G(\rho)$ be denoted by

$$\left[\begin{array}{c|c} \mathcal{A}(\rho) & \mathcal{B}(\rho) \\ \hline \mathcal{C}(\rho) & \mathcal{D}(\rho) \end{array}\right] = (\pi_{m,L} \otimes I_d) \begin{bmatrix} G(\rho) \\ I_d \end{bmatrix}.$$

The following theorem gives a sufficient condition for performance analysis.

Theorem 3.4. *If $\exists \mathcal{X} \succ 0, P \in \mathbb{P}$ such that, for any $\bar{\rho} \in \mathcal{P} \subseteq \mathbb{R}^{n_\rho}$ ($\bar{\rho}$ is a vector, whereas ρ is a function),*

$$\begin{bmatrix} \mathcal{A}(\bar{\rho})^T\mathcal{X} + \mathcal{X}\mathcal{A}(\bar{\rho}) + 2\alpha\mathcal{X} & \mathcal{X}\mathcal{B}(\bar{\rho}) \\ \mathcal{B}(\bar{\rho})^T\mathcal{X} & \mathbf{0} \end{bmatrix} + \begin{bmatrix} \mathcal{C}(\bar{\rho})^T \\ \mathcal{D}(\bar{\rho})^T \end{bmatrix} P_{(d)}(*) \preceq 0, \tag{3.26}$$

then, the state trajectories generated by the dynamics (3.25) with any $\psi \in \mathcal{S}(m, L)$ remain bounded and the output trajectory y converges exponentially to the minimizer y_{opt} of ψ with rate α, i.e., $\exists \kappa \geqslant 0$ such that $||y(t) - y_{\text{opt}}|| \leqslant \kappa e^{-\alpha t}$ holds for all $t \geqslant 0$.

Proof. Consider the equilibrium η_*, $u_* = 0$, y_{opt} such that for any trajectory $\rho : [0, \infty) \to \mathcal{P}$,

$$\begin{aligned} 0 &= A_G(\rho(t))\eta_*, \\ y_{\text{opt}} &= C_G(\rho(t))\eta_*, \\ 0 &= \nabla\psi(y_{\text{opt}}). \end{aligned} \tag{3.27}$$

Note that since the system $G(\rho)$ has the structure depicted in Fig. 3.1, it contains an integrator. Therefore, by following the same arguments as in [Scherer and Ebenbauer, 2021, Theorem 2.1], the existence of an equilibrium η_* satisfying the equations (3.27) is guaranteed by quadratic detectability, i.e., if there exists a matrix L_o such that $(A_G(\bar{\rho}) + L_o C_G(\bar{\rho}))$ is Hurwitz for

all $\bar{\rho} \in \mathcal{P}$. Note that the $(1,1)$ block of LMI (3.26) ensures that there exists an $\mathcal{X}_G \succ 0$ such that

$$A_G(\bar{\rho})^T \mathcal{X}_G + \mathcal{X}_G A_G(\bar{\rho}) - C_G(\bar{\rho})^T C_G(\bar{\rho}) \prec 0,$$

which implies that the detectability condition [Caverly and Forbes, , Section 3.12.1] is verified so that the existence of the equilibrium is established. Now let $\xi = \begin{bmatrix} \eta - \eta_* \\ x_\pi \end{bmatrix}$, where η is the state of $G(\rho)$, x_π is the filter state and η_* is the equilibrium defined above. For any trajectory ρ, such that, $\rho(t) \in \mathcal{P} \quad \forall t \in [0, \infty)$, the dynamics of ξ can be represented by

$$\begin{aligned} \dot{\xi} &= \mathcal{A}(\rho(t))\xi + \mathcal{B}(\rho(t))\tilde{u}, \qquad \xi(0) = [\tilde{\eta}_0^T \quad \mathbf{0}]^T, \\ \tilde{z} &= \mathcal{C}(\rho(t))\xi + \mathcal{D}(\rho(t))\tilde{u}. \end{aligned} \tag{3.28}$$

Since (3.28) is the serial interconnection $(\pi_{m,L} \otimes I_d) \begin{bmatrix} G(\rho) \\ I \end{bmatrix}$, the output $\tilde{z}$ of (3.28) can be obtained from (3.22) with signals $\tilde{u}$ and $\tilde{y}$, where $\tilde{y}$ is the output of $G(\rho)$ for input $\tilde{u}$. Furthermore, dynamics (3.25) imply that $\tilde{u}, \tilde{y}$ satisfy $\tilde{u} = \nabla\psi(\tilde{y} + y_{\text{opt}})$. Hence, Theorem 3.2 implies

$$\int_0^T e^{2\alpha t} \tilde{z}^T(t)(P \otimes I_d)\tilde{z}(t)dt \geqslant 0 \quad \forall P \in \mathbb{P}, \forall T \geqslant 0. \tag{3.29}$$

Define a storage function $V(\xi) = \xi^T \mathcal{X} \xi$. Using (3.28), (3.26) and the assumption that $\rho(t) \in \mathcal{P} \quad \forall t \in [0, \infty)$, we get

$$\begin{aligned} &\frac{d}{dt}(V(\xi(t))) + 2\alpha V(\xi(t)) \\ &= \begin{bmatrix} \xi & \tilde{u} \end{bmatrix} \begin{bmatrix} \mathcal{A}(\rho(t))^T \mathcal{X} + \mathcal{X}\mathcal{A}(\rho(t)) + 2\alpha\mathcal{X} & \mathcal{X}\mathcal{B}(\rho(t)) \\ \mathcal{B}(\rho(t))^T \mathcal{X} & \mathbf{0} \end{bmatrix} \begin{bmatrix} \xi \\ \tilde{u} \end{bmatrix} \\ &\leqslant - \begin{bmatrix} \xi & \tilde{u} \end{bmatrix} \begin{bmatrix} \mathcal{C}(\rho(t))^T \\ \mathcal{D}(\rho(t))^T \end{bmatrix} (P \otimes I_d) \begin{bmatrix} \mathcal{C}(\rho(t)) & \mathcal{D}(\rho(t)) \end{bmatrix} \begin{bmatrix} \xi \\ \tilde{u} \end{bmatrix} \\ &= -\tilde{z}^T(t)(P \otimes I_d)\tilde{z}(t). \end{aligned}$$

Rearranging, multiplying by $e^{2\alpha t}$ and integrating from 0 to T, we obtain

$$\begin{aligned} \frac{d}{dt}(e^{2\alpha t} V(\xi(t))) + e^{2\alpha t} \tilde{z}^T(t)(P \otimes I_d)\tilde{z}(t) \leqslant 0, \\ e^{2\alpha T} V(\xi(T)) + \int_0^T e^{2\alpha\tau} \tilde{z}^T(\tau)(P \otimes I_d)\tilde{z}(\tau)d\tau \leqslant V(\xi(0)). \end{aligned}$$

Using (3.29) and $\mathcal{X} succ 0$, we get that $V(\xi(t)) \leqslant e^{-2\alpha T} V(\xi(0))$ implying $||\tilde{y}(T)|| \leqslant ||C_G|| \sqrt{\text{cond}(\mathcal{X})} ||\xi(0)|| e^{-\alpha T}$ for all $T \geqslant 0$. □

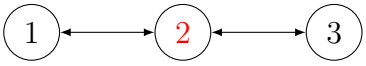

Figure 3.6: Example graph with agent 2 as the informed agent for illustration of Definition 3.2 and Lemma 3.5.

An attempt to apply Theorem 3.3 to Problem 3.1 when $N > 1$ prompts the following questions:

1. Is $f_c \in \mathcal{S}(m, L)$ for some m, L if $\psi \in \mathcal{S}(m_\psi, L_\psi)$ for some m_ψ, L_ψ and how to verify it?

2. How to characterize minimizers of f_c?

3. The size of the LMI (3.24) grows with N, but has a lot of structure. Can we exploit this structure and derive equivalent LMIs independent of N?

These questions are addressed in Sections 3.2.4, 3.2.5 and 3.2.6, respectively.

3.2.4 Smoothness and Convexity Properties of f_c

For convenience, let us define two grounded Laplacians.

Definition 3.2. *For a given graph $\mathcal{G}$ of order N (with its corresponding Laplacian $\mathcal{L}$), a set of informed agents $\mathcal{V}_l$ and constants $0 < m_\psi \leqslant L_\psi$, let the grounded Laplacians $\mathcal{L}_s$ and $\mathcal{L}_b$ be defined by*

$$\mathcal{L}_s = \mathcal{L} + m_\psi E \text{ and } \mathcal{L}_b = \mathcal{L} + L_\psi E, \tag{3.30}$$

where E is a diagonal matrix with the i^{th} diagonal entry equal to 1 if $i \in \mathcal{V}_l$ and equal to 0 otherwise.

Remark 3.6. *To illustrate the compatibility with the conventional definition of grounded Laplacian from the literature, consider an undirected super graph $\mathcal{G}_s$ of the given graph $\mathcal{G}$ by adding an $(N+1)^{\text{th}}$ node which is grounded and has an edge with all informed agents in $\mathcal{V}_l$ with an edge weight m_ψ. The grounded Laplacian for $\mathcal{G}_s$ as defined in [Xia and Cao, 2017] then equals $\mathcal{L}_s$.*

To illustrate the above definition, consider a graph depicted in Fig. 3.6 where the informed agent 2 is shown in red. Furthermore, let constants

$m_\psi = 1$ and $L_\psi = 2$. The grounded Laplacians for this setup as defined above are given by

$$\mathcal{L}_s = \mathcal{L} + 1E = \begin{bmatrix} 1 & -1 & 0 \\ -1 & 2 & -1 \\ 0 & -1 & 1 \end{bmatrix} + \begin{bmatrix} 0 & 0 & 0 \\ 0 & 1 & 0 \\ 0 & 0 & 0 \end{bmatrix} = \begin{bmatrix} 1 & -1 & 0 \\ -1 & 3 & -1 \\ 0 & -1 & 1 \end{bmatrix},$$
$$\mathcal{L}_b = \mathcal{L} + 2E = \begin{bmatrix} 1 & -1 & 0 \\ -1 & 2 & -1 \\ 0 & -1 & 1 \end{bmatrix} + \begin{bmatrix} 0 & 0 & 0 \\ 0 & 2 & 0 \\ 0 & 0 & 0 \end{bmatrix} = \begin{bmatrix} 1 & -1 & 0 \\ -1 & 4 & -1 \\ 0 & -1 & 1 \end{bmatrix}.$$

Lemma 3.5. *For a given graph $\mathcal{G}$ of order N (with its corresponding Laplacian $\mathcal{L}$), a set of informed agents $\mathcal{V}_l$, a scalar field ψ, a formation reference vector $\hat{r}$ and constants m_ψ, L_ψ such that $0 < m_\psi \leqslant L_\psi$, let f_c be as defined in Definition 3.1 and $\mathcal{L}_s$, $\mathcal{L}_b$ be as defined in Definition 3.2. Then, for constants m, L such that $0 < m \leqslant L$, the following statements are equivalent:*

1) $f_c \in \mathcal{S}(m, L)$ for all $\psi \in \mathcal{S}(m_\psi, L_\psi)$,

2) $mI \preceq \mathcal{L}_s$ *and* $\mathcal{L}_b \preceq LI$.

Proof. From Definition 3.1 and u_ψ as defined in (3.5), we have, for any $x, y \in \mathbb{R}^{Nd}$,

$$(\nabla f_c(x) - \nabla f_c(y))^T(x - y) = (x - y)^T(\mathcal{L} \otimes I_d)(x - y) + (x - y)^T u_\psi,$$

where

$$(x - y)^T u_\psi = \sum_{i \in \mathcal{V}_l} (x_i - y_i)^T(\nabla\psi(x_i) - \nabla\psi(y_i)).$$

Let us first show that statement 2) implies statement 1). For any $\psi \in \mathcal{S}(m_\psi, L_\psi)$,

$$m_\psi ||x_i - y_i||^2 \leqslant (x_i - y_i)^T(\nabla\psi(x_i) - \nabla\psi(y_i)) \leqslant L_\psi ||x_i - y_i||^2.$$

Using Definition 3.2, this implies

$$(\nabla f_c(x) - \nabla f_c(y))^T(x - y) \leqslant (x - y)^T(\mathcal{L}_b \otimes I_d)(x - y) \tag{3.31}$$

and

$$(\nabla f_c(x) - \nabla f_c(y))^T(x - y) \geqslant (x - y)^T(\mathcal{L}_s \otimes I_d)(x - y). \tag{3.32}$$

Finally, $mI \preceq \mathcal{L}_s$, $\mathcal{L}_b \preceq LI$, equations (3.31), (3.32) and the fact that the spectrum of X and $X \otimes I$ is identical together imply that $f_c \in \mathcal{S}(m, L)$. The

reverse direction, i.e., statement 1) implies statement 2), can be shown by choosing the functions

$$\psi_s(z) = m_\psi ||z||^2 \text{ and } \psi_b(z) = L_\psi ||z||^2,$$

defining functions f_s and f_b using Definition 3.1 for functions ψ_s and ψ_b, respectively,

$$\begin{aligned} (\nabla f_s(x) - \nabla f_s(y))^T (x-y) &= (x-y)^T (\mathcal{L}_s \otimes I_d)(x-y), \\ (\nabla f_b(x) - \nabla f_b(y))^T (x-y) &= (x-y)^T (\mathcal{L}_b \otimes I_d)(x-y). \end{aligned} \tag{3.33}$$

This implies statement 2) using the fact that $f_s,\ f_b \in \mathcal{S}(m, L)$. □

Continuing our example from Fig. 3.6 with $m_\psi = 1$ and $L_\psi = 2$, observe that $0.2679 \cdot I \preceq \mathcal{L}_s \preceq \mathcal{L}_b \preceq 4.5616 \cdot I$, which implies because of Lemma 3.5 that $f_c \in \mathcal{S}(0.2679, 4.5616)$ for all $\psi \in \mathcal{S}(1, 2)$

The next lemma shows that Assumption 3.2 is necessary and sufficient for f to belong to $\mathcal{S}(m, L)$.

Lemma 3.6. *Let $0 < m_\psi \leqslant L_\psi$ be fixed. There exist constants m, L with $0 < m \leqslant L$ such that $f_c \in \mathcal{S}(m, L)$ for every $\psi \in \mathcal{S}(m_\psi, L_\psi)$ if and only if the graph $\mathcal{G}$ and the set of informed agents $\mathcal{V}_l$ satisfy Assumption 3.2.*

Proof. Let $\mathcal{G}$ and $\mathcal{V}_l$ satisfy Assumption 3.2. This implies that every connected component of $\mathcal{G}$ contains at least one node from $\mathcal{V}_l$. Therefore, $\mathcal{L}_s$ according to Definition 3.2, can be transformed with a permutation of node numbering (similarity transformation), into a block diagonal matrix with each diagonal block being a grounded Laplacian corresponding to each connected component. Since each diagonal block is a grounded Laplacian with at least one grounded node, the smallest eigenvalue m_i of each diagonal block is positive [Xia and Cao, 2017]. By defining m as the minimum over all m_i, we obtain $mI \preceq \mathcal{L}_s$ with $m > 0$. On the other hand, defining L as the maximum eigenvalue of $\mathcal{L}_b$, we obtain $\mathcal{L}_b \preceq LI$. Using Lemma 3.5, $mI \preceq \mathcal{L}_s$ and $\mathcal{L}_s \preceq LI$ implies $f_1 \in \mathcal{S}(m, L)$. This proves the first part of the lemma.

Let us now show the necessity of Assumption 3.2. Without loss of generality, let $v_1 \in \mathcal{V}$ be such that $\mathcal{G}$ contains no path from v_1 to any node in $\mathcal{V}_l$ and let $\mathcal{V}_1 = \{v_1, v_2, \cdots, v_{n_1}\}$ be the set of nodes that have a path from v_1. Thus, the grounded Laplacian $\mathcal{L}_s$ as defined in Definition 3.2 is a block diagonal matrix of the following form

$$\mathcal{L}_s = \begin{bmatrix} \mathcal{L}_1 & \mathbf{0} \\ \mathbf{0} & \mathcal{L}_g \end{bmatrix},$$

where $\mathcal{L}_1 \in \mathbb{R}^{n_1 \times n_1}$ is a Laplacian without any grounded nodes. Therefore, $\mathcal{L}\mathbf{1}_{n_1} = \mathbf{0}$. Hence, a $y \in \mathbb{R}^N$ can be constructed as $y = \begin{bmatrix}\mathbf{1}_{n_1}^T & \mathbf{0}\end{bmatrix}^T$, with the property that $||y||^2 > 0$ and $y^T\mathcal{L}_s y = 0$. Hence, there does not exist an $m > 0$ such that $mI \preceq \mathcal{L}_s$. From Lemma 3.5, this means that if Assumption 3.2 is violated, there does not exist an $m > 0$ such that $f_1 \in \mathcal{S}(m, L)$. □

3.2.5 Minimizers of f_c

Lemma 3.7 characterizes the minimizers for the case of consensus ($r = 0$) and formation control with a single informed agent ($|\mathcal{V}_l| = 1$) as depicted in Fig. 3.7 and only necessary conditions are obtained for the general case in Lemma 3.8.

Lemma 3.7. *Let ψ satisfy Assumption 3.1, $\mathcal{G}$ and $\mathcal{V}_l$ satisfy Assumption 3.2 and f_c be as defined in Definitions 3.1. Then the following statements hold:*

1) *If $r = 0$, then z is the minimizer of f_c if and only if $z = \mathbf{1}_N \otimes y_{\text{opt}}$.*
2) *If $\mathcal{V}_l = \{i\}$ for some $i \in \mathcal{V}$, then z is the minimizer of f_c if and only if $z_j = y_{\text{opt}} + (r_j - r_i)$ for all $j \in \mathcal{V}$.*

Proof. First, let $r = 0$. Using Definition 3.1, we get, for all $y \in \mathbb{R}^{Nd}$,

$$f_c(y) = \frac{1}{2}y^T\mathcal{L}_{(d)}y + \sum_{i\in\mathcal{V}_l}\psi(y_i) \geqslant \sum_{i\in\mathcal{V}_l}\psi(y_i) \geqslant |\mathcal{V}_l|\psi(y_{\text{opt}}),$$

where the first inequality is obtained by using the fact that the Laplacian $\mathcal{L}$ (and $(\mathcal{L}\otimes I_d)$) is positive semi-definite [Bullo, 2021] and the second inequality is obtained using Assumption 3.1. Since $\mathcal{L}\mathbf{1}_N = \mathbf{0}$, $f(\mathbf{1}_N \otimes y_{\text{opt}}) = |\mathcal{V}_l|\psi(y_{\text{opt}})$ which together with the above argument implies $f_c(y) \geqslant f_c(\mathbf{1}_N \otimes y_{\text{opt}})$ for all $y \in \mathbb{R}^{Nd}$, i.e., $\mathbf{1}_N \otimes y_{\text{opt}}$ minimizes f_c. Since Assumption 3.1 also implies uniqueness of the minimizer, this already completes the proof for part 1).

For part 2), let us assume without loss of generality that $1 \in \mathcal{V}_l$. Similar to the arguments in part 1), we get, for all $y \in \mathbb{R}^{Nd}$,

$$f_c(y) = \frac{1}{2}(y - r)^T\mathcal{L}_{(d)}(y - r) + \psi(y_1) \geqslant \psi(y_1) \geqslant \psi(y_{\text{opt}}).$$

Let $z_1 = y_{\text{opt}}$ and $z_j = y_{\text{opt}} + (r_j - r_1)$ as specified in the statement of the lemma. Thus, $z = (\mathbf{1}_N \otimes y_{\text{opt}}) + r - (\mathbf{1}_N \otimes r_1)$ and $z - r = \mathbf{1}_N \otimes (y_{\text{opt}} - r_1)$. Since $\mathcal{L}\mathbf{1}_N = \mathbf{0}$, $f_c(z) = \psi(z_1) = \psi(y_{\text{opt}})$ which implies $f_c(y) \geqslant f_c(z)$ for all $y \in \mathbb{R}^{Nd}$, i.e., z minimizes f. As in part 1), uniqueness of the minimizer (implied by Assumption 3.1) completes the proof for part 2).

□

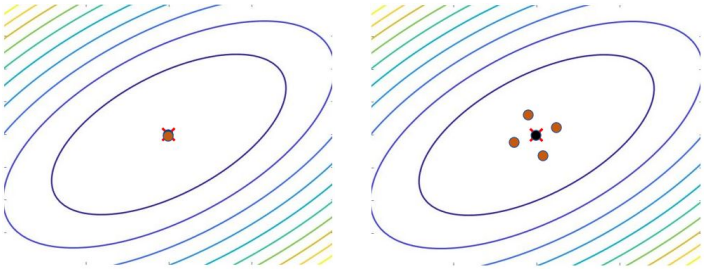

Figure 3.7: Sketch depicting the minimizers for the case of consensus ($r = 0$) (left) and formation control with a single informed agent ($|\mathcal{V}_l| = 1$) (right) considered in Lemma 3.7. Black solid circles represents the informed agents, orange solid circles represent the non-informed agents, red cross represents the minimizer of the field.

Remark 3.7. *Note that if r is chosen such that $r_i = 0$ for the informed agent $i \in \mathcal{V}_l$, then r just encodes the desired positions of the agents with the coordinate system such that the source and the informed agent are located at the origin (see Fig. 3.7 (right)).*

Remark 3.8. *Scenarios involving multiple informed agents and a non-zero formation reference $\hat{r}$ are difficult to characterize because the terms $\frac{1}{2}(y - r)^T \mathcal{L}_{(d)}(y - r)$ and $\sum_{i \in \mathcal{V}_l} \psi(y_i)$ have competing objectives. The equilibrium can thus result in a situation where none of the informed agents are at the source and agents are not at desired relative distances.*

Lemma 3.8. *Let ψ satisfy Assumption 3.1, $\mathcal{G}$ and $\mathcal{V}_l$ satisfy Assumption 3.2 and f_c be as defined in Definition 3.1 with z minimizing f_c. Then*

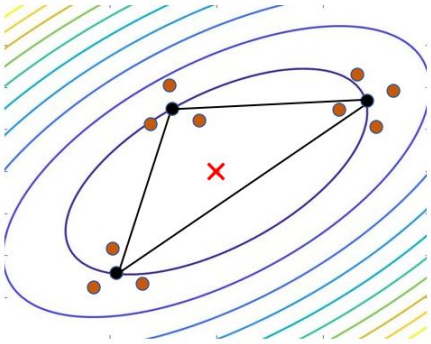

Figure 3.8: Sketch depicting minimizer for the case of a quadratic field. Black solid circles represents the informed agents, orange solid circles represent the non-informed agents, red cross represents the minimizer of the field as considered in Lemma 3.8 item 2).

$\{y|\nabla\psi(z_i)^T(z_i - y) \geqslant 0 \text{ for all } i \in \mathcal{V}_l\}$ *contains* y_{opt}. *Furthermore, we obtain the following stronger conclusions if* ψ *is quadratic or radially symmetric.*

1) *If* ψ *is radially symmetric around the source, i.e., it has the form* $\psi(y) = \psi_r(||y - y_{\text{opt}}||)$ *for some function* $\psi_r : \mathbb{R} \to \mathbb{R}$, *then the minimizer* z *of* f_c *is such that* y_{opt} *lies in the convex hull of* $\{z_i|i \in \mathcal{V}_l\}$.

2) *If* ψ *is quadratic, i.e., it has the form* $\psi(y) = y^TQy + b^Ty + c$, *then, the minimizer* z *of* f_c *satisfies* $y_{\text{opt}} = \frac{1}{|\mathcal{V}_l|}\sum_{i\in\mathcal{V}_l} z_i$, *i.e., the center of mass of informed agents is at the minimizer* y_{opt} *of* ψ *(see Fig. 3.8).*

Proof. Convexity of ψ implies that $\nabla\psi(y)(y - y_{\text{opt}}) \geqslant 0$ for all $y \in \mathbb{R}^d$. This implies that for any $z_i \in \mathbb{R}^d$, y_{opt} belongs to the half-space $\{y|\nabla\psi(z_i)(z_i - y) \geqslant 0\}$. Repeating this argument for each informed agent, we get that y_{opt} belongs to the intersection of N half-space defined above, i.e., $y_{\text{opt}} \in \{y|\nabla\psi(z_i)(z_i - y) \geqslant 0 \text{ for all } i \in \mathcal{V}_l\}$.

The proof for part 1) involves identical arguments to the ones used in the proof of Theorem 2.1 item 1) and are repeated here only for convenience. Assume that $\psi(y) = \psi_r(||y - y_{\text{opt}}||)$, which implies that if $y \neq y_{\text{opt}}$, $\nabla\psi(y) = \frac{\psi_r'(||y-y_{\text{opt}}||)}{||y-y_{\text{opt}}||}(y - y_{\text{opt}})$ and $\nabla\psi(y_{\text{opt}}) = 0$. Additionally, strong convexity of ψ implies $\psi_r'(||y - y_{\text{opt}}||) > 0$ for all $y \neq y_{\text{opt}}$. Using the fact that $\mathbf{1}_N$ is a left eigenvector of $\mathcal{L}$ with eigenvalue 0, we get

$$\begin{aligned}(\mathbf{1}_N^T \otimes I_d)\nabla f_c(z) &= \sum_{i\in\mathcal{V}_l} \nabla\psi(z_i) \\ &= \sum_{i\in\mathcal{V}_l, z_i\neq y_{\text{opt}}} \frac{\psi_r'(||z_i - y_{\text{opt}}||)}{||z_i - y_{\text{opt}}||}(z_i - y_{\text{opt}}).\end{aligned}$$

If z minimizes f_c, then $\nabla f_c(z) = 0$ and we obtain

$$0 = \sum_{i\in\mathcal{V}_l, z_i\neq y_{\text{opt}}} \frac{\psi_r'(||z_i - y_{\text{opt}}||)}{||z_i - y_{\text{opt}}||}(z_i - y_{\text{opt}}). \tag{3.34}$$

Now assume that y_{opt} does not belong to the convex hull of $\{z_i|i \in \mathcal{V}_l\}$. This implies that there is a separating hyperplane characterized by an $h \in \mathbb{R}^d$ and an offset $c_h \in \mathbb{R}$ such that $h^Tz_i + c_h \geqslant 0$ for all $i \in \mathcal{V}_l$ and $h^Ty_{\text{opt}} + c_h < 0$.

Multiplying both sides of equation (3.34) from the left by h^T, we get

$$\begin{aligned} 0 &= \sum_{i\in\mathcal{V}_l, z_i\neq y_{\text{opt}}} \frac{\psi_r'(||z_i - y_{\text{opt}}||)}{||z_i - y_{\text{opt}}||} h^T(z_i - y_{\text{opt}}) \\ &= \sum_{i\in\mathcal{V}_l, z_i\neq y_{\text{opt}}} \frac{\psi_r'(||z_i - y_{\text{opt}}||)}{||z_i - y_{\text{opt}}||} ((h^T z_i + c_h) - (h^T y_{\text{opt}} + c_h)) \\ &\geqslant \sum_{i\in\mathcal{V}_l, z_i\neq y_{\text{opt}}} -\frac{\psi_r'(||z_i - y_{\text{opt}}||)}{||z_i - y_{\text{opt}}||} (h^T y_{\text{opt}} + c_h). \end{aligned}$$

If $h^T y_{\text{opt}} + c_h < 0$, each term in the sum above is positive and we have a contradiction. Therefore, there exists no hyperplane separating $\{z_i | i \in \mathcal{V}_l\}$ and y_{opt} which implies that y_{opt} is in the convex hull of $\{z_i | i \in \mathcal{V}_l\}$.

For part 2) assume that $\psi(y) = \frac{1}{2} y^T Q y + b^T y + c$ which implies $\nabla\psi(y) = Qy + b$ and the unique minimizer is given by $y_{\text{opt}} = -Q^{-1}b$. Defining E to be a diagonal matrix of size N such that the i^{th} diagonal entry is equal to 1 if $i \in \mathcal{V}_l$ and equal to 0 otherwise, we get,

$$\nabla f_c(z) = (\mathcal{L} \otimes I_d)z + (E \otimes Q)z + (E\mathbf{1}_N) \otimes b. \tag{3.35}$$

Multiplying both sides from the left by $\mathbf{1}_N^T \otimes I_d$, and using the fact that $\mathbf{1}_N$ is a left eigenvector of $\mathcal{L}$ with eigenvalue 0, we get,

$$(\mathbf{1}_N^T \otimes I_d)\nabla f_c(z) = Q(\sum_{i\in\mathcal{V}_l} z_i) + |\mathcal{V}_l| b.$$

Finally, if z is a minimizer of f_c, then $\nabla f_c(z) = 0$ which implies $\frac{1}{\mathcal{V}_l}(\sum_{i\in\mathcal{V}_l} z_i) = -Q^{-1}b = y_{\text{opt}}$.

□

Remark 3.9. *One can construct examples of strongly convex non-quadratic and non-radially symmetric fields such that y_{opt} does not belong to the convex hull of $\{z_i | i \in \mathcal{V}_l\}$ showing that specializations of quadratic and radially symmetric cases in Lemma 3.8 cannot be extended to the general case without further assumptions on ψ. See Fig. 3.9 for a sketch of a non-smooth strongly convex example field.*

3.2.6 Decomposition of the Analysis Condition

This section finally addresses Remark 3.5. Using the structure of matrices in the LMI (3.24), it can be reduced without any additional conservatism

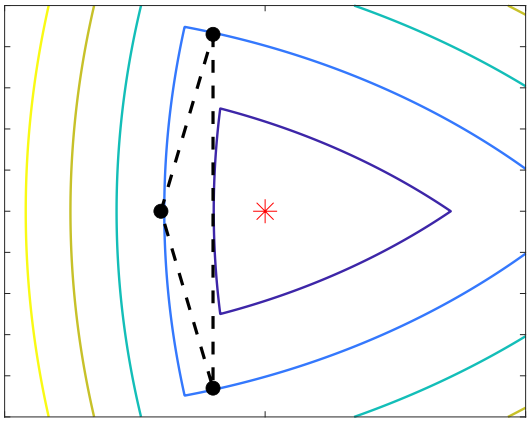

Figure 3.9: A sketch of a strongly convex (albeit non-differentiable) scalar field of the form $\psi(y) = \max(c_i^T y + b_i) + m||y||^2$ with an equilibrium configuration such that the source is outside the convex hull of agent positions (see Remark 3.9).

to a smaller LMI independent of N. Note that this is possible due to the specific diagonal and repeated structure of the multiplier and the plant and is common in the literature on robust control. The key idea is that once the uncertainty consisting of the interconnections is characterized by an IQC with a diagonal repeated multiplier, the nominal plant and the multiplier form repeated decoupled systems leading to repeated decoupled system matrices entering the verification LMIs.

Lemma 3.9. *The following statements are equivalent:*

1. $\exists \mathcal{X} \succ 0, P \in \mathbb{P}$ *such that* (3.24) *is satisfied.*
2. $\exists \mathcal{X}_0 \succ 0, P \in \mathbb{P}$ *such that*

$$\begin{bmatrix} \mathcal{A}_0^T \mathcal{X}_0 + \mathcal{X}_0 \mathcal{A}_0 + 2\alpha \mathcal{X}_0 & \mathcal{X}_0 \mathcal{B}_0 \\ \mathcal{B}_0^T \mathcal{X}_0 & \mathbf{0} \end{bmatrix} + \begin{bmatrix} \mathcal{C}_0^T \\ \mathcal{D}_0^T \end{bmatrix} P_{(d)}(*) \leq 0, \tag{3.36}$$

where $\left[\begin{array}{c|c} \mathcal{A}_0 & \mathcal{B}_0 \\ \hline \mathcal{C}_0 & \mathcal{D}_0 \end{array}\right] = (\pi_{m,L} \otimes I_d) \begin{bmatrix} G \\ I_d \end{bmatrix}$

Proof. It can be shown that there exist permutation matrices T_1, T_2 of appropriate dimensions such that $T_1^T (X \otimes I) T_2 = I \otimes X$ holds for any real matrix X [Magnus and Neudecker, 1979]. This can be used together with

the equivalence of LTI systems under similarity transformations to show that there exist permutation matrices T and T_π such that,

$$(\pi \otimes I_{Nd}) \begin{bmatrix} I_N \otimes G \\ I_{Nd} \end{bmatrix} = (I_{2(\nu+1)} \otimes T_\pi)(\left[\begin{array}{c|c} \mathcal{A}_0 & \mathcal{B}_0 \\ \hline \mathcal{C}_0 & \mathcal{D}_0 \end{array}\right] \otimes I_N)T. \tag{3.37}$$

Substituting in LMI (3.24) and using properties of the Kronecker products, the condition reduces to

$$\begin{bmatrix} (\mathcal{A}_0 \otimes I_N)^T \mathcal{X} + \mathcal{X}(\mathcal{A}_0 \otimes I_N) + 2\alpha\mathcal{X} & \mathcal{X}(\mathcal{B}_0 \otimes I_N)T \\ T^T(\mathcal{B}_0 \otimes I_N)^T \mathcal{X} & \mathbf{0} \end{bmatrix} \\ + (*)(P \otimes I_d \otimes I_N) \begin{bmatrix} (\mathcal{C}_0 \otimes I_N) & (\mathcal{D}_0 \otimes I_N)T \end{bmatrix} \preceq 0, \tag{3.38}$$

where we have used $(I_{2(\nu+1)} \otimes T_\pi)^T (P \otimes I_d \otimes I_N)(I_{2(\nu+1)} \otimes T_\pi) = (P \otimes I_d \otimes T_\pi^T T_\pi) = (P \otimes I_d \otimes I_N)$. Now, applying a congruence transformation using the permutation matrix $\begin{bmatrix} I & \mathbf{0} \\ \mathbf{0} & T^T \end{bmatrix}$, we obtain the following equivalent LMI,

$$\begin{bmatrix} (\mathcal{A}_0 \otimes I_N)^T \mathcal{X} + \mathcal{X}(\mathcal{A}_0 \otimes I_N) + 2\alpha\mathcal{X} & \mathcal{X}(\mathcal{B}_0 \otimes I_N) \\ (\mathcal{B}_0 \otimes I_N)^T \mathcal{X} & \mathbf{0} \end{bmatrix} \\ + \begin{bmatrix} (*)(P \otimes I_d) \begin{bmatrix} \mathcal{C}_0 & \mathcal{D}_0 \end{bmatrix} \otimes I_N \end{bmatrix} \preceq 0. \tag{3.39}$$

The equivalence between statements 1) and 2) can now be shown by making an argument exactly as in [Lessard et al., 2016, Section 4.2]. □

3.2.7 Main Robust Analysis Result

Before presenting the main result, let us define an appropriate uncertainty set for the dynamics (3.9). Let the underlying graph $\mathcal{G}$, the set of informed agents $\mathcal{V}_l$ and the external field ψ be such that f_c (see Definition 3.1) belongs to $\mathcal{S}(m, L)$. This can be verified by looking at spectrum of the grounded Laplacians defined in Definition 3.2 (see Lemma 3.5).

Definition 3.3.

$$\mathbf{\Delta}_{m,L} = \{(\mathcal{G}, \mathcal{V}_l, \psi) | f_c \in \mathcal{S}(m, L)\}. \tag{3.40}$$

Remark 3.10. *Note that with $\mathcal{V} = \mathcal{V}_l = \{1\}$ and $\mathcal{E} = \{\}$, we get $f_c = \psi$ and the setup reduces to the scenario of a single agent embedded in a scalar field.*

Theorem 3.10 (Analysis for Problem 3.1)**.** *Let graph $\mathcal{G}$, set of informed agents $\mathcal{V}_l$ and scalar field ψ be such that $(\mathcal{G}, \mathcal{V}_l, \psi) \in \mathbf{\Delta}_{m,L}$ for some $0 < m \leqslant L$. Let y_* be the minimizer of f_c. If $\exists \mathcal{X}_0 \succ 0, P \in \mathbb{P}$ such that* (3.36) *is satisfied, then the state trajectories generated under dynamics* (3.9) *remain bounded and the output trajectory y converges exponentially to y_* with rate α, i.e., $\exists \kappa \geqslant 0$ such that, $||y(t) - y_*|| \leqslant \kappa e^{-\alpha t}$ holds for all $t \geqslant 0$.*

Proof. Since $(\mathcal{G}, \mathcal{V}_l, \psi) \in \mathbf{\Delta}_{m,L}$, $f_c \in \mathcal{S}(m, L)$. Using the hypothesis of this theorem and Lemma 3.9, $\exists \mathcal{X} \succ 0, P \in \mathbb{P}$ such that (3.24) is satisfied. Finally, application of Theorem 3.3 completes the proof. □

3.3 Numerical Examples: Single Agent

3.3.1 Single Quadrotor in $\psi \in \mathcal{S}(1, L_\psi)$

A 12^{th} order linear model of a quadrotor is considered with an LQR-based state-feedback controller tuned for zero steady-state error for step references. See Appendix B.1 for more details on the quadrotor modeling and control. As discussed in Section 3.1, we let this closed-loop system be represented by state-space realization (3.1) and augment it with dynamics (3.2) to obtain the system G.

The following questions are addressed next to demonstrate the applicability of the theoretical results.

1 How robust is the given controller with respect to different fields $\psi \in \mathcal{S}(m_\psi, L_\psi)$?

2 How can the gain k_d be designed for the given closed-loop quadrotor system?

3 How conservative are the estimates of the convergence rates given by our analysis for static multipliers (circle criterion) and causal/anti-causal/non-causal ZF multipliers (See Remark 3.2)?

For fixed gains k_p and k_d and given closed-loop quadrotor dynamics, Fig. 3.10 shows the convergence rate estimates provided by different multipliers for fields $\psi \in \mathcal{S}(1, L_\psi)$ with increasing L_ψ. Since increasing L_ψ enlarges the set of allowable fields, i.e., $\mathcal{S}(1, L_1) \subseteq \mathcal{S}(1, L_2) \quad \forall L_1 \leqslant L_2$, the estimates are non-increasing with increasing L_ψ. It can be seen that while the circle criterion can certify stability ($\alpha \geqslant 0$) for fields $\psi \in \mathcal{S}(1, 5.1)$, the general non-causal ZF multipliers along with the ZF multipliers restricted to the causal case ($P_3 = 0$) can certify stability for all fields $\psi \in \mathcal{L}(1, 8.1)$. Furthermore, for each L_ψ,

$$\psi(x) = \frac{1}{2}(x - y_{\text{opt}})^T \begin{bmatrix} 1 & \\ & L_\psi \end{bmatrix} (x - y_{\text{opt}})$$

achieves the convergence rate guaranteed by the analysis showing that, in this example, the estimates are tight. The conservatism incurred by restricting the search to causal multipliers is minor in this example. Since performance

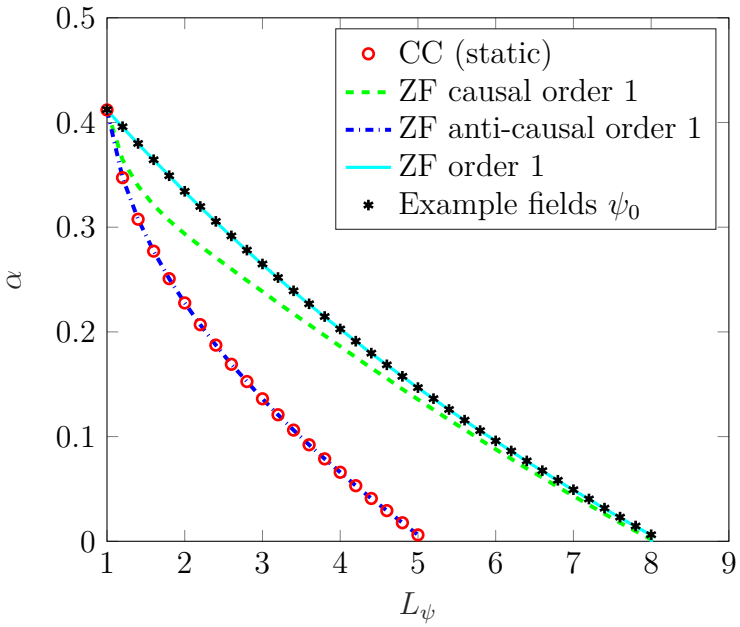

Figure 3.10: Convergence rate estimates for quadrotor dynamics provided by different multipliers (see Remark 3.2) for fields $\psi \in \mathcal{S}(1, L_\psi)$ and convergence rates for example fields $\psi_0(x) = \frac{1}{2}(x - y_{\text{opt}})^T \text{diag}(1, L_\psi)(x - y_{\text{opt}})$.

analysis was not included in Chapter 2, this example illustrates the extension to a non-conservative performance analysis. Note that this comes at the cost of the additional assumption of strong convexity of ψ (in comparison to only strict convexity as required in Chapter 2).

The effect of varying k_d on the performance estimates for a fixed allowable field set $\mathcal{S}(1, 10)$ is shown in Fig. 3.11, where $k_p = 1$. It shows that the highest convergence rate of 0.148 can be achieved for $k_d = 8.2$ and demonstrates a method for tuning the gains for optimal convergence rates. It can also be observed that tuning the gains by using static multipliers (circle criterion) would lead to a rather slower performance. Sample trajectories of a quadrotor locating the source at (-50,-50) is shown in Fig. 3.12, where k_d is chosen optimal with respect to the circle criterion (dashed lines) and ZF (solid lines). Although leading to a higher overshoot, the gains tuned with respect to ZF lead to faster convergence.

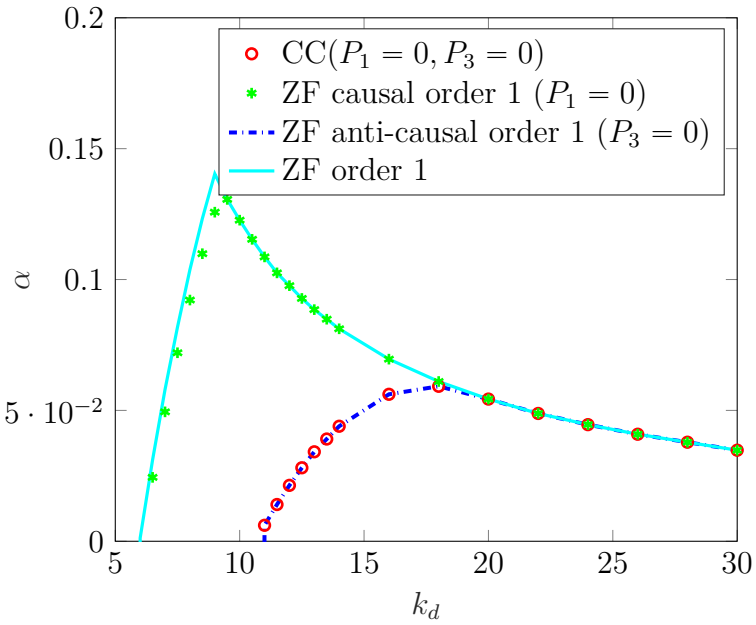

Figure 3.11: Performance estimates for quadrotor dynamics provided by different multipliers for $\psi \in \mathcal{S}(1, 10)$ and varying k_d.

3.3.2 Example Showing the Benefit of Non-Causal Multipliers

An academic example is now presented that brings out the benefit of using general non-causal multipliers over causal multipliers. Let $G(s) = 5\frac{(s-1)}{s(s^2+s+25)}$ and consider fields $\psi \in \mathcal{S}(1, L_\psi)$. The convergence rate estimates provided by different multipliers for increasing L are shown in Fig. 3.13. It can be seen that while the circle criterion and causal ZF multipliers certify stability for fields $\psi \in \mathcal{S}(1, 1.9)$, the anti-causal ZF multipliers can certify stability for fields $\psi \in \mathcal{S}(1, 2)$ and the general non-causal ZF multipliers can certify stability for fields $\psi \in \mathcal{S}(1, 2.4)$. Furthermore, convergence rates with $\psi_0(x) = \frac{1}{2}L_\psi x^2$ hit the convergence rate estimates showing that these estimates are tight. Note that the gap between the actual convergence rates for example fields and the estimates obtained from non-causal ZF multipliers for $L_\psi \in \{1.1, 1.2, \cdots, 1.6\}$ does not imply conservatism since the example field used at $L_\psi = 1$ is included for any larger L_ψ.

3.3.3 LPV Generic Vehicle Model

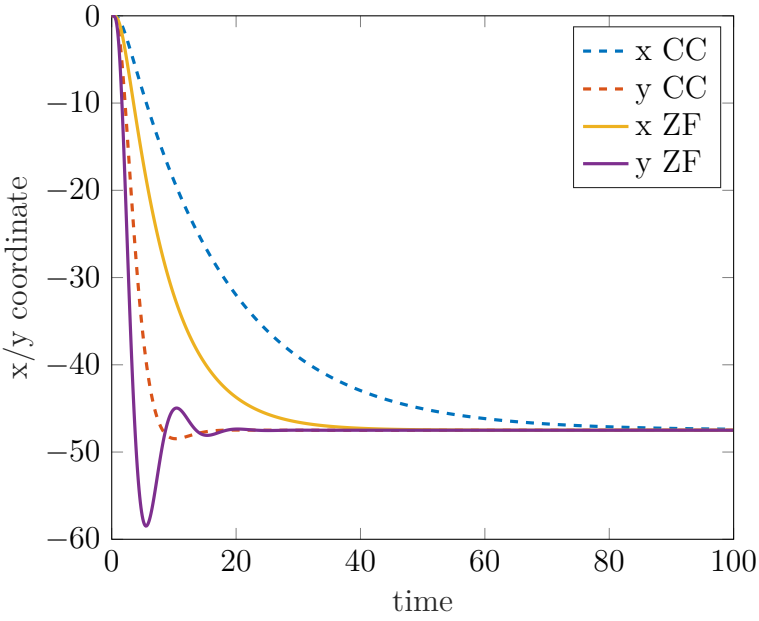

Figure 3.12: Sample trajectories of a quadrotor in a 2D-field with minimum at (-50,-50) with optimal k_d based on CC (dashed lines) and optimal k_d based on ZF (solid lines).

We now consider an LPV system $G(\rho)$ described by

$$\begin{aligned} \dot{x} &= v, \\ \dot{v} &= -\rho(t)v - u, \end{aligned} \tag{3.41}$$

where $\rho(t) \in \mathcal{P} = [0.8, 1.2] \quad \forall t \in [0, \infty)$. The scheduling parameter ρ can be seen as a time-varying or adaptive damping coefficient and can be either fixed and unknown or time-varying. It can be verified that (3.26) for this example is affine in $\bar{\rho}$ and hence satisfaction of the inequality for $\bar{\rho} = 0.8$ and $\bar{\rho} = 1.2$ implies the satisfaction for any $\bar{\rho} \in [0.8, 1.2]$ [Scherer and Weiland, 2000]. This reduces the condition (3.26) to a finite dimensional feasibility problem that is implemented to produce the results discussed next. Figure 3.14 shows the convergence rate estimates provided by different multipliers for fields $\psi \in \mathcal{S}(1, L_\psi)$ with increasing L_ψ. As in the previous examples, example fields (quadratic) are chosen to get an upper bound on the convergence rate. The reduction in conservatism with increasing order of multiplier can be clearly seen. For this example, fifth order ZF multipliers show negligible conservatism. This analysis essentially guarantees that for this chosen example, poorly conditioned fields do not affect the convergence rate. For constant trajectories, i.e., $\rho(t) = \bar{\rho} \in [0.8, 1.2] \quad \forall t$, and for quadratic fields

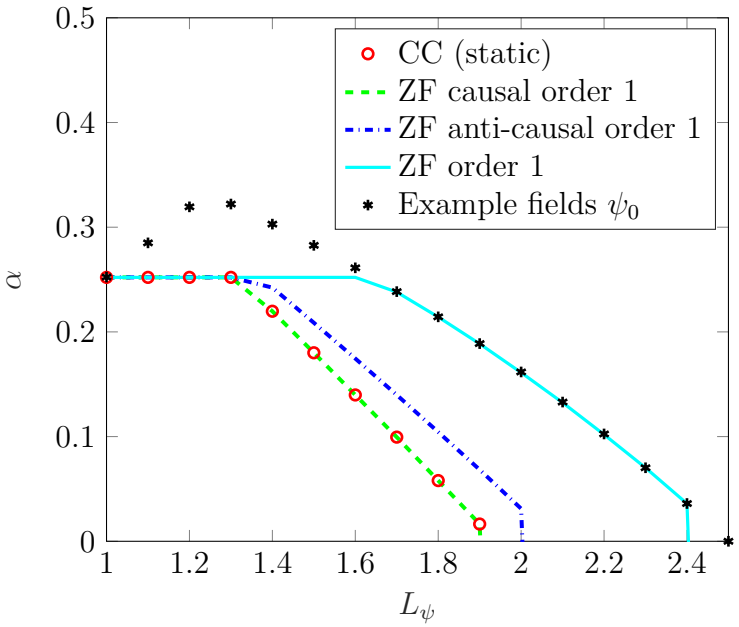

Figure 3.13: Convergence rate estimates for $G(s) = \frac{5(s-1)}{s(s^2+s+25)}$ provided by different multipliers (see Remark 3.2) for fields $\psi \in \mathcal{S}(1, L_\psi)$ and convergence rates for example fields $\psi_0(x) = \frac{1}{2}L_\psi x^2$.

(linear gradients), a root-locus argument can be used to show that $\alpha = 0.4$ for any $L_\psi \geqslant m_\psi$. With the current performance analysis, we can see that this holds even for any non-constant trajectories ρ restricted to the allowable parameter range and for any strongly convex field $\psi \in \mathcal{S}(m_\psi, L_\psi)$. This example also illustrates the benefit of non-causal multipliers over causal ones and the reduction in conservatism with increasing order of the ZF multiplier.

3.3.4 Quadrotor with two Modes

The next scenario is that of a quadrotor, as in Section 3.3.1, but with two operating modes. One operating mode corresponds to the quadrotor carrying some load and the other mode corresponds to no-load. This is modeled by considering two masses $m \in \{0.2, 2\}$ with LQR controllers designed as in Section 3.3.1 for each mode separately. Consider an arbitrary switching between the two modes and this can be modeled as an LPV (or switching) system with $\mathcal{P} = \{1, 2\}$ and $\rho(t) \in \mathcal{P} \quad \forall t$. Figure 3.15 shows the convergence rate estimates provided by different multipliers for fields $\psi \in \mathcal{S}(1, L_\psi)$. In comparison to the LTI case (Fig. 3.10 from Section 3.3.1), the performance is

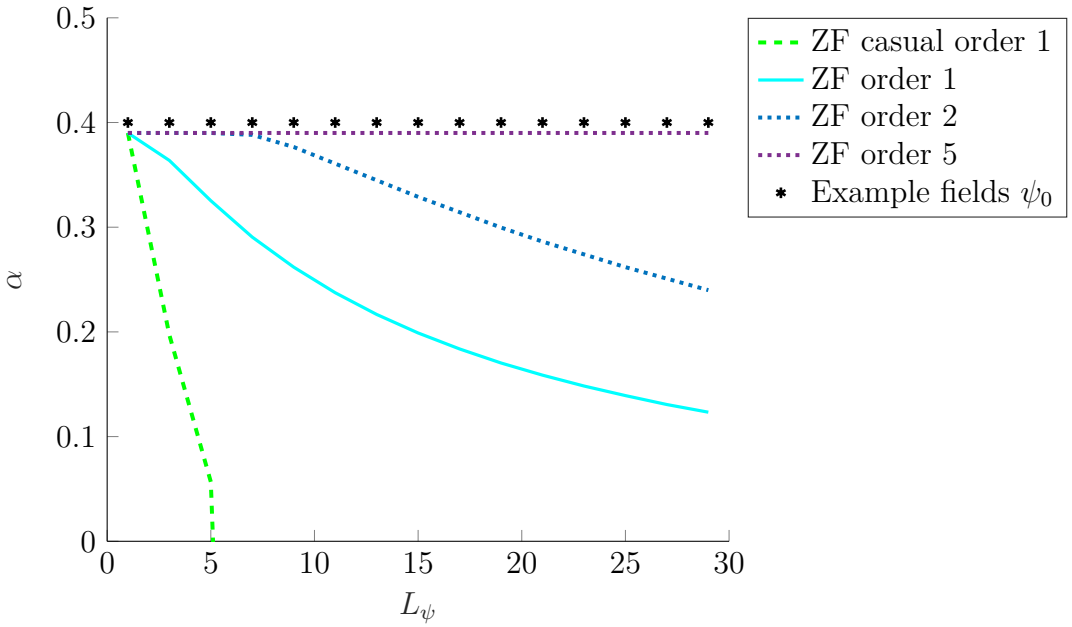

Figure 3.14: Convergence rate estimates for LPV system (3.41) provided by different multipliers (see Remark 3.2) for fields $\psi \in \mathcal{S}(1, L_\psi)$ and convergence rates for example fields $\psi_0(x) = \frac{1}{2}(x - y_{\text{opt}})^T \text{diag}(1, L_\psi)(x - y_{\text{opt}})$.

slightly reduced due to the possibility of arbitrary switching between modes. Furthermore, the estimates with first-order ZF multipliers are not tight anymore and better results are obtained with second-order ZF multipliers. No further improvement in the estimates was observed up to 5th order ZF multipliers.

3.4 Numerical Examples: Formation Control

The LQR-based quadrotor model considered in Section 3.3.1 is now used in a scenario with multiple quadrotors embedded in a field ψ with a given communication graph $\mathcal{G}$ and a set of informed agents $\mathcal{V}_l$. This scenario is posed in Problem 3.1 and the conservatism involved in the analysis condition is first investigated for this example. Assume that the bounds on the spectrum of Laplacians are known for the conservatism analysis in Section 3.4.1. When the bounds on the spectrum of the Laplacians are unknown, these bounds could be estimated using the maximum degree, a minimal graph consisting of edges that are present in all allowable graphs, the set of informed agents and the constants m_ψ, L_ψ from the assumption on $\psi \in \mathcal{S}(m_\psi, L_\psi)$. This is

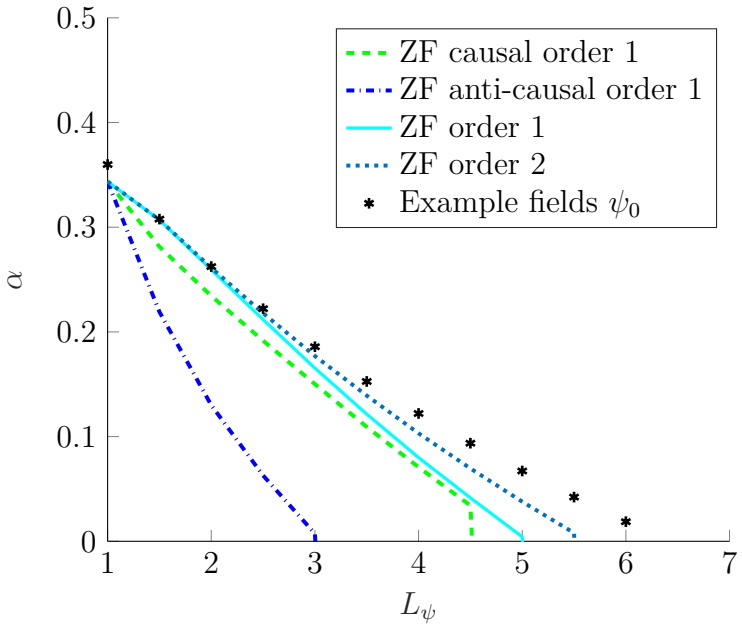

Figure 3.15: Convergence rate estimates for quadrotor dynamics with uncertain or switching mass $m \in \{0.2, 2\}$ provided by different multipliers (see Remark 3.2) for fields $\psi \in \mathcal{S}(1, L_\psi)$ and convergence rates for fields $\psi_0(x) = \frac{1}{2}(x - y_{\text{opt}})^T \text{diag}(1, L_\psi)(x - y_{\text{opt}})$.

considered in Section 3.4.2. For convenience, let the star and the cycle graphs be denoted by

$$\mathcal{G}^N_{\text{star}} = (\{1, \cdots, N\}, \{(1,1), \cdots, (1,N)\}),$$
$$\mathcal{G}^N_{\text{cycle}} = (\{1, \cdots, N\}, \{(1,2), (2,3), \cdots, (N-1,N), (N,1)\}).$$

3.4.1 Conservatism Analysis: Known Laplacian Spectrum

The theoretical results are applied to the uncertainty set

$$\mathbf{\Delta}_{0.3,L} = \{(\mathcal{G}, \mathcal{V}_l, \psi) | f_c \in \mathcal{S}(0.3, L)\}.$$

In order to estimate the conservatism, worst-case examples are sought and presented along with the performance guarantees given by the theory. For this purpose, define

$$\Delta_1 = \{(\mathcal{G}, \mathcal{V}_l, \psi) | \mathcal{G} = \mathcal{G}^5_{\text{star}}, \mathcal{V}_l = \{1\}, \psi \in \mathcal{S}(m_\psi, L_\psi)\}. \tag{3.42}$$

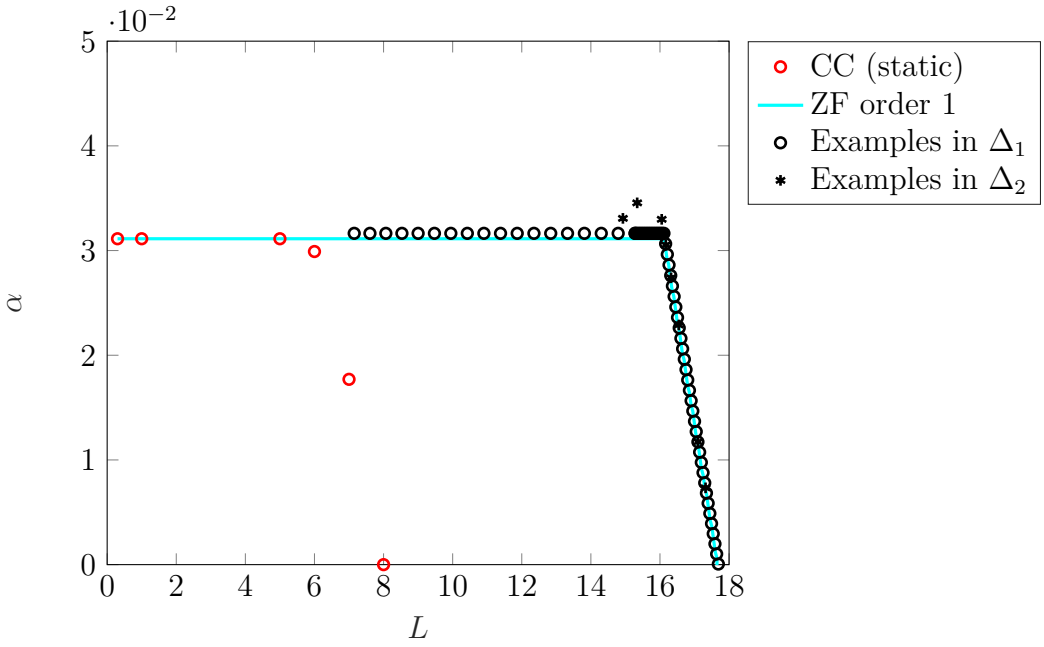

Figure 3.16: Convergence rate estimates for quadrotor dynamics under formation control provided by different multipliers (see Remark 3.2) for $f_c \in \mathcal{S}(0.3, L)$ and convergence rates for examples in Δ_1 and Δ_2.

The graph is kept fixed to a star graph in Δ_1 with the first agent as the informed agent and the central node in the star topology. Constants m_ψ and L_ψ are chosen such that $\Delta_1 \subseteq \mathbf{\Delta}_{m,L}$. Let Δ_2 be constructed with a fixed scalar field and graphs $\mathcal{G}^{25}$ consisting of 25 nodes such that $\Delta_2 \subseteq \mathbf{\Delta}_{m,L}$, i.e.,

$$\Delta_2 = \{(\mathcal{G}^{25}, \mathcal{V}_l, \psi) | \psi = 1.85||y - y_*||^2\}. \tag{3.43}$$

Figure 3.16 shows the exponential performance estimates for increasing L guaranteed by the ZF multipliers and the circle criterion along with some examples that achieve the worst case performance bounds. It can be noted that while the circle criterion can certify stability for any $(\mathcal{G}, \mathcal{V}_l, \psi)$ such that $f_c \in \mathcal{S}(0.3, 7)$, the ZF multipliers can certify stability for any $(\mathcal{G}, \mathcal{V}_l, \psi)$ such that $f_c \in \mathcal{S}(0.3, 17.64)$. Examples achieving the worst case performance show that performance estimates given by the ZF multipliers are tight in this example.

3.4.2 Robust Analysis: Unknown Laplacian Spectrum

If the spectrum of the Laplacian is unknown, it can be estimated by using some structural properties of the graph. Assume that $\psi \in \mathcal{S}(m_\psi, L_\psi)$ and a

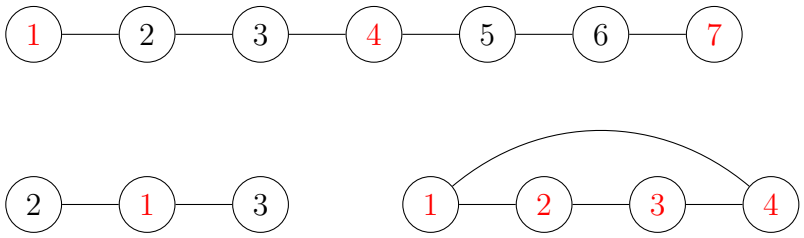

Figure 3.17: Three examples of graphs satisfying Assumption 3.3 where the informed agents are shown in red and worst case examples from the set Δ_3 (bottom right) and Δ_4 (bottom left) defined in (3.44).

minimal structure in the graph is known in the form of essential edges that are present in all allowable graphs. This means that all allowable graphs could be obtained by adding edges to the minimal graph. Let the graph Laplacian associated with this minimal graph be denoted by $\mathcal{L}_0$. As defined in 3.2, let the grounded graph Laplacian associated with this minimal graph be denoted by $\mathcal{L}_m = \mathcal{L}_0 + m_\psi E$. Using the fact that adding edges can only increase the eigenvalues of the graph Laplacian (see Lemma 6.9 from [Bullo, 2021]), we have that $\mathcal{L}_m = \mathcal{L}_0 + m_\psi E \preceq \mathcal{L} + m_\psi E = \mathcal{L}_s$. Furthermore, assuming that the maximum degree, denoted by $d_{\max}$, is known and using the fact that $2d_{\max}$ is an upper bound on the largest eigenvalue of the graph Laplacian (apply Geršgorin Disks theorem [Bullo, 2021, Theorem 2.8]) together with $\psi \in \mathcal{S}(m_\psi, L_\psi)$, we get, $\mathcal{L}_b \preceq (2d_{\max} + L_\psi) I_N$. The uncertainty set can then be defined to be $\mathbf{\Delta}_{m,L}$ with $m = \lambda_{\min}(\mathcal{L}_m)$ and $L = (2d_{\max} + L_\psi)$.

This is now illustrated on a concrete example. Let $\mathbf{\Delta}$ be the set of all $(\mathcal{G}, \mathcal{V}_l, \psi)$ that satisfy the Assumption 3.3 (see Fig. 3.17).

Assumption 3.3. *1. At least one third of total number of agents are informed agents (have access to the gradient).*

2. Every agent that is not an informed agent has an edge with at least one informed agent.

3. Maximum degree of all agents is 2*.*

4. $\psi \in \mathcal{S}(3, L_\psi)$*.*

As outlined in the paragraph above, a minimal Laplacian for graphs satisfying the above properties needs to be constructed. Since any informed agent $i \in \mathcal{V}_l$ is either connected to 0, 1 or 2 other agents, a suitable ordering of the agents will lead to a minimal grounded Laplacian of the form

$\mathcal{L}_m = \text{blkdiag}(m_\psi I, \mathcal{L}_1, \cdots, \mathcal{L}_1, \mathcal{L}_2, \cdots, \mathcal{L}_2)$, where

$$\mathcal{L}_1 = \begin{bmatrix} 1+m_\psi & -1 \\ -1 & 1 \end{bmatrix}, \mathcal{L}_2 = \begin{bmatrix} 2+m_\psi & -1 & -1 \\ -1 & 1 & 0 \\ 0 & -1 & 1 \end{bmatrix}.$$

Therefore,

$$\begin{aligned} m &= \lambda_{\min}(\mathcal{L}_m) = \min(m_\psi, \lambda_{\min}(\mathcal{L}_1), \lambda_{\min}(\mathcal{L}_2)) = 0.4116, \\ L &= L_\psi + 2 * d_{\max} = L_\psi + 4. \end{aligned}$$

In other words, $\mathbf{\Delta} \subseteq \mathbf{\Delta}_{0.4116, L_\psi+4}$. Figure 3.18 shows performance curves for increasing values of L_ψ. As in previous examples, worst-case examples that achieve the theoretical estimates are found showing again that the analysis is without any conservatism. The worst case examples are found here in the sets $\Delta_3 \subseteq \mathbf{\Delta}$ and $\Delta_4 \subseteq \mathbf{\Delta}$, given by,

$$\begin{aligned} \Delta_3 &= \{(\mathcal{G}, \mathcal{V}_l, \psi) | \mathcal{G} = \mathcal{G}^4_{\text{cycle}}, \mathcal{V}_l = \mathcal{V}, \psi = \psi_0\}, \\ \Delta_4 &= \{(\mathcal{G}, \mathcal{V}_l, \psi) | \mathcal{G} = \mathcal{G}^3_{\text{star}}, \mathcal{V}_l = \{1\}, \psi = \psi_0\}, \end{aligned} \tag{3.44}$$

where

$$\psi_0(x) = (x - y_{\text{opt}})^T \begin{bmatrix} 3 & \\ & L_\psi \end{bmatrix} (x - y_{\text{opt}}).$$

It is emphasized that the robust analysis demonstrated here requires no knowledge of the spectrum but general structural properties that can be verified locally by every agent in a distributed manner.

3.5 Robustness Against Noisy Gradients

This section demonstrates how information about noise involved in the gradient measurements can be incorporated in the analysis. For simplicity, it is assumed that $N = 1$, i.e., there is a single agent measuring a noisy gradient as $u_n(t) = \nabla\psi(y(t)) + e(t)$ with multiplicative noise e such that the overall vehicle dynamics from u to y denoted by G, can be represented by

$$\begin{aligned} \dot{\eta}(t) &= A_G\eta(t) + B_G u(t) + B_G e(t), \qquad \eta(0) = \eta_0, \\ y(t) &= C_G\eta(t), \\ u(t) &= \nabla\psi(y(t)). \end{aligned} \tag{3.45}$$

The knowledge about the multiplicative noise is assumed to be available in the form of the following assumption.

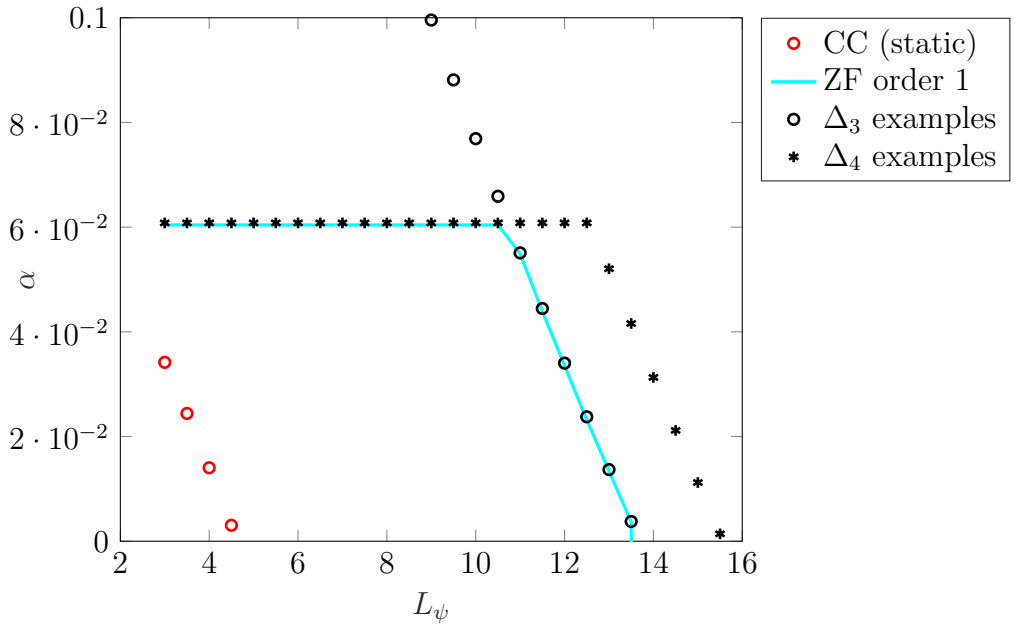

Figure 3.18: Convergence rate estimates for quadrotor dynamics under formation control provided by different multipliers (see Remark 3.2) for fields $(\mathcal{G}, \mathcal{V}_l, \psi)$ satisfying Assumption 3.3 and convergence rates for examples in Δ_3 and Δ_4.

Assumption 3.4. *For a non-negative constant δ and arbitrary trajectories $y(t)$ and $e(t)$ under dynamics (3.45), let $||e(t)|| \leqslant \delta||\nabla\psi(y(t))||$, i.e.,*

$$\begin{bmatrix} e(t) \\ \nabla\psi(y(t)) \end{bmatrix}^T \begin{bmatrix} -I_d & 0 \\ 0 & \delta^2 I_d \end{bmatrix} \begin{bmatrix} e(t) \\ \nabla\psi(y(t)) \end{bmatrix} \geqslant 0 \qquad \text{for all } t \geqslant 0. \tag{3.46}$$

The following theorem provides a performance analysis of dynamics (3.45).

Theorem 3.11. *Let the multiplicative noise e satisfy Assumption 3.4. If there exists $\mathcal{X} \succ 0$, $P \in \mathbb{P}$, $\alpha > 0$ and $\lambda \geqslant 0$ such that*

$$\begin{bmatrix} \mathcal{A}^T\mathcal{X} + \mathcal{X}\mathcal{A} + 2\alpha\mathcal{X} & (*) \\ \mathcal{B}^T\mathcal{X} & \mathbf{0} \end{bmatrix} + (*) \begin{bmatrix} P \otimes I_d & \\ & \lambda M \end{bmatrix} \begin{bmatrix} \mathcal{C}_1 & \mathcal{D}_1 \\ \mathcal{C}_2 & \mathcal{D}_2 \end{bmatrix} \preceq 0, \tag{3.47}$$

where $\left[\begin{array}{c|c} \mathcal{A} & \mathcal{B} \\ \hline \mathcal{C}_1 & \mathcal{D}_1 \\ \mathcal{C}_2 & \mathcal{D}_2 \end{array}\right] = \left[\begin{array}{cc} \pi_{m_\psi, L_\psi} \otimes I_d & 0 \\ 0 & I_{2d} \end{array}\right] \left[\begin{array}{c|cc} A_G & B_G & B_G \\ \hline C_G & \mathbf{0} & \mathbf{0} \\ \mathbf{0} & I_d & \mathbf{0} \\ \hline \mathbf{0} & \mathbf{0} & I_d \\ \mathbf{0} & I_d & \mathbf{0} \end{array}\right]$ *and*

$$M = \begin{bmatrix} -I_d & 0 \\ 0 & \delta^2 I_d \end{bmatrix},$$

then the state trajectories generated by the dynamics (3.45) *with any* $\psi \in \mathcal{S}(m, L)$ *remain bounded and the output trajectory* y *converges exponentially to the minimizer* y_{opt} *of* ψ *with rate* α*, i.e.,* $\exists \kappa \geqslant 0$ *such that* $||y(t) - y_{\text{opt}}(t)|| \leqslant \kappa e^{-\alpha t}$ *holds for all* $t \geqslant 0$*.*

Proof. Similar to the proof of Theorem 3.4, let $\xi = \begin{bmatrix} \eta - \eta_* \\ x_\pi \end{bmatrix}$, where η is the state of G, x_π is the filter state and η_* is the equilibrium state satisfying

$$\begin{aligned} 0 &= A_G \eta_*, \\ y_{\text{opt}} &= C_G \eta_*, \\ 0 &= \nabla \psi(y_{\text{opt}}). \end{aligned} \tag{3.48}$$

Since $\nabla \psi(y_{\text{opt}}) = 0$, $\tilde{u} = u$ and therefore $\tilde{e} = e$. The dynamics of ξ can be represented by

$$\begin{aligned} \dot{\xi} &= \mathcal{A}\xi + \mathcal{B}\begin{bmatrix} u \\ e \end{bmatrix}, \qquad \xi(0) = [\tilde{\eta}_0^T \quad \mathbf{0}]^T, \\ \begin{bmatrix} \tilde{z} \\ e \\ u \end{bmatrix} &= \begin{bmatrix} \mathcal{C}_1 \\ \mathcal{C}_2 \end{bmatrix} \xi + \begin{bmatrix} \mathcal{D}_1 \\ \mathcal{D}_2 \end{bmatrix} \begin{bmatrix} u \\ \tilde{e} \end{bmatrix}, \end{aligned} \tag{3.49}$$

where $\tilde{z}$ can be obtained from (3.22) with signals $\tilde{u}$ and $\tilde{y}$, where $\tilde{y}$ is the output of G for input $\tilde{u}$. Furthermore, dynamics (3.45) imply that $\tilde{u}, \tilde{y}$ satisfy $\tilde{u} = \nabla \psi(\tilde{y} + y_{\text{opt}})$. Hence, Theorem 3.2 implies

$$\int_0^T e^{2\alpha t} \tilde{z}^T(t)(P \otimes I_d)\tilde{z}(t)dt \geqslant 0 \quad \forall P \in \mathbb{P}, \forall T \geqslant 0. \tag{3.50}$$

Define a storage function $V(\xi) = \xi^T \mathcal{X} \xi$. Using (3.47), we get,

$$\begin{aligned} \frac{d}{dt}(V(\xi(t))) + 2\alpha V(\xi(t)) &= (*) \begin{bmatrix} \mathcal{A}^T\mathcal{X} + \mathcal{X}\mathcal{A} + 2\alpha\mathcal{X} & \mathcal{X}\mathcal{B} \\ \mathcal{B}^T\mathcal{X} & \mathbf{0} \end{bmatrix} \begin{bmatrix} \xi(t) \\ \tilde{u}(t) \\ e(t) \end{bmatrix} \\ &\leqslant -(*) \begin{bmatrix} P \otimes I_d & \\ & \lambda M \end{bmatrix} \begin{bmatrix} \mathcal{C}_1 & \mathcal{D}_1 \\ \mathcal{C}_2 & \mathcal{D}_2 \end{bmatrix} \begin{bmatrix} \xi(t) \\ \tilde{u}(t) \\ e(t) \end{bmatrix} \\ &= -\tilde{z}^T(t)(P \otimes I_d)\tilde{z}(t) - \lambda \begin{bmatrix} e^T & u^T \end{bmatrix} M \begin{bmatrix} e \\ u \end{bmatrix} \\ &\leqslant -\tilde{z}^T(t)(P \otimes I_d)\tilde{z}(t), \end{aligned}$$

where the last inequality follows from Assumption 3.4. Rearranging, multiplying by $e^{2\alpha t}$ and integrating from 0 to T, we obtain,

$$\frac{d}{dt}(e^{2\alpha t}V(\xi(t))) + e^{2\alpha t}\tilde{z}^T(t)(P \otimes I_d)\tilde{z}(t) \leqslant 0,$$
$$e^{2\alpha T}V(\xi(T)) + \int_0^T e^{2\alpha t}\tilde{z}^T(t)(P \otimes I_d)\tilde{z}(t)dt \leqslant V(\xi(0)).$$

Using (3.50) and $\mathcal{X} \succ 0$, we get that $V(\xi(T)) \leqslant e^{-2\alpha T}V(\xi(0))$ implying $||\tilde{y}(T)|| \leqslant ||C_G||\sqrt{\text{cond}(\mathcal{X})}||\xi(0)||e^{-\alpha T}$ for all $T \geqslant 0$. □

3.5.1 Numerical Example

Consider again, the quadrotor example from Section 3.3.1 but now with noisy gradient measurements. Let δ vary in the set $\{0.1, \cdots, 0.9\}$. Figure 3.11 is now reproduced using Theorem 3.11 for each of the above values of δ in Fig. 3.19 when using first-order ZF multipliers. The trade-off between nominal performance and robustness against noise can be clearly seen. The optimal values of k_d increases as δ increases (thereby demanding more robustness) and the estimated performance therefore reduces.

3.6 Proof of a Supporting Lemma

This section proves a lemma that is central in the derivation of the ZF IQCs and is used in the proof of Theorem 3.1. It is covered by [Freeman, 2018, Lemma 3] where the result is presented in a very general setting of Bochner spaces. Moreover, since the proof of [Freeman, 2018, Lemma 3] is unavailable, we present a self-contained proof here making all arguments in time-domain.

Lemma 3.12. *Let $\alpha \geqslant 0$ be fixed and let $\beta(\tau) = \min\{1, e^{-2\alpha\tau}\}$ for $\tau \in \mathbb{R}$. Let $\tilde{u}, \tilde{y} \in \mathcal{L}_{2e}[0, \infty)$ be related by $\tilde{u} = \nabla f(\tilde{y} + y_*)$, where $f \in \mathcal{S}(m, L)$ and y_* minimizes f. Then, the signals p and q defined in* (3.12) *satisfy, $\forall \tau \in \mathbb{R}$, $\forall T \geqslant 0$,*

$$\int_0^T e^{2\alpha t}p(t)^T(q(t) - \beta(\tau)q_T(t-\tau))dt \geqslant 0, \tag{3.51}$$

where q_T denotes the extension defined in (1.2).

Proof. The proof goes along the lines of [Lessard et al., 2016] and borrows some ideas from [Scherer and Ebenbauer, 2021].

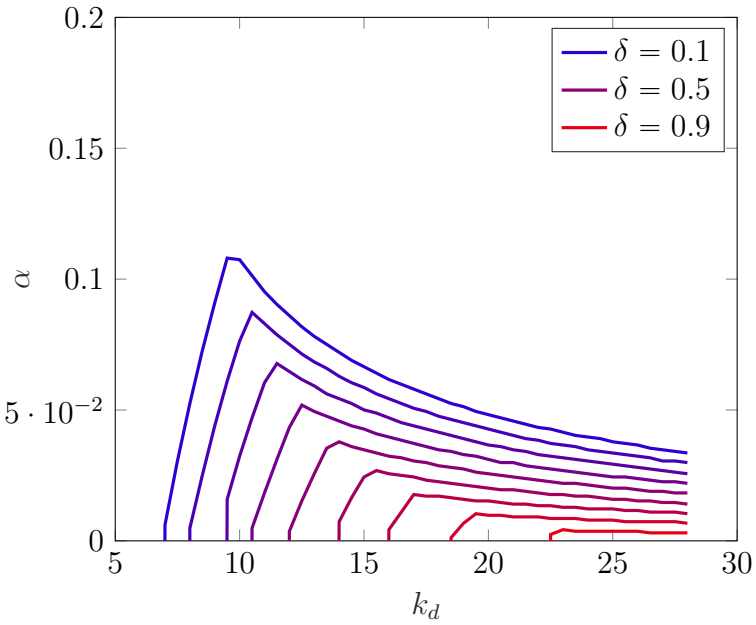

Figure 3.19: Performance estimates for quadrotor dynamics provided by first order ZF multipliers for $\psi \in \mathcal{S}(1, 10)$ and varying k_d with different bound $\delta \in \{0.1, 0.2 \cdots, 0.9\}$ on the multiplicative noise (see Assumption 3.4).

The central idea behind the proof is to exhibit a non-negative function $F : \mathbb{R} \to \mathbb{R}$ with support $[0, T]$ such that the integrand of (3.51) can be lower-bounded for all $\tau \in \mathbb{R}$ and all $t \in [0, T]$ as

$$e^{2\alpha t} p(t)^T (q(t) - \beta(\tau) q_T(t - \tau)) \geqslant F(t) - F(t - \tau). \tag{3.52}$$

If such a function F exists, integrating both sides of (3.52) from 0 to T and using the non-negativity of F along with the fact that F is zero outside $[0, T]$,

we get the desired result as

$$\begin{aligned}\int_0^T e^{2\alpha t} p(t)^T (q(t) - \beta(\tau) q_T(t-\tau)) dt &\geqslant \int_0^T (F(t) - F(t-\tau)) dt \\ &= \int_0^T F(t)dt - \int_{-\tau}^{T-\tau} F(t)dt \\ &= \begin{cases} \int_{T-\tau}^{T} F(t)dt \geqslant 0 & \text{if } \tau \geqslant 0, \\ \int_0^{-\tau} F(t)dt \geqslant 0 & \text{if } \tau < 0. \end{cases}\end{aligned} \tag{3.53}$$

The arguments that follow serve to produce this function F discussed above.

For convenience, let the dimension of $\tilde{y}$ be denoted by n_y, i.e., $\tilde{y} \in \mathbb{R}^{n_y}$. Let $g : \mathbb{R}^{n_y} \to \mathbb{R}$ be defined for any $\tilde{y} \in \mathbb{R}^{n_y}$ by

$$g(\tilde{y}) = f(\tilde{y} + y_*) - f(y_*) - \frac{m}{2}||\tilde{y}||^2, \tag{3.54}$$

where $f \in \mathcal{S}(m, L)$ and y_* minimizes f. This can be used to show that $g \in \mathcal{S}(0, L-m)$, $g(\mathbf{0}) = 0$ and $\nabla g(\mathbf{0}) = \mathbf{0}$. It can be further shown [Lessard et al., 2016] that for all $\tilde{y}$, $\tilde{y}_1$, $\tilde{y}_2 \in \mathbb{R}^{n_y}$,

$$(L-m)g(\tilde{y}) - \frac{1}{2}||\nabla g(\tilde{y})||^2 \geqslant 0, \tag{3.55}$$

$$(L-m)\nabla g(\tilde{y})^T \tilde{y} \geqslant (L-m)g(\tilde{y}) + \frac{1}{2}||\nabla g(\tilde{y})||^2, \tag{3.56}$$

$$\nabla g(\tilde{y}_1)^T (\tilde{y}_1 - \tilde{y}_2) \geqslant g(\tilde{y}_1) - g(\tilde{y}_2) + \frac{||\nabla g(\tilde{y}_1) - \nabla g(\tilde{y}_2)||^2}{2(L-m)}. \tag{3.57}$$

Using (3.55), we define a non-negative function $r : \mathbb{R}^{n_y} \to \mathbb{R}$ as

$$r(\tilde{y}) = (L-m)g(\tilde{y}) - \frac{1}{2}||\nabla g(\tilde{y})||^2. \tag{3.58}$$

Using definitions (3.12), we verify that for $\tilde{u}$, $\tilde{y}$ satisfying $\tilde{u} = \nabla f(\tilde{y} + y_*)$,

$$\begin{aligned} p(t) &= \nabla g(\tilde{y}(t)), \\ q(t) &= (L-m)\tilde{y}(t) - \nabla g(\tilde{y}(t)). \end{aligned} \tag{3.59}$$

Consider for $t_1 \in [0, \infty)$,

$$\begin{aligned} p(t_1)^T q(t_1) &= \nabla g(\tilde{y}(t_1))^T ((L-m)\tilde{y}(t_1) - \nabla g(\tilde{y}(t_1))) \\ &= (L-m)\nabla g(\tilde{y}(t_1))^T \tilde{y}(t_1) - ||\nabla g(\tilde{y}(t_1))||^2 \\ &\geqslant (L-m)g(\tilde{y}(t_1)) - \frac{1}{2}||\nabla g(\tilde{y}(t_1))||^2 \\ &= r(\tilde{y}(t_1)) \geqslant 0, \end{aligned} \tag{3.60}$$

where the inequality in the third line above is obtained using (3.56). We now consider signal extensions $\tilde{u}_T, \tilde{y}_T, p_T$ and q_T as defined in (1.2) and since the map f is static, we have $\forall t \in \mathbb{R}$,

$$\begin{aligned} p_T(t) &= \tilde{u}_T(t) - m\tilde{y}_T(t), \\ q_T(t) &= L\tilde{y}_T(t) - \tilde{u}_T(t). \end{aligned} \tag{3.61}$$

So, for $t_1, t_2 \in \mathbb{R}$,

$$\begin{aligned} &p_T(t_1)^T[q_T(t_1) - q_T(t_2)] \\ &= \nabla g(\tilde{y}_T(t_1))^T((L-m)\tilde{y}_T(t_1) - \nabla g(\tilde{y}_T(t_1)) - (L-m)\tilde{y}_T(t_2) + \nabla g(\tilde{y}_T(t_2))) \\ &= (L-m)\nabla g(\tilde{y}_T(t_1))^T(\tilde{y}_T(t_1) - \tilde{y}_T(t_2)) \\ &\qquad - ||\nabla g(\tilde{y}_T(t_1))||^2 + \nabla g(\tilde{y}_T(t_1))^T \nabla g(\tilde{y}_T(t_2)) \\ &\geqslant (L-m)(g(\tilde{y}_T(t_1)) - g(\tilde{y}_T(t_2))) + \frac{1}{2}||\nabla g(\tilde{y}_T(t_1)) - \nabla g(\tilde{y}_T(t_2))||^2 \\ &\qquad - ||\nabla g(\tilde{y}_T(t_1))||^2 + \nabla g(\tilde{y}_T(t_1))^T \nabla g(\tilde{y}_T(t_2)) \\ &= ((L-m)g(\tilde{y}_T(t_1)) - \frac{1}{2}||\nabla g(\tilde{y}_T(t_1))||^2) - ((L-m)g(\tilde{y}_T(t_2)) \\ &\qquad - \frac{1}{2}||\nabla g(\tilde{y}_T(t_2))||^2) \\ &= r(\tilde{y}_T(t_1)) - r(\tilde{y}_T(t_2)), \end{aligned} \tag{3.62}$$

where the inequality in the third line above is obtained using (3.57). For any $\beta \in [0,1]$, multiplying (3.60) by $(1-\beta)$, multiplying (3.62) by β and adding the so-obtained equations together, we can show that

$$p_T(t_1)^T[q_T(t_1) - \beta q_T(t_2)] \geqslant r(\tilde{y}_T(t_1)) - \beta r(\tilde{y}_T(t_2)). \tag{3.63}$$

For any $\tau \in \mathbb{R}$, let $\beta(\tau) = \min\{1, e^{-2\alpha\tau}\}$. Noting that $\beta(\tau) \in [0,1]$ and $\beta(\tau) \leqslant e^{-2\alpha\tau} \quad \forall \tau \in \mathbb{R}$, we use (3.63) and non-negativity of r to obtain

$$\begin{aligned} p_T(t)^T[q_T(t) - \beta(\tau)q_T(t-\tau)] &\geqslant r(\tilde{y}_T(t)) - \beta(\tau)r(\tilde{y}_T(t-\tau)) \\ &\geqslant r(\tilde{y}_T(t)) - e^{-2\alpha\tau}r(\tilde{y}_T(t-\tau)). \end{aligned} \tag{3.64}$$

Multiplying both sides by $e^{2\alpha t}$ and using that signal extensions are equal to the non-extended signals on $[0,T]$, we get for all $\tau \in \mathbb{R}$ and $t \in [0,T]$,

$$e^{2\alpha t}p(t)^T(q(t) - \beta(\tau)q_T(t-\tau)) \geqslant e^{2\alpha t}r(\tilde{y}_T(t)) - e^{2\alpha(t-\tau)}r(\tilde{y}_T(t-\tau)).$$

Observe that the function $F(t) := e^{2\alpha t}r(\tilde{y}_T(t))$ is non-negative on its support $[0,T]$ and satisfies the desired property (3.52) completing the proof. $\square$

Chapter 4

Distributed Control Over a Decoupled Architecture

In this chapter, the decoupled architecture (see Fig. 1.2), introduced in Section 1, is closely investigated. The goal is to understand the extent to which the decoupled architecture is reasonable. The key tools used in this chapter are the induced l_2 to l_∞ norm for obtaining a measure of local tracking performance and the recent results on scalable analysis and control of positive systems [Rantzer and Valcher, 2018], [Rantzer, 2015] which are used to analyze the simplified dynamics. The results presented in this chapter have been reported in [Datar and Werner, 2021] along with the extension to quasi-LPV systems in continuous time systems in [Hespe et al., 2020].

4.1 Problem Setup

Consider a large-scale interconnected system of N vehicles governed by general discrete-time LTI dynamics with state x^i, input u^i and output y^i (for agent i) neither of which are communicated with neighboring agents. At the same time, the interaction mechanism between different agents is modeled by first-order protocols with the virtual state p^i (for agent i) which is communicated with neighboring agents. The key idea is to see the first-order protocol as a reference generator, generating the reference trajectory p. Local feedback controllers are wrapped around the reference so that complex vehicles with higher order dynamics track these references. The resulting system dynamics and the controller structure for agent i are depicted in Fig. 4.1 and Fig. 4.2, respectively, and is discussed next in detail.

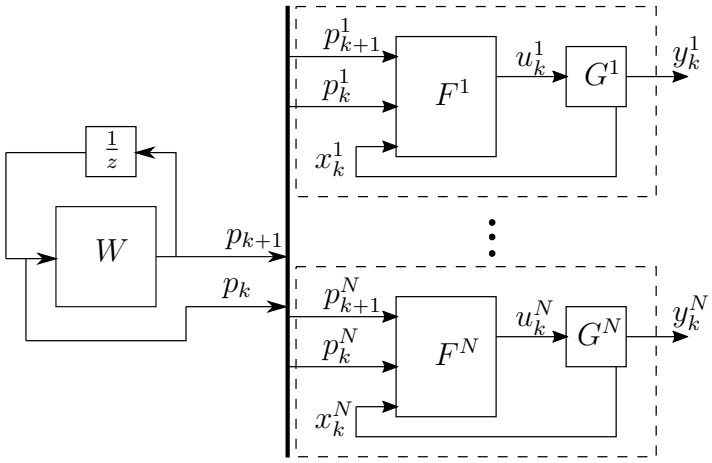

Figure 4.1: Interconnected system (4.7) under a decoupled architecture.

4.1.1 First Order Protocols

Let $p^i_k \in \mathbb{R}$ be a virtual state of the i^{th} agent at time k that is communicated with neighboring agents. Let the interconnection topology between the agents be represented by an undirected graph $\mathcal{G}$ with the corresponding Laplacian matrix $\mathcal{L}$. The 1^{st} agent is assumed to be the leader. The leader is externally controlled to the desired state which is assumed without the loss of generality to be the origin. Define $\mathcal{L}_c = \mathcal{L} + K_{\text{lead}} \cdot e_1 e_1^T$ for some given $K_{\text{lead}} > 0$. Discrete-time first-order protocols [Bullo, 2021] can be represented by

$$p^i_{k+1} = w^{ii} p^i_k + \sum_{j \in \mathcal{N}_i} w^{ij} p^j_k, \tag{4.1}$$

where $w^{ij} \in \mathbb{R}$ represent the weights corresponding to the edge between node i and j, and w^{ii} represents the weight associated with the self-state. Let W be matrix of weights w^{ij} with $w^{ij} = 0$, if the edge $(i,j) \notin \mathcal{E}$. By defining $p_k = [p^1_k \cdots p^N_k]^T$, the dynamics in (4.1) can be represented by

$$p_{k+1} = W p_k. \tag{4.2}$$

W is further assumed to be of the form $W = I - E\mathcal{L}_c$, where K_{lead} is assumed fixed and E is a diagonal matrix seen as a design parameter (control variable) such that $W \succcurlyeq 0$. Using a bound on the maximum degree $d_{\max}$, one can ensure that K_{lead} and E are such that $W \succcurlyeq 0$ and it does not require the knowledge of the spectrum of the Laplacian. The requirement of $W \succcurlyeq 0$ is justified by scalability aspects from the theory of positive systems analysis [Rantzer, 2015], which is discussed briefly in the following section.

Remark 4.1. *Generalizing this to the vector-valued case, i.e., when* $p_k^i \in \mathbb{R}^{n_p}$ *where* $n_p > 1$*, could be done by running independent first-order protocols along each canonical direction, i.e.,* $p_{k+1} = (W \otimes I_{n_p})p_k$.

4.1.2 Wrapping Local Tracking Controllers

The physical dynamics of the N vehicles are now considered along with local tracking controllers wrapped around the simplified first-order dynamics (4.2). For $i \in \{1, \cdots, N\}$, the i-th vehicle is modeled as a discrete-time LTI system

$$\begin{aligned} x_{k+1}^i &= A^i x_k^i + B_u^i u_k^i + B_w^i w_k^i, \\ y_k^i &= C^i x_k^i, \end{aligned} \tag{4.3}$$

where $x_k^i \in \mathbb{R}^{n_x}$, $u_k^i \in \mathbb{R}^{n_u}$, $w_k^i \in \mathbb{R}^{n_w}$ and $y_k^i \in \mathbb{R}$ are the state, the control input, the disturbance and the output of the i^{th} system at time k, respectively and A^i, B_u^i, B_w^i and C^i are constant matrices of appropriate dimensions.

Remark 4.2. *The system defined above is a multi-input single output system. In the light of Remark 4.1, it is possible to generalize the results to multiple outputs, whenever* p_k^i *is a vector-valued signal.*

Assumption 4.1. *The disturbance signal* w^i *for all vehicles is bounded in the sense of the* l_2 *norm and this bound is known a priori, i.e,* $||w^i||_{l_2} \leqslant \beta$.

The controller running on board communicates with neighboring agents and first calculates p_{k+1}^i according to (4.1) which is the desired output at time $k+1$ and uses this to compute the control input u_k^i, i.e., the controller implements

$$u_k^i = F_1^i x_k^i + F_2^i p_k^i + F_3^i p_{k+1}^i = F_1^i x_k^i + F_2^i p_k^i + F_3^i (w^{ii} p_k^i + \sum_{j \in \mathcal{N}_i} w^{ij} p_k^j), \tag{4.4}$$

where $F_1^i \in \mathbb{R}^{n_u \times n_x}$, $F_2^i \in \mathbb{R}^{n_u}$ and $F_3^i \in \mathbb{R}^{n_u}$ represent the control variables. This is shown in Fig. 4.2. The closed-loop agent dynamics with $\eta_k^i = \begin{bmatrix} x_k^i \\ p_k^i \end{bmatrix}$ as state and the tracking error $e_k^i = p_k^i - y_k^i$ as output can then be represented along with (4.1) by

$$\forall i: \quad \begin{cases} \eta_{k+1}^i &= \mathcal{A}^i \eta_k^i + \mathcal{B}_q^i q_k^i + \mathcal{B}_w^i w_k^i, \\ e_k^i &= \mathcal{C}^i \eta_k^i, \end{cases} \tag{4.5}$$

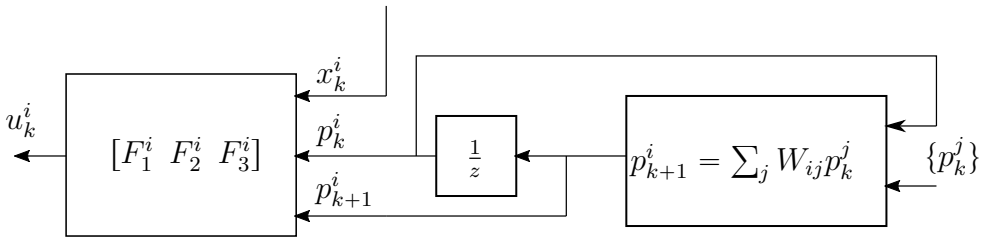

Figure 4.2: Controller implementation on agent i.

where $q_k^i = p_{k+1}^i$ and

$$\begin{aligned} \mathcal{A}^i &= \begin{bmatrix} A^i + B_u^i F_1^i & B_u^i F_2^i \\ \mathbf{0} & 0 \end{bmatrix}, \mathcal{B}_q^i = \begin{bmatrix} B_u^i F_3^i \\ I \end{bmatrix}, \mathcal{B}_w^i = \begin{bmatrix} B_w^i \\ 0 \end{bmatrix}, \\ \mathcal{C}^i &= \begin{bmatrix} -C^i & 1 \end{bmatrix}. \end{aligned} \tag{4.6}$$

The overall interconnected system is shown in Fig. 4.1 and is governed by

$$\begin{aligned} p_{k+1} &= W p_k, \\ \forall i: \quad &\begin{cases} \eta_{k+1}^i &= \mathcal{A}^i \eta_k^i + \mathcal{B}_q^i q_k^i + \mathcal{B}_w^i w_k^i, \\ e_k^i &= \mathcal{C}^i \eta_k^i, \end{cases} \end{aligned} \tag{4.7}$$

where $q_k^i = p_{k+1}^i$, $\eta_k^i = \begin{bmatrix} x_k^i \\ p_k^i \end{bmatrix}$ and initial conditions are such that $p_0^i = y_0^i = Cx_0^i$ for all i.

4.1.3 Objectives

The goal is to design controllers $(E, \{F_1^i, F_2^i, F_3^i\}_{i=1}^N)$ and analyze stability and performance of the interconnected system (4.7). More precisely, an upper bound is found on the peak norm of the tracking error, i.e., $||e^i||_{l_\infty}$, under bounded disturbances (see Assumption 4.1). This bound can be seen as a measure of how far the actual trajectories of the vehicles are as compared to their virtual (communicated) trajectories generated by the first-order protocols. This can then be used to conclude that the actual trajectories are collision-free by simply looking at the virtual trajectories generated by the first-order protocols. It can also serve to validate or invalidate the applicability of the decoupled architecture. For example, if the tracking errors are large, it would make sense to communicate rather the actual outputs of the vehicles and change the architecture. For more details on a comparison between these architectures, see [Hespe, 2020]. A coarse-grained performance

measure is next defined to quantify the deviation of the actual system in comparison to the simplified system as

$$\zeta_k = |\text{avg}(y_k) - \text{avg}(p_k)|. \tag{4.8}$$

If the desired relative displacements between agents i and j are denoted by r^{ij} (which for consensus can be set to 0), a measure for cooperation is defined for the actual system and the simplified system as

$$\begin{aligned} J_k &= \frac{1}{|\mathcal{E}|} \sum_{(i,j)\in\mathcal{E}} |y_k^j - y_k^i - r^{ij}|, \\ M_k &= \frac{1}{|\mathcal{E}|} \sum_{(i,j)\in\mathcal{E}} |p_k^j - p_k^i - r^{ij}|, \end{aligned} \tag{4.9}$$

respectively.

Problem 4.1. *Derive sufficient conditions in the form of LMIs to search for control gains E, $\{F_1^i, F_2^i, F_3^i\}_{i=1}^N$ guaranteeing an upper bound on $||e^i||_{l_\infty}$ under dynamics* (4.7) *for all bounded disturbances satisfying Assumption 4.1 such that the size of the LMIs grows at most linearly with network size N.*

4.2 Theoretical Results

In this section, two preliminary theorems (Theorem 4.1 and Theorem 4.2) are first presented which are needed as building blocks in the analysis. Analogous to the result reported in [Scherer and Weiland, 2000] and [Rotea, 1993], for continuous-time dynamical systems, an LMI condition is derived to find a bound on $||e||_{l_\infty}$ for inputs with a finite $||w||_{l_2}$ for discrete-time dynamical systems which corresponds to the generalized H_2 norm of the system. The following theorem is a straight-forward translation of [Scherer and Weiland, 2000, Proposition 3.15] to the discrete-time setting.

Theorem 4.1 (Discrete-time analogue of Proposition 3.15 from [Scherer and Weiland, 2000])**.** *For a discrete-time dynamical system governed by*

$$\begin{aligned} \eta_{k+1} &= \mathcal{A}\eta_k + \mathcal{B}_q q_k + \mathcal{B}_w w_k, \qquad \eta_0 = 0, \\ e_k &= \mathcal{C}\eta_k, \end{aligned} \tag{4.10}$$

where $\eta_k \in \mathbb{R}^{n_\eta}$, $q_k \in \mathbb{R}^{n_q}$, $w_k \in \mathbb{R}^{n_w}$ and $e_k \in \mathbb{R}^{n_e}$, if $\exists K > 0$, $\gamma_q > 0$, $\gamma_w > 0$ such that

$$\begin{bmatrix} \mathcal{A}^T \\ \mathcal{B}_q^T \\ \mathcal{B}_w^T \end{bmatrix} K \begin{bmatrix} \mathcal{A} & \mathcal{B}_q & \mathcal{B}_w \end{bmatrix} \prec \begin{bmatrix} K & 0 & 0 \\ 0 & \gamma_q^2 I & 0 \\ 0 & 0 & \gamma_w^2 I \end{bmatrix} \tag{4.11}$$

and

$$\begin{bmatrix} K & \mathcal{C}^T \\ * & I \end{bmatrix} \succ 0 \tag{4.12}$$

hold, then, $\forall w, q \in l_2,\ \forall k,$

$$||\eta_k|| \leqslant \frac{(\gamma_q||q||_{l_2} + \gamma_w||w||_{l_2})}{\sqrt{\lambda_{\min}(K)}},$$
$$||e_k||_2 \leqslant \gamma_q||q||_{l_2} + \gamma_w||w||_{l_2}.$$

Proof. Condition (4.11) is equivalent to the existence of $\epsilon > 0$ such that $\forall \eta_k \in \mathbb{R}^{n_\eta}, \forall w_k \in \mathbb{R}^{n_w}, \forall q_k \in \mathbb{R}^{n_q}$,

$$\eta_{k+1}^T K \eta_{k+1} \leqslant \eta_k^T (K - \epsilon I)\eta_k + (\gamma_q^2 - \epsilon)||q_k||_2^2 + (\gamma_w^2 - \epsilon)||w_k||_2^2.$$

Considering the storage function $V_k = \eta_k^T K \eta_k$, we have

$$\begin{aligned} V_{k+1} &\leqslant V_k + \gamma_q^2||q_k||_2^2 + \gamma_w^2||w_k||_2^2 \\ &\leqslant V_0 + \gamma_q^2 \sum_{i=0}^{k} ||q_i||_2^2 + \gamma_w^2 \sum_{i=0}^{k} ||w_i||_2^2. \end{aligned}$$

Then, using $\eta_0 = 0$, a bound on V_k can be obtained $\forall w, q \in l_2$ as

$$V_k \leqslant \gamma_q^2 \sum_{i=0}^{k-1} ||q_i||_2^2 + \gamma_w^2 \sum_{i=0}^{k-1} ||w_i||_2^2 \leqslant \gamma_q^2||q||_{l_2}^2 + \gamma_w^2||w||_{l_2}^2. \tag{4.13}$$

Using $\lambda_{\min}(K)||\eta_k||_2^2 \leqslant V_k$,

$$||\eta_k||^2 \leqslant \frac{\left(\gamma_q^2||q||_{l_2}^2 + \gamma_w^2||w||_{l_2}^2\right)}{\lambda_{\min}(K)}.$$

Since $\sqrt{a^2 + b^2} \leqslant \sqrt{a^2 + b^2 + 2ab} = a + b$ holds for any $a \geqslant 0, b \geqslant 0$, the above implies

$$||\eta_k|| \leqslant \frac{(\gamma_q||q||_{l_2} + \gamma_w||w||_{l_2})}{\sqrt{\lambda_{\min}(K)}}.$$

Using the Schur complement [Scherer and Weiland, 2000, Proposition 1.27], condition (4.12) can be converted to the equivalent condition

$$K - C^T C \succ 0, \tag{4.14}$$

which implies

$$V_k = \eta_k^T K \eta_k \geqslant \eta_k^T C^T C \eta_k = e_k^T e_k \quad \forall \eta_k \in \mathbb{R}^{n_\eta}$$

and together with equation (4.13), we get that $\forall w, q \in l_2$, $\forall k$,

$$||e_k||_2^2 \leqslant V_k \leqslant \gamma_q^2 ||q||_{l_2}^2 + \gamma_w^2 ||w||_{l_2}^2$$

and

$$||e_k||_2 \leqslant \gamma_q ||q||_{l_2} + \gamma_w ||w||_{l_2}.$$

□

The next theorem forms the second main ingredient of the analysis and allows for non-conservative analysis conditions that scale linearly with the network size (See Remark 4.3) for a large interconnected system.

Theorem 4.2 ([Rantzer, 2015])**.** *Consider a discrete-time autonomous system governed by*

$$p_{k+1} = W p_k, \tag{4.15}$$

where $p_k \in \mathbb{R}^N$ and $W \geqslant 0$.

The following statements are equivalent:

(1) The spectral radius of W is less than 1, i.e., W is Schur.

(2) $\lim_{k\to\infty} p_k = \mathbf{0} \ \ \forall p_0 \in \mathbb{R}^N$.

(3) There exists a diagonal matrix $P \succ 0$ such that $P - W^T P W \succ 0$.

(4) There exists a diagonal matrix P such that $\begin{bmatrix} P & W^T P \\ PW & P \end{bmatrix} \succ 0$.

Remark 4.3. *As P is a diagonal matrix, the matrix in condition (4) is sparse based on the sparsity structure of W. Sparse techniques for Semi-Definite Programs (SDP) can be exploited to decompose this problem into smaller SDPs [Mason and Papachristodoulou, 2014] and the verification of condition (4) leads to an analysis condition that scales linearly with N under some conditions on the sparsity structure of W. Details can be found in [Mason and Papachristodoulou, 2014].*

Building on Theorem 4.1 and Theorem 4.2, one of the main results of this chapter is presented next.

Theorem 4.3. *For the interconnected system (4.7) with given control variables F_1^i, F_2^i, F_3^i and E and matrices defined in* (4.6)*, if for some $0 < \alpha < 1$, there exists a diagonal matrix P such that*

$$\begin{bmatrix} \alpha^2 P & W^T P \\ PW & P \end{bmatrix} \succ 0, \tag{4.16}$$

and for all i, there exist $K^i \succ 0$ and $\gamma_q^i > 0$, $\gamma_w^i > 0$ such that

$$\begin{bmatrix} \mathcal{A}^{i\,T} \\ \mathcal{B}_q^{i\,T} \\ \mathcal{B}_w^{i\,T} \end{bmatrix} K^i \begin{bmatrix} \mathcal{A}^i & \mathcal{B}_q^i & \mathcal{B}_w^i \end{bmatrix} \prec \begin{bmatrix} K^i & 0 & 0 \\ 0 & {\gamma_q^i}^2 I & 0 \\ 0 & 0 & {\gamma_w^i}^2 I \end{bmatrix}, \tag{4.17}$$

$$\begin{bmatrix} K^i & \mathcal{C}^{i\,T} \\ * & I \end{bmatrix} \succ 0, \tag{4.18}$$

then the interconnected system, defined in (4.7), is stable, i.e., the trajectories remain bounded for disturbances satisfying Assumption 4.1 and for all $k \geqslant 0$,

$$|e_k^i|_2 \leqslant \gamma_q^i \sqrt{\frac{\mathrm{cond}(P)}{1-\alpha^2}} ||p_0||_2 + \gamma_w^i \beta, \tag{4.19}$$

$$||\eta_k^i||_2 \leqslant \frac{\gamma_q^i \sqrt{\frac{\mathrm{cond}(P)}{(1-\alpha^2)}} ||p_0||_2 + \gamma_w^i \beta}{\sqrt{\lambda_{\min}(K^i)}}. \tag{4.20}$$

Proof. Condition (4.16) is equivalent to the existence of a diagonal $P \succ 0$ such that

$$\alpha^2 P - W^T P W \succ 0$$

which implies

$$p_{k+1} P p_{k+1} \leqslant \alpha^2 p_k P p_k \quad \forall p_k \in \mathbb{R}^{n_p}.$$

Therefore,

$$||p_k||_2^2 \leqslant \alpha^{2k} \mathrm{cond}(P) ||p_0||_2^2 \quad \forall p_0 \in \mathbb{R}^{n_p}.$$

The infinite sum for a converging geometric series gives

$$||p||_{l_2}^2 \leqslant \frac{1}{1-\alpha^2} \mathrm{cond}(P) ||p_0||_2^2$$

and therefore,

$$||p^i||_{l_2} \leqslant ||p||_{l_2} \leqslant \sqrt{\frac{\mathrm{cond}(P)}{1-\alpha^2}} ||p_0||_2.$$

The bounds (4.19) and (4.20) are then obtained by simply applying Theorem 4.1 and using the bound derived above on $||p^i||_{l_2}$. □

Corollary 4.4. *If condition* (4.19) *holds, the loss in performance due to imperfect tracking can be bounded as*

$$\zeta_k \leqslant \gamma_q^{\text{avg}} \sqrt{\frac{\text{cond}(P)}{1-\alpha^2}} ||p_0||_2 + \gamma_w^{\text{avg}} \beta, \tag{4.21}$$

$$J_k \leqslant M_k + \frac{\sum_i \gamma_q^i \cdot d^i}{|\mathcal{E}|} \sqrt{\frac{\text{cond}(P)}{(1-\alpha^2)}} ||p_0||_2 + \frac{\sum_i \gamma_w^i \cdot d^i}{|\mathcal{E}|} \beta, \tag{4.22}$$

where γ_q^{avg} *and* γ_w^{avg} *denote the arithmetic mean of* $\{\gamma_q^1, \cdots, \gamma_q^N\}$ *and* $\{\gamma_w^1, \cdots, \gamma_w^N\}$*, respectively.*

Proof. Using definitions (4.8) and bound (4.19), the bound on ν_k can be derived as

$$\begin{aligned}
\zeta_k &= |\text{avg}(y_k) - \text{avg}(p_k)| \\
&= |\text{avg}(e_k)| \\
&\leqslant \frac{1}{N} \sum_{i=1}^{N} (\gamma_q^i \sqrt{\frac{\text{cond}(P)}{1-\alpha^2}} ||p_0||_2 + \gamma_w^i \beta) \\
&\leqslant \gamma_q^{\text{avg}} \sqrt{\frac{\text{cond}(P)}{1-\alpha^2}} ||p_0||_2 + \gamma_w^{\text{avg}} \beta.
\end{aligned}$$

Now using definition (4.9) and bound (4.19), we can derive the bound on J_k as

$$\begin{aligned}
J_k &= \frac{1}{|\mathcal{E}|} \sum_{(i,j)\in\mathcal{E}} |y_k^j - y_k^i| \\
&= \frac{1}{|\mathcal{E}|} \sum_{(i,j)\in\mathcal{E}} |(p_k^j - p_k^i) - (e_k^j - e_k^i)| \\
&\leqslant M_k + \frac{1}{|\mathcal{E}|} \sum_{(i,j)\in\mathcal{E}} |e_k^j| + |e_k^i| \\
&= M_k + \frac{1}{|\mathcal{E}|} \sum_{i=1}^{N} d^i |e_k^i| \\
&\leqslant M_k + \frac{\sum_i \gamma_q^i \cdot d^i}{|\mathcal{E}|} \sqrt{\frac{\text{cond}(P)}{(1-\alpha^2)}} ||p_0||_2 + \frac{\sum_i \gamma_w^i \cdot d^i}{|\mathcal{E}|} \beta.
\end{aligned} \tag{4.23}$$

□

The analysis conditions (4.16), (4.17) and (4.18) can be converted into synthesis conditions for finding optimal control variables F_1^i, F_2^i, F_3^i and E. For this purpose, define matrices

$$\begin{aligned} \mathcal{A}_o^i &= \begin{bmatrix} A^i & 0 \\ \mathbf{0} & 0 \end{bmatrix}, \\ \mathcal{B}_o^i &= \begin{bmatrix} B_u^i \\ 0 \end{bmatrix}, \\ \mathcal{F}^i &= \begin{bmatrix} F_1^i & F_2^i \end{bmatrix}. \end{aligned} \tag{4.24}$$

The following theorem gives LMI conditions for synthesis.

Theorem 4.5 (Solution to Problem 4.1)**.** *For the interconnected system (4.7), if there exist diagonal matrices $P \succ 0$ and X, such that, for an $\alpha \in (0,1)$,*

$$\begin{bmatrix} \alpha^2 P & P^T - \mathcal{L}_c^T X^T \\ P - X\mathcal{L}_c & P \end{bmatrix} \succ 0, \tag{4.25}$$

and $\forall i$, there exist $Q^i \succ 0$, Y^i, F_3^i, $\gamma_p^i > 0$,$\gamma_w^i > 0$ such that

$$\left[\begin{array}{c|cc|c} Q^i & * & & * \\ \hline \mathbf{0} & \gamma_q^{i\,2} I & \mathbf{0} & \\ & \mathbf{0} & \gamma_w^{i\,2} I & * \\ \hline \mathcal{A}_o^i Q^i + \mathcal{B}_o^i Y^i & \bar{B}_u^i F_3^i & \bar{B}_w & \\ & \mathbf{1} & \mathbf{0} & Q^i \end{array}\right] \succ 0, \tag{4.26}$$

$$\left[\begin{array}{c|c} Q^i & * \\ \hline \begin{bmatrix} -\bar{C}^i & \bar{I} \end{bmatrix} \bar{Q}^i & \bar{I} \end{array}\right] \succ 0, \tag{4.27}$$

then $\mathcal{F}^i = Y^i Q^{i^{-1}}$, F_3 and $E = P^{-1}X$ stabilize the networked system, i.e., (4.19) *and* (4.20) *hold and performance bounds (4.21) and (4.22) hold.*

Proof. Using the Schur complement, condition (4.17) can be written in a compact form as

$$\left[\begin{array}{ccc|c} K^i & 0 & 0 & \mathcal{A}^{i\,T} K^i \\ 0 & \gamma_q^{i\,2} I & 0 & \mathcal{B}_q^{i\,T} K^i \\ 0 & 0 & \gamma_w^{i\,2} I & \mathcal{B}_w^{i\,T} K^i \\ \hline \bar{K}^i \bar{\mathcal{A}}^i & \bar{K}^i \bar{\mathcal{B}}_q^i & \bar{K} \bar{\mathcal{B}}_w^i & \bar{K}^i \end{array}\right] \succ 0.$$

A congruence transformation with a non-singular matrix

$$\begin{bmatrix} K^{i-1} & 0 & 0 \\ 0 & I & 0 \\ 0 & 0 & K^{i-1} \end{bmatrix}$$

gives us the equivalent condition

$$\left[\begin{array}{ccc:c} Q^i & 0 & 0 & Q^i\mathcal{A}^{i^T} \\ 0 & \gamma_q^{i\,2} I & 0 & \mathcal{B}_q^{i\,T} \\ 0 & 0 & \gamma_w^{i\,2} I & \mathcal{B}_w^{i\,T} \\ \hdashline \mathcal{A}^i Q^i & \mathcal{B}_q^i & \mathcal{B}_w^i & Q^i \end{array}\right] \succ 0, \tag{4.28}$$

where $Q^i = K^{i^{-1}}$.

Similarly, condition (4.18), i.e.,

$$\begin{bmatrix} K^i & \mathcal{C}^{i^T} \\ * & I \end{bmatrix} \succ 0$$

is equivalent to

$$\begin{bmatrix} Q^i & Q^i\mathcal{C}^{i^T} \\ \mathcal{C}^i Q^i & I \end{bmatrix} \succ 0. \tag{4.29}$$

With definitions (4.6), (4.24) and $\mathcal{F}^i Q^i = Y^i$, equivalent conditions (4.26) and (4.27) are obtained. By substituting $W = I - E\mathcal{L}_c$ in condition (4.16) and defining $X = PE$, condition (4.25) can be obtained. The proof then follows simply as a consequence of Theorem 4.3.

□

Remark 4.4. *It should be noted that although* (4.16) *and* (4.25) *are not LMIs in α and P, a standard bisection algorithm can be used to find the minimum α that renders the LMIs feasible [Boyd et al., 1994]. See Remark 3.4.*

Extension of the analysis and synthesis results to more general non-linear agent dynamics modeled as quasi-LPV systems is straightforward and is demonstrated in the continuous-time setting in [Hespe et al., 2020].

4.3 Practical Aspects and Scalability

4.3.1 Remarks on Tuning

In order to consider control input in the performance channel, one could replace the LMI condition (4.27) by

$$\left[\begin{array}{c:c} Q^i & * \\ \hdashline \begin{bmatrix} -C^i & 1 \\ \mathbf{0} & 0 \end{bmatrix} Q^i + \rho \begin{bmatrix} \mathbf{0} \\ 1 \end{bmatrix} Y^i & I \end{array}\right] \succ 0, \tag{4.30}$$

where $\rho > 0$ acts as a tuning knob punishing the control effort in the performance channel.

4.3.2 Synthesis with H_∞ Techniques

Alternatively, one could use standard H_∞ loop-shaping techniques to obtain a controller and then use the analysis LMIs to obtain l_∞ bounds on the error. A controller that guarantees a finite H_∞ norm (induced l_2 to l_2 norm) of the closed-loop necessarily leads to a finite induced l_2 to l_∞ norm (See [Hespe et al., 2020], [Hespe, 2020]).

4.3.3 Scalability

The feasibility LMI conditions (4.16) and (4.25) for analysis and synthesis of first-order protocols are *large* SDPs with a sparsity structure that depends on the sparsity structure of W (which depends on the underlying graph $\mathcal{G}$). Referring to Remark 4.3, these LMIs can be decomposed into N *smaller* LMIs using ideas from [Mason and Papachristodoulou, 2014] thereby allowing a scalable analysis. Knowledge of the spectrum of the graph Laplacian, if available, can be used to avoid solving (4.16). The analysis LMIs (4.17) and (4.18) and synthesis LMIs (4.26) and (4.27) are N separate conditions with the size of each LMI corresponding to the respective order of the agent dynamics. The complexity thus scales linearly with the network size N. This also means that if the network is homogeneous with identical agent dynamics, these LMIs are identical for all i which reduces to a single LMI.

4.4 Illustrative Examples

In this section, the theoretical results are applied on illustrative examples.

4.4.1 Perfect Tracking Controller

Together with a general first-order protocol (4.2), consider the following dynamics for all first-order agents $i \in \{1, 2, \cdots, N\}$

$$\begin{aligned} x_{k+1}^i &= a^i x_k^i + b_u^i u_k^i + b_w^i w_k^i, \\ y_k^i &= x_k^i, \end{aligned} \tag{4.31}$$

along with the controller

$$u_k^i = f_1^i x_k^i + f_2^i p_{k+1}^i. \tag{4.32}$$

It can be seen that for $f_1^i = -a^i/b_u^i$ and $f_2^i = 1/b_u^i$, the closed-loop agent dynamics are

$$\begin{aligned} x_{k+1}^i &= p_{k+1}^i + b_w^i w_k^i, \\ y_k^i &= x_k^i \end{aligned} \tag{4.33}$$

along with the first-order protocol (4.2). It can be shown that minimizing γ_q^i subject to constraint (4.17) gives $\gamma_q^{i*} = 0$. This can be easily seen intuitively by observing that we have perfect tracking for arbitrary p_k^i whenever $w_k^i \equiv 0$.

Thus applying Theorem 4.3, we get the following $\forall k$

$$|e_k^i|_2 \leqslant \gamma_w^i \beta, \tag{4.34}$$

$$\zeta_k \leqslant \gamma_w^{\text{avg}} \beta, \tag{4.35}$$

$$J_k \leqslant M_k + \frac{\sum_i \gamma_w^i \cdot d^i}{|\mathcal{E}|} \beta. \tag{4.36}$$

This result can be interpreted as follows. For scenarios with very good tracking controllers acting locally on the agents, i.e., when $\gamma_q \approx 0$, the performance loss due to input disturbances acting on the agents can be estimated a priori by (4.35) and (4.36). Moreover, the boundedness of trajectories is implied just by analyzing the system of simple agents as seen in (4.34). It also has an interesting implication for non-linear differentially flat systems [van Nieuwstadt et al., 1998] where it is possible to achieve perfect tracking in the absence of disturbances. This needs to be investigated further.

4.4.2 Generic Vehicle Model

A slightly more realistic example of a generic second-order vehicle model is considered next, where the governing equations are

$$m\ddot{q} + b\dot{q} = u + w \tag{4.37}$$

where m, b, q, u and w represent the mass, damping coefficient, position, forcing input and disturbance input, respectively. This model can be written in a state space form and discretized using Zero-Order-Hold (ZOH) with a time-step of 0.1 to obtain a discrete-time state space model.

Disturbance Rejection in Platooning

A platooning scenario is first considered with a heterogeneous network of agents perturbed by an l_2 input disturbance. A heterogeneous group of five agents modeled by (4.37) is considered with the following parameter values:

- Agent 1: $m^1 = 1$, $b^1 = 3$
- Agent 2: $m^2 = 1$, $b^2 = 10$
- Agents 3, 4 and 5: $m^3 = 0.1$, $b^3 = 1$

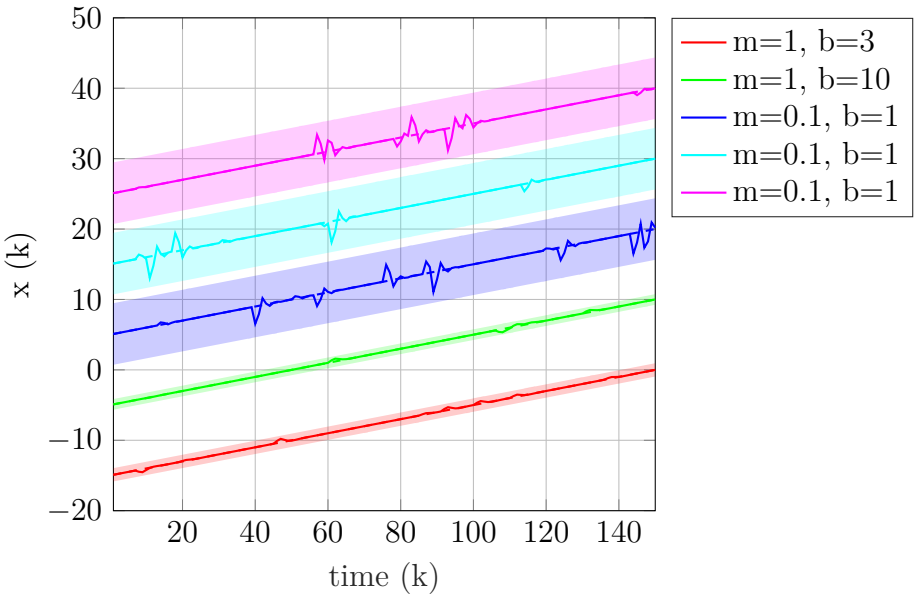

Figure 4.3: Disturbance rejection in platooning.

A desired platoon velocity of 0.1 units is considered. In the absence of disturbances, a constant feed-forward control input will lead to the desired trajectory. The error dynamics are again governed by (4.37) where the control input is the deviation from the feed-forward control input. A controller for the error dynamics of each agent is designed by solving the following convex optimization problem for each i:

$$\min \gamma_q^i + \gamma_w^i \quad \text{s.t. (4.26) and (4.30) hold.}$$

The closed-loop dynamics under a disturbance signal with $\beta = 100$ along with theoretical bounds (depicted by shaded regions) are shown in Figure 4.3. Note that because agents 3, 4 and 5 have the least mass and are identical, the deviation bound are the greatest whereas agents 1 and 2 are heavy, leading to a smaller bound. it can be concluded that as long as the bounds on the input disturbances are valid, the trajectories will remain collision free. Note that if $\beta \cdot (\gamma_w^i + \gamma_w^j)$ is higher than the distance between the nominal trajectories of agents i and j, generated by the first-order protocol,the bounding boxes would intersect allowing the possibility of a collision and thereby demonstrating a need for a coupled architecture or a redesign.

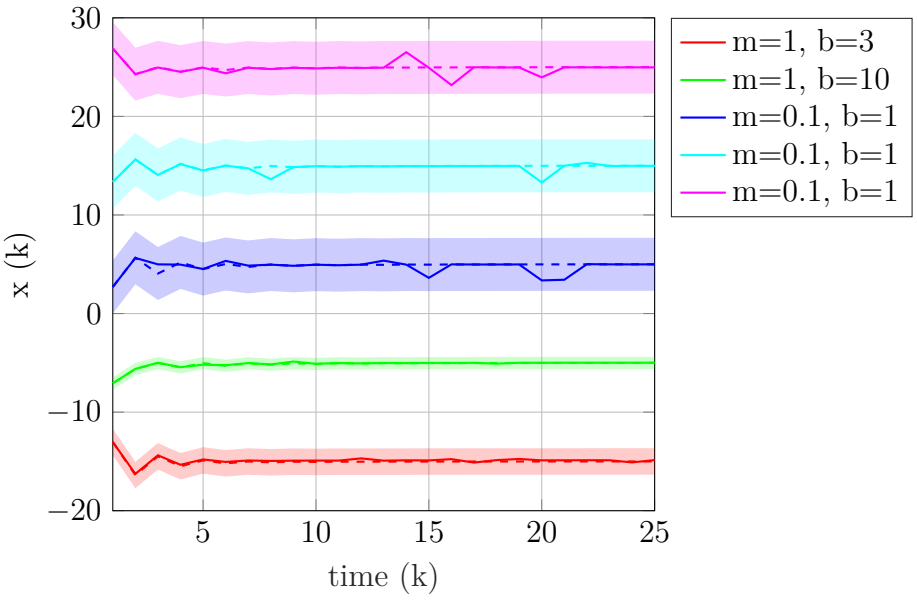

Figure 4.4: Formation stabilization.

Formation Forming at Arbitrary Locations

The problem of formation attainment is considered next with a network of the above described five agents with a first-order protocol as the interaction mechanism. A graph is randomly generated by setting the probability of having an edge between any two nodes to 0.6. We assume that the agent 1 is externally controlled as in (4.2) with $K_{\text{lead}} = 5$. The following convex optimization problem is solved to obtain controllers.

$$\min \gamma_q + \gamma_w \quad \text{s.t. (4.25), (4.26), (4.27) hold.}$$

Figure 4.4 shows the trajectories for the formation attainments problem along with the theoretical bounds depicted by shaded regions. The dashed trajectories are the trajectories of the simplified dynamics (first-order protocol) which are reasonably well tracked. Since the shaded regions do not intersect, the actual trajectories can be declared collision free by simply studying the simplified dynamics. On the contrary, if the shaded regions do intersect, there would be a possibility of a collision which calls for a redesign or a coupled architecture.

Chapter 5

Consensus Under Packet Dropouts

This chapter focuses on the interaction dynamics with simplified agent models (left feedback loop from Fig. 1.2). Moving away from ideal communication channels treated so far, this chapter deals with network imperfections in the form of packet dropouts. A novel first-order consensus protocol is proposed in Section 5.2 as a generalization of two standard consensus protocols used in the literature on lossy networks. Analysis of the proposed protocol along with simulation results demonstrate the benefit of the proposed protocol in terms of allowing for large sampling times. These results have been reported in [Datar et al., 2018].

The standard deterministic consensus protocol with ideal communication is first reviewed in Section 5.1. Section 5.2 introduces the mathematical framework which formalizes the proposed protocol followed by a review of the available tools for mean-square stability analysis in Section 5.3. The analysis tools are applied to an example illustrating the benefit of the proposed protocol in Section 5.4 and Section 5.5 presents the numerical simulations to validate the results.

5.1 Consensus Protocol in Lossless Networks

Consider an undirected graph $\mathcal{G}$ of order N characterized by the adjacency matrix $A \in \mathbb{R}^{N\times N}$. First order integrator dynamics with states $x_i \in \mathbb{R}$ for agent i are given by

$$\dot{x_i}(t) = u_i(t), \qquad x(0) = x_0, \tag{5.1}$$

where $u \in \mathbb{R}$ is the output from a sampled-data controller together with a zero order hold implemented on each agent with a uniform sampling time

T. Let t_k denote the sampling instants such that $t_{k+1} - t_k = T \; \forall k \in \mathbb{N}$. Applying the control protocol similar to the one suggested in [Olfati-Saber et al., 2007] for a sampled data controller with gain $K \in \mathbb{R}$ and followed by a ZOH, the control law can be obtained as

$$u_i(t) = K \sum_{v_j \in \mathcal{N}_i} (x_j(t_k) - x_i(t_k)), \qquad \forall t \in [t_k, t_{k+1}). \tag{5.2}$$

Using exact ZOH discretization, the discrete-time dynamics are given by

$$\begin{aligned} x(k+1) &= (I - KT \cdot \mathcal{L})x(k) \\ &= (I - \epsilon \cdot \mathcal{L})x(k) = Px(k), \end{aligned} \tag{5.3}$$

where the *discrete gain* $\epsilon \in \mathbb{R}$ is defined as $\epsilon = KT$, $\mathcal{L}$ is the graph Laplacian and $P \in \mathbb{R}^{N \times N}$, given by $P = I - \epsilon \cdot \mathcal{L}$, is called the Perron matrix induced by the graph $\mathcal{G}$ [Olfati-Saber et al., 2007].

Remark 5.1. *Note that for a fixed discrete gain ϵ, the discrete time response sequences are identical for different combinations of K and T as long as $KT = \epsilon$. However, the same value of discrete gain ϵ leads to significantly different responses in the continuous time. This is illustrated in Fig. 5.1 for an example of a group of 3 agents connected in a line-topology.*

Remark 5.2. *The agents of a network are said to have reached consensus if and only if $x_i = x_j \; \forall i, \; j \in \mathcal{V}, i \neq j$. For connected graphs, it can be shown that the dynamics in equation (5.3) lead to consensus if and only if $\epsilon < \frac{2}{\lambda_{max}(\mathcal{L})}$. Let this bound be denoted by $\epsilon_{max} = \frac{2}{\lambda_{max}(\mathcal{L})}$. This work investigates such bounds in lossy networks.*

5.2 Memory Weighted Protocol for Lossy Networks with Packet Dropouts

As one of the important aspects of non-ideal communication, packet dropouts are considered next and a novel consensus protocol specifically geared towards packet loss is proposed. Let r denote the probability that a message in an arbitrary communication link in the network is lost. Although the formalism allows for different loss rates r_{ij} in different links $(i, j) \in \mathcal{E}$, this work is restricted to a global loss rate $r_{ij} \equiv r$. For any link $(i, j) \in \mathcal{E}$, let $\theta_{ij}(k)$ be a stochastic Bernoulli process modeling the packet loss in the following way. A packet from agent j to agent i is considered lost at instance k if and only if $\theta_{ij}(k) = 1$ and the packet is considered received at instance k if and only

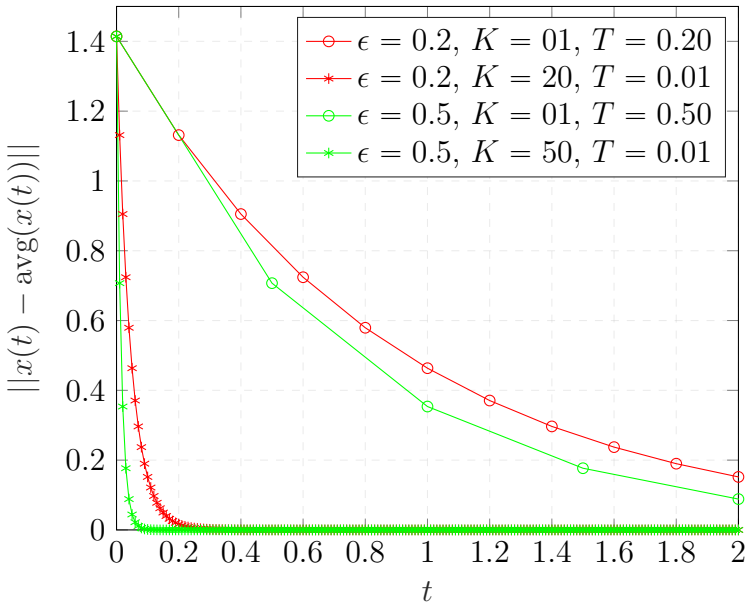

Figure 5.1: Continuous time responses for different values of *discrete gain*, sampling times T and gains K. Each color represents a fixed value of *discrete gain*.

if $\theta_{ij}(k) = 0$ and thus, the probability that $\theta_{ij}(k) = 1$ is r for all $k \in \mathbb{N}$ and for all $(i, j) \in \mathcal{E}$. The motivation behind this notation is to be able to define the *lossy* adjacency matrix at time k as $A_\theta(k) = A - \theta(k)$, where A is the adjacency matrix if the communication is ideal. Therefore, for all pairs of agents without a link, $(m, n) \notin \mathcal{E}$ (even in the case of ideal communication), let $\theta_{mn}(k) = 0$, i.e., the probability that $\theta_{mn}(k) = 0$ is 1 for all $k \in \mathbb{N}$ and for all $(m, n) \notin \mathcal{E}$. The overall packet loss in the network can now be modeled by composing an $(N \times N)$ stochastic matrix process $\theta(k)$ whose entries are $\theta_{ij}(k)$ as defined above. For convenience, let $\theta_{ij}(k)' = 1 - \theta_{ij}(k)$ and the argument k is suppressed in $\theta(k)$ when it is clear from context.

Consider a scenario when a packet containing the information x_j sent by agent j is not received at agent i. Agent i can either disregard agent j by considering the link in the topology as broken or use the most recent stored information $\hat{x}_i^j$ about agent j. The latter needs an available memory storage. These two ideas can be expressed as the *switching protocol* and the *memory protocol* as follows:

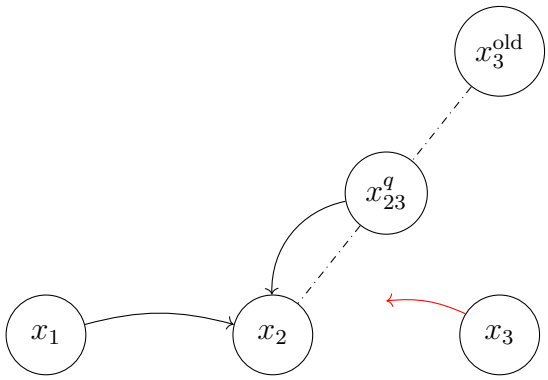

Figure 5.2: A packet from agent 3 containing information x_3 is lost at agent 2. Agent 2 therefore uses a convex combination of x_3^{old}, the last information received by agent 2 from agent 3, and the self state x_2 depending on the memory weight $q \in [0, 1]$, i.e., $x_{23}^q = (1-q)x_2 + qx_3^{\text{old}}$ as a replacement for the lost package.

$$\begin{aligned} u_i^{switch} &= K \sum_{v_j \in \mathcal{N}_i} \theta'_{ij}(x_j - x_i) = K \sum_{v_j \in \mathcal{N}_i} (\theta'_{ij} x_j + \theta_{ij} x_i) - x_i, \\ u_i^{mem} &= K \sum_{v_j \in \mathcal{N}_i} [\theta'_{ij} x_j + \theta_{ij} \hat{x}_i^j - x_i]. \end{aligned} \tag{5.4}$$

Comparing this with the standard protocol in equation (5.2), the lost information x_j in the switching protocol is replaced by x_i whereas as in the memory protocol, the lost information x_j is replaced by $\hat{x}_i^j$. A previous work [Wang et al., 2010] has compared these two protocols in a simplified case, where at any time, all packets in a network are either lost or received.

A free parameter called as the memory weight q_i is introduced which could be chosen such that $0 \leqslant q_i \leqslant 1$. The following *memory weighted protocol* is proposed as a generalization and defined by

$$u_i^{mwp} = K \sum_{v_j \in \mathcal{N}_i} [\theta'_{ij} x_j + (q_i - 1)\theta_{ij} x_i + q_i \theta_{ij} \hat{x}_i^j - x_i]. \tag{5.5}$$

The stored information is assigned a memory weight $q_i \in \mathbb{R}$ which can be tuned based on the agent dynamics, network characteristics like the loss rate, *discrete gain*, etc., and this can be interpreted as saying that at agent i, the lost state of the neighbor is assumed to be somewhere on the line segment joining the past state of the neighbor and present state of agent i. This idea is depicted in Fig. 5.2. The ideas discussed above are now formalized to represent the update equations of the complete system in a compact form.

Assume that there is a fixed underlying communication topology represented by a graph $\mathcal{G}$ characterized by the adjacency matrix A. Existing links from this fixed topology can be broken and reconnected but no new links which are not present in the underlying topology can be created. The instantaneous adjacency matrix is then given by $A_\theta(k) = A - \theta(k)$.

Assume that each agent has an available memory storage and it stores the most recent state of its neighbors. Let d_i denote the in-degree at node i (number of neighbors agent i is listening to) and let $\hat{x}_i \in \mathbb{R}^{d_i}$ be the stored positions of neighbors of agent i and $\theta_i \in \mathbb{R}^{d_i}$ be the vector of the binary variables representing the success/failure of packet reception at the incoming channels of agent i. Let the projection matrix $B_i \in \mathbb{R}^{d_i \times N}$ be constructed from d_i canonical unit basis vectors as rows such that it selects the d_i number of neighbors of agent i from the total number of agents N. So the matrix B_i contains all zeros except for exactly one entry equal to 1 in each row.

Let the vectors of stacked $\hat{x}_i$ and θ_i be denoted by $\hat{x}$ and $\theta_{\text{vec}} \in \mathbb{R}^{d_1+\ldots+d_N}$, respectively, and the block matrix of stacked B_i be $B \in \mathbb{R}^{(d_1+\ldots+d_N)\times N}$. Each agent assumes its own location as the initial condition for its stored variable, i.e., $\hat{x}(0) = \text{blkdiag}(\mathbf{1}_{d_1}, \mathbf{1}_{d_2}, ..., \mathbf{1}_{d_N})x(0)$. Define $x_{\text{aug}} \in \mathbb{R}^{\bar{N}}$ such that $x_{\text{aug}} = [x^T \quad \hat{x}^T]^T$ where $\bar{N} = N + d_1 + d_2 + \ldots + d_N$. Define the *memory weight matrix* $Q \in \mathbb{R}^{N\times N}$ as $\text{diag}(q_1, q_2, \ldots, q_N)$. Using (5.5), one can work out the system dynamics as in equation (5.3) and show that the network dynamics with appropriate initial condition $x_{\text{aug}}(0)$ are

$$\begin{aligned} x_{\text{aug}}(k+1) &= \begin{bmatrix} W_{11}^c & W_{12}^c \\ W_{21}^c & W_{22}^c \end{bmatrix} x_{\text{aug}}(k) \\ &= W^c x_{\text{aug}}(k), \end{aligned} \tag{5.6}$$

where

$$\begin{aligned} W_{11}^c &= P - \epsilon\theta + \epsilon(I - Q)(\text{diag}(\theta \cdot \mathbf{1})), \\ W_{12}^c &= \epsilon \cdot Q \cdot \text{blkdiag}(\theta_1^T, \theta_2^T, \ldots, \theta_N^T), \\ W_{21}^c &= (I - \text{diag}(\theta_{\text{vec}})) \cdot B, \\ W_{22}^c &= \text{diag}(\theta_{\text{vec}}). \end{aligned}$$

For convenience, define a model as follows:

Definition 5.1 (Model)**.** *For a given undirected graph $\mathcal{G}$ characterized by the adjacency matrix A, loss probability r for the Bernoulli random variables θ_{ij} as defined above, discrete gain ϵ and given memory weight matrix Q, a model is defined uniquely by a tuple (ϵ, Q, A, r) which leads to network dynamics as in equation (5.6) and is abbreviated as $M(\epsilon, Q, A, r)$.*

Note that $M(\epsilon, \mathbf{0}, A, r)$ and $M(\epsilon, I, A, r)$ correspond to the models due to *switching protocol* and *memory protocol* respectively. These are referred to as the *switching model* and the *memory model* respectively. The results in this chapter are restricted to Q of the form qI and the following problem precisely states the objectives.

Problem 5.1. *Compare the different models $M(\epsilon, qI, A, r)$ by analyzing the network dynamics* (5.6) *and demonstrate, if any, the advantage of the generalized memory-weighted protocol ($0 < q < 1$) over the standard first-order consensus protocols ($q = 0$ or $q = 1$).*

5.3 Mean Square Consensus Analysis

This section defines mean-square consensus and presents necessary and sufficient conditions to assess mean-square consensus of dynamics (5.6) which facilitate a comparison between different protocols presented in Section 5.4. It can be seen (from the definition of W^c) that $W^c\mathbf{1} = \mathbf{1}$. Defining the projection matrix $P_r = I - \frac{1}{N}\mathbf{1}\mathbf{1}^T$, observe that

$$\begin{aligned} P_r W^c P_r &= (I - \frac{1}{N}\mathbf{1}\mathbf{1}^T)W^c(I - \frac{1}{N}\mathbf{1}\mathbf{1}^T) \\ &= (I - \frac{1}{N}\mathbf{1}\mathbf{1}^T)(W^c - \frac{1}{N}\mathbf{1}\mathbf{1}^T) \\ &= (I - \frac{1}{N}\mathbf{1}\mathbf{1}^T)W^c - (I - \frac{1}{N}\mathbf{1}\mathbf{1}^T)\frac{1}{N}\mathbf{1}\mathbf{1}^T \\ &= (I - \frac{1}{N}\mathbf{1}\mathbf{1}^T)W^c = P_r W^c. \end{aligned} \tag{5.7}$$

Therefore, if the deviation variable δ is defined as $\delta(k) = P_r x_{\text{aug}}(k)$, the dynamics of the deviation variables can be derived to be

$$\delta(k+1) = P_r W^c x_{\text{aug}}(k) = P_r W^c P_r x_{\text{aug}}(k) = P_r W^c \delta(k). \tag{5.8}$$

Definition 5.2. *$M(\varepsilon, Q, A, r)$ is said to achieve mean square consensus if there exist $M \geqslant 0$ and $0 \leqslant c < 1$ such that*

$$\mathbb{E}\left[||(I - \frac{1}{N}\mathbf{1}\mathbf{1}^T)x_{\text{aug}}(k)||^2\right] = \mathbb{E}\left[||\delta(k)||^2\right] \leqslant Mc^k \tag{5.9}$$

holds for all $k \geqslant 0$ under dynamics (5.6).

A necessary and sufficient condition for mean square exponential stability from [Costa et al., 2010] is summarized in the next result adapted to the setting in this chapter.

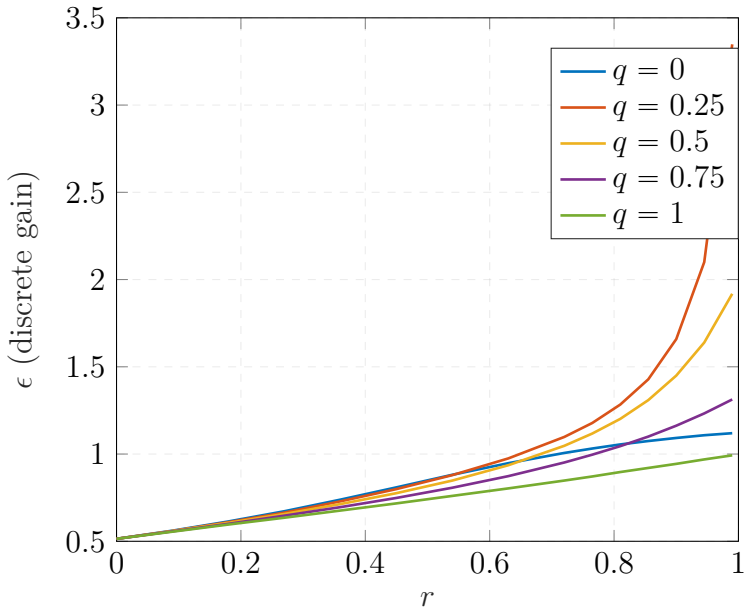

Figure 5.3: Maximum allowable ϵ with varying loss rates considering a line topology for $N = 9$ agent for different values of the memory weights.

Theorem 5.1 (adapted from [Costa et al., 2010]). *$M(\epsilon, Q, A, r)$ achieves mean square consensus if and only if*

$$r_2(\epsilon, Q, A, r) := \rho(\mathbb{E}\left[(I - \frac{1}{\bar{N}}\mathbf{1}\mathbf{1}^T)W^c \otimes (I - \frac{1}{\bar{N}}\mathbf{1}\mathbf{1}^T)W^c\right]) < 1. \quad (5.10)$$

5.4 Analysis of Different Protocols for Line Topology

The network dynamics for an example of 9 agents connected in a line topology is now analyzed. Let the standard adjacency matrix of the line topology be denoted by $A_{\text{line}} \in \mathbb{R}^{9\times 9}$. Additionally, assume a structure $Q = qI$. Qualitatively similar behavior is observed for $N = 3, 5, 7$ agents and with a cycle and star topology. Figure 5.3 show the maximum allowable *discrete gain* that still achieves mean square consensus for 9 agents in a line topology. One can see that the allowable ϵ increases for higher loss rates. Additionally, if ϵ is smaller than ϵ_{max}, the value of maximum allowable ϵ for the loss-free situation ($r = 0$), all models lie within the stability region. This agrees with [Fagnani and Zampieri, 2009], where it is shown that if $\epsilon < \epsilon_{max}$ (see Remark 5.2), packet losses cannot cause divergence. Interestingly, the bound on

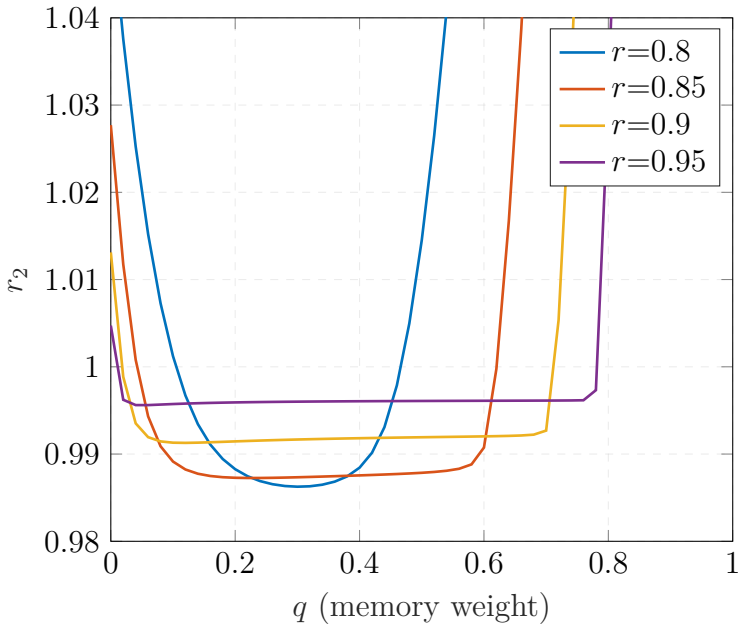

Figure 5.4: Effect of variation in q on r_2 for $\epsilon = 1.25$.

the *discrete gain* is increased in the presence of network losses. Intuitively, since the maximum eigenvalue of the *averaged* graph Laplacian over a large number of steps is reduced because of losses, the upper bound is increased. Figure 5.4 shows the effect of the variation of the memory weight q on r_2 for a high value of $\epsilon = 1.25$. It can be seen that the minimum value of r_2 is achieved approximately near $q = 0.25$ and in fact, mean square consensus is achieved only for a limited range of q. It is in this high ϵ regime, that the *memory weighted models* $M(\epsilon, q \cdot I, A_9, r)$ with $0 < q < 1$ seem most effective. For a low value of $\epsilon = 0.1$, Fig. 5.5 shows that the *memory model* is better than the *switching model* and the *memory weighted models* do not show any special advantage in this low ϵ regime. Numerical simulations verify these analytical calculations in the next section.

5.5 Numerical Studies

In order to further investigate these different protocols, numerical simulations are presented that validate the theoretical observations. Consider 9 agents connected in a line topology and as before, let A_9 denote the standard adjacency matrix for the line topology.

Figure 5.6 shows the empirical mean (top) and empirical variance (below)

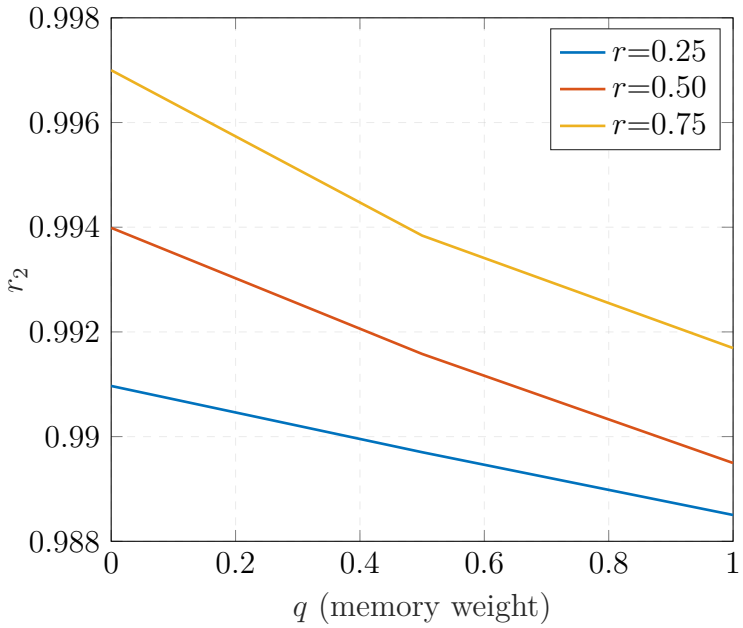

Figure 5.5: Effect of variation in q on r_2 for $\epsilon = 0.1$.

of the norm of the disagreement vector over 1000 simulations for $\epsilon = 1.25$. The initial conditions of the agents are $x(0) = [1, 2, \ldots, 9]$. The trajectories from the *switching model* and the *memory model* diverge and one can see that trajectories from $M(1.25, 0.3, A_9, 0.8)$ converge faster than the other two weighted models. This agrees well with the analytical results obtained in Fig. 5.4 which shows that r_2 is minimized around $q = 0.3$. Further numerical investigations are reported in [Datar et al., 2018].

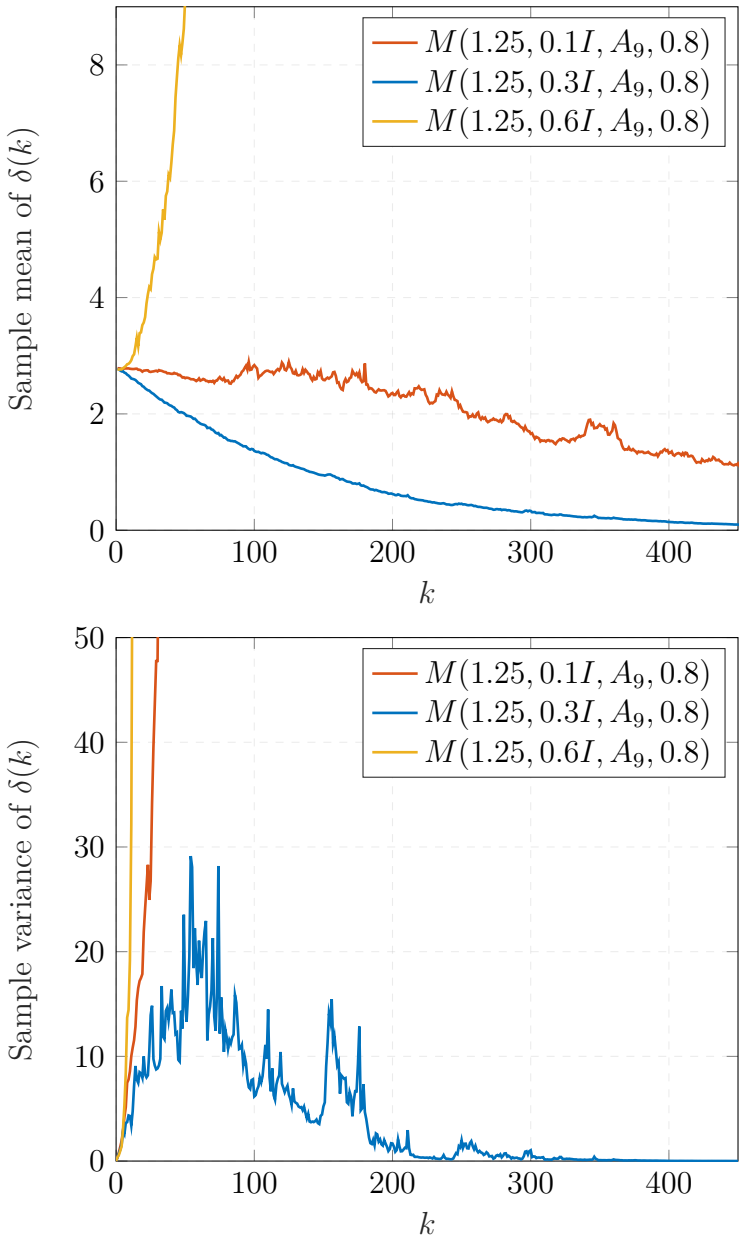

Figure 5.6: Comparison of the expectation (top) and variance (bottom) of the norm of the disagreement vector for different models for $\epsilon = 1.25$ over 1000 simulations with $x(0) = [1, 2, \ldots, 9]^T$.

Chapter 6

Summary and Open Directions

This work studies modular architectures introduced in Chapter 1 from an analytical standpoint with simulations and experiments complementing the theory. The coupled architecture introduced in Fig. 1.1 is studied in Chapter 2 and Chapter 3 with a focus on gradient-based cooperative control. On the other hand, results on the decoupled architecture introduced in Fig. 1.2 are presented in Chapter 4 and Chapter 5. The next section summarizes the presented work and proposes possible extensions requiring further study and Section 6.2 presents open research directions on a broader level.

6.1 Summary and Possible Extensions

The standard flocking dynamics are augmented to address the source-seeking problem and analyzed in Chapter 2 along with experimental results on the Crazyflie 2.1 platform. This is done by adding a forcing term using the local gradient and/or Hessian information. The analysis first addresses simple double integrator models and presents experimental results with quadrotors by using a fast velocity controller and gradient and Hessian estimation heuristics. Motivated by the successful experimental results, the theoretical results on stability analysis with double integrator models are extended by explicitly considering general vehicle dynamics with a guaranteed tracking performance. Although qualitative in nature, these theoretical results provide a rationale for the proposed architecture. Complementing the stability analysis, simulation results with complex non-holonomic vehicle dynamics are presented as a proof-of-concept showing the effectiveness of the proposed architecture for various situations. Finally, as a first step towards automatic stability verification with LMIs and as a prelude to the Chapter 3, a generalization of the stability analysis results using the framework of IQCs is

finally presented along with an application example with quadrotors. The qualitative stability analysis results are extended to more quantitative performance analysis results with the help of dynamics IQCs in Chapter 3, where sufficient conditions (independent of the size of the network) are presented for the verification of robust exponential performance of source-seeking dynamics with convex interaction potentials among agents and strongly convex external fields. By extending the ZF parameterization to the α-IQC setting, a quasi-convex feasibility problem which can be used to obtain estimates on exponential convergence rates. Various numerical examples including an LTI quadrotor model with an LQR-based controller and two LPV examples are presented in Chapter 3, where the conservatism can be reduced by increasing the order of the ZF multiplier demonstrating the effectiveness of the approach. The reduction in conservatism by searching over general non-causal multipliers is also evident in some of the examples considered. All sufficient conditions developed are independent of the size of the network owing to the diagonal repeated structure in the multipliers thereby allowing the analysis of large networks.

A number of interesting directions as possible extensions of the presented results are open for further study. These include extending the results to non-differentiable fields using sub-gradients/sub-differentials, controller synthesis (possibly based on [Holicki and Scherer, 2021]), extension to the stochastic setting based on [Hu et al., 2017] and performance analysis with flocking interactions using sum-of-squares (SOS) [Papachristodoulou and Prajna, 2005] tools. Furthermore, when considering obstacles in the source-seeking problem, recent results on the use of control barrier functions [Seiler et al., 2022], [Ames et al., 2019] may open the doors to prove that trajectories remain collision free and this looks like a promising direction for research. Extension of the analysis results to controller synthesis is highly desirable and a starting point for this direction could be [Scherer and Ebenbauer, 2021]. A systematic synthesis procedure based on quasi-LPV systems using the analysis from Chapter 2 is proposed in [Attallah and Werner, 2022], where scenarios such as level surface tracking and level surface monitoring are considered.

On the theoretical front, various models of flocking with continuum agents are studied in the literature. For example, [Shu and Tadmor, 2020] considers continuum agents with external fields exactly in the same class as the one studied here. It would be exciting to see if the results developed here can be extended to such models of flocking. In addition, the Cucker-Smale [Cucker and Smale, 2007], [Choi et al., 2020] flocking models consider only velocity alignment terms and it is worth investigating if the analysis via IQCs pursued here can be extended to such models.

On a somewhat parallel track, Chapter 4 considers a decoupled network

architecture of LTI vehicles and analyzes the performance by considering first-order protocols as the interaction mechanism and wrapping local controllers around these dynamics. LMIs that scale linearly with the number of agents can be obtained for bounding the l_∞ norm of local tracking error. Initial steps towards extending analysis LMIs to synthesis for local controller design and protocol design have been presented. The applicability of the synthesized controllers on generic second-order vehicle models is demonstrated in simulations.

Extension along the lines of [Hespe et al., 2020] to quasi LPV vehicle models is straightforward. An extension of these results to the class of differentially flat non-linear systems where the interaction mechanism generates perfectly trackable trajectories can be further investigated with possible applications to non-holonomic models. On another note, extension of the results to networks with non-ideal communications can be made by modeling the first-order protocols within the framework of Markovian jump linear systems along with deterministic tracking agent dynamics. Extensions of the results to more involved flocking dynamics [Olfati-Saber, 2006] is an interesting open problem especially relevant in applications where local closed-loop tracking dynamics of the agent can be well approximated with linear second-order systems and the disturbances acting on agents are low. An l_∞ bound on the tracking error can be possibly used with energy-based arguments from [Olfati-Saber, 2006] to prove that the actual trajectories remain collision free. This closely related architecture, albeit with a different techniques from high gain adaptive control is considered in [Mastellone et al., 2008].

Focusing on the interaction dynamics of the simplified agent models, Chapter 5 proposes a generalization in the form of the *memory weighted protocol* emerging from the two standard consensus protocols for networks with packet dropouts. An example with a group of 9 agents in a line-topology is presented which shows the benefit of the proposed protocol. A further generalization using heterogeneous memory weights instead of assuming the diagonal structure in weighting matrix can help tackle heterogeneous loss rates and needs to be investigated further. Although not presented in this work, initial experiments with a decoupled architecture using first-order consensus protocols as the simplified dynamics have been successfully conducted [Paulsen, 2019], where artificial packet loss is introduced by dropping messages with a specified probability and the different consensus protocols introduced in Chapter 5 have been tested. More elaborate experimental work on these lines is required to compare the different architectures studied in this work.

6.2 Broader Open Directions

Taking a bird's eye view, a number of different research directions that are not merely extensions of the presented work are presented next.

6.2.1 Modeling Aspects in Modular Architectures

This work considers first or second-order agents in the *Simplified Dynamics* (see Fig. 1.1 and Fig. 1.2). The reason for this is that networks of first and second-order dynamics have been very well studied in the literature and the ideas presented in this work leverage on this knowledge. However, it is not clear how to systematically model this abstracted simplified model. A systematic modeling methodology on capturing the necessary phenomena (such as inertia) in the simplified network dynamics and precise measures for comparing the obtained performance with different levels of abstraction is highly desirable from a practical standpoint and this direction seems to be largely unexplored.

6.2.2 Architectures with Predictive Controllers

This work considers non-predictive controllers and the study of control architectures involving real-time optimization (such as model predictive control (MPC)) blocks is becoming increasingly relevant owing to fast computation capabilities on hardware. This brings with it an interesting set of mathematical problems and the framework of distributed optimization is foundational in this context. A simple extension of the current work to include predictive controllers is to use MPC as the local velocity tracking controller on each vehicle in the decoupled architecture. Some promising experimental results with such an architecture have been obtained on the Crazyflie platform discussed in this work [Dio, 2021]. Consideration of more involved predictive control strategies for the coupled architecture with flocking protocols is another exciting direction.

6.2.3 Non-ideal Communication Aspects

Finally, in addition to the packet dropouts considered in this work, time-delay and finite data-rate (quantization) play a critical role especially when considering scenarios involving underwater communication. Explicit consideration of these communication aspects typically requires a stochastic framework for analysis and the extension of the results obtained here in these directions

is an important research direction. Another interesting direction in this regard is to develop a framework involving stochastic network dynamics with simplified agents as a module in combination with a module containing deterministic tracking dynamics of vehicles with local controllers. Speculating a little bit, the results from Chapter 5 may be used in conjunction with the results from Chapter 4 in a decoupled architecture to derive a bound on the local tracking error $\mathbb{E}\left[||e_k||^2\right]$ and may help in computing probability of collisions for example. As an intermediate step, moving from mean square consensus analysis of the memory weighted protocol considered in Section 5.3 to specific performance measures such as an appropriate stochastic version of H_∞ performance (studied in [Seiler and Sengupta, 2005]) is an interesting direction. Results on coupled architectures that include stochastic and deterministic modules seem harder to analyze and opens up possibilities for further study.

Bibliography

[Alvarez et al., 2002] Alvarez, F., Attouch, H., Bolte, J., and Redont, P. (2002). A second-order gradient-like dissipative dynamical system with hessian-driven damping. *Journal de Mathématiques Pures et Appliquées*, 81(8):747–779.

[Ames et al., 2019] Ames, A. D., Coogan, S., Egerstedt, M., Notomista, G., Sreenath, K., and Tabuada, P. (2019). Control barrier functions: Theory and applications. In *2019 18th European Control Conference*, pages 3420–3431.

[Angelico et al., 2021] Angelico, B. A., Chamon, L. F., Paternain, S., Ribeiro, A., and Pappas, G. J. (2021). Source seeking in unknown environments with convex obstacles. In *2021 American Control Conference (ACC)*. IEEE.

[Arcak et al., 2016] Arcak, M., Meissen, C., and Packard, A. (2016). *Networks of dissipative systems: Compositional certification of stability, performance, and safety / Murat Arcak, Chris Meissen, Andrew Packard*. SpringerBriefs in electrical and computer engineering, Control, automation and robotics, 2191-8112. Springer, Cham.

[Attallah et al., 2020] Attallah, A., Datar, A., and Werner, H. (2020). Flocking of linear parameter varying agents: Source seeking application with underwater vehicles. *IFAC-PapersOnLine*, 53(2):7305–7311.

[Attallah and Werner, 2022] Attallah, A. and Werner, H. (2022). Distributed control for complex missions: Quasi–linear parameter varying approach. *International Journal of Robust and Nonlinear Control*, 32(12):6983–7000.

[Attouch and Redont, 2001] Attouch, H. and Redont, P. (2001). The second-order in time continuous newton method. In Lassonde, M., editor, *Approximation, Optimization and Mathematical Economics*, pages 25–36, Berlin. Springer-Verlag.

[Awad et al., 2015] Awad, A., Chapman, A., Schoof, E., Narang-Siddarth, A., and Mesbahi, M. (12/15/2015 - 12/18/2015). Time-scale separation on networks: Consensus, tracking, and state-dependent interactions. In *2015 54th IEEE Conference on Decision and Control (CDC)*, pages 6172–6177. IEEE.

[Awad et al., 2019] Awad, A., Chapman, A., Schoof, E., Narang-Siddarth, A., and Mesbahi, M. (2019). Time-scale separation in networks: State-dependent graphs and consensus tracking. *IEEE Transactions on Control of Network Systems*, 6(1):104–114.

[Aznar et al., 2014] Aznar, F., Sempere, M., Pujol, M., Rizo, R., and Pujol, M. J. (2014). Modelling oil-spill detection with swarm drones. *Abstract and Applied Analysis*, 2014.

[Bartels and Werner, 2014] Bartels, M. and Werner, H. (2014). Cooperative and consensus-based approaches to formation control of autonomous vehicles. *IFAC Proceedings Volumes*, 47(3):8079–8084.

[Boyd et al., 1994] Boyd, S., El Ghaoui, L., Feron, E., and Balakrishnan, V. (1994). *Linear Matrix Inequalities in System and Control Theory*. Society for Industrial and Applied Mathematics.

[Bullo, 2021] Bullo, F. (2021). *Lectures on Network Systems*. Kindle Direct Publishing, 1.5 edition.

[Bullo et al., 2009] Bullo, F., Cortés, J., and Martínez, S. (2009). *Distributed Control of Robotic Networks: A mathematical approach to motion coordination algorithms*. Princeton series in applied mathematics. Princeton University Press, Princeton, N.J. and Woodstock.

[Burgués et al., 2019] Burgués, J., Hernández, V., Lilienthal, A. J., and Marco, S. (2019). Smelling nano aerial vehicle for gas source localization and mapping. *Sensors (Basel, Switzerland)*, 19(3):478.

[Byrnes and Martin, 1995] Byrnes, C. I. and Martin, C. F. (1995). An integral-invariance principle for nonlinear systems. *IEEE Transactions on Automatic Control*, 40(6):983–994.

[Caverly and Forbes,] Caverly, R. J. and Forbes, J. R. Lmi properties and applications in systems, stability, and control theory.

[Chen and Ren, 2019] Chen, F. and Ren, W. (2019). On the control of multi-agent systems: A survey. *Foundations and Trends in Systems and Control*, 6(4):339–499.

[Choi et al., 2020] Choi, S.-H., Kwon, D., and Seo, H. (2020). *Cucker-Smale type flocking models on a sphere*.

[Cortés and Egerstedt, 2017] Cortés, J. and Egerstedt, M. (2017). Coordinated control of multi-robot systems: A survey. *SICE Journal of Control, Measurement, and System Integration*, 10(6):495–503.

[Costa et al., 2010] Costa, O. L. V., Fragoso, M. D., and Marques, R. P. (2010). *Discrete-Time Markov Jump Linear Systems*. Probability and its applications. Springer, London.

[Cucker and Smale, 2007] Cucker, F. and Smale, S. (2007). Emergent behavior in flocks. *IEEE Transactions on Automatic Control*, 52(5):852–862.

[Datar et al., 2022] Datar, A., Hespe, C., and Werner, H. (2022). *Robust Performance Analysis of Cooperative Control Dynamics via Integral Quadratic Constraints (under review)*. arXiv.

[Datar et al., 2020] Datar, A., Paulsen, P., and Werner, H. (5/12/2020 - 5/15/2020). Flocking towards the source: Indoor experiments with quadrotors. In *2020 European Control Conference (ECC)*, pages 1638–1643. IEEE.

[Datar et al., 2018] Datar, A., Schneider, D., Mirali, F., Werner, H., and Frey, H. (6/27/2018 - 6/29/2018). A memory weighted protocol for sampled-data systems subjected to packet dropouts. In *2018 Annual American Control Conference (ACC)*, pages 2485–2490. IEEE.

[Datar and Werner, 2021] Datar, A. and Werner, H. (12/14/2021 - 12/17/2021). Distributed control of heterogeneous networks of vehicles with positive systems theory and generalized h 2 norm. In *2021 60th IEEE Conference on Decision and Control (CDC)*, pages 5982–5987. IEEE.

[Datar and Werner, 2022] Datar, A. and Werner, H. (2022). Robust performance analysis of source-seeking dynamics with integral quadratic constraints. In *2022 Annual American Control Conference*.

[de Campos et al., 2012] de Campos, G. R., Briñón-Arranz, L., Seuret, A., and Niculescu, S.-I. (2012). On the consensus of heterogeneous multi-agent systems: a decoupling approach. *IFAC Proceedings Volumes*, 45(26):246–251.

[Dio, 2021] Dio, M. (2021). *Cooperative control of multiple quadrotors with model predictive control in an indoor experimental setup*. Project Work, Hamburg University of Technology.

[Dörfler and Francis, 2009] Dörfler, F. and Francis, B. (2009). Formation control of autonomous robots based on cooperative behavior. In *2009 European Control Conference (ECC)*. IEEE.

[Dücker et al., 2018a] Dücker, D. A., Hackbarth, A., Johannink, T., Kreuzer, E., and Solowjow, E. (2018a). Micro underwater vehicle hydrobatics: A submerged furuta pendulum. In *2018 IEEE International Conference on Robotics and Automation (ICRA)*. IEEE.

[Dücker et al., 2018b] Dücker, D. A., Kreuzer, E., Maerker, G., and Solowjow, E. (2018b). Parameter identification for micro underwater vehicles. *PAMM*, 18(1).

[Duisterhof et al., 2021] Duisterhof, B. P., Krishnan, S., Cruz, J. J., Banbury, C. R., Fu, W., Faust, A., de Croon, G. C. H. E., and Reddi, V. J. (2021). *Learning to Seek: Autonomous Source Seeking with Deep Reinforcement Learning Onboard a Nano Drone Microcontroller*.

[Dürr et al., 2017] Dürr, H.-B., Krstić, M., Scheinker, A., and Ebenbauer, C. (2017). Extremum seeking for dynamic maps using lie brackets and singular perturbations. *Automatica*, 83:91–99.

[Fagnani and Zampieri, 2009] Fagnani, F. and Zampieri, S. (2009). Average consensus with packet drop communication. *SIAM Journal on Control and Optimization*, 48(1):102–133.

[Fax and Murray, 2004] Fax, J. A. and Murray, R. M. (2004). Information flow and cooperative control of vehicle formations. *IEEE Transactions on Automatic Control*, 49(9):1465–1476.

[Fazlyab et al., 2018] Fazlyab, M., Ribeiro, A., Morari, M., and Preciado, V. M. (2018). Analysis of optimization algorithms via integral quadratic constraints: Nonstrongly convex problems. *SIAM Journal on Optimization*, 28(3):2654–2689.

[Fossen, 2011] Fossen, T. I. (2011). *Handbook of marine craft hydrodynamics and motion control: Vademecum de Navium Motu Contra Aquas et de Motu Gubernando / Thor I. Fossen*. Wiley and Chichester : John Wiley [distributor], Hoboken, N.J.

[Francis and Maggiore, 2016] Francis, B. A. and Maggiore, M. (2016). *Flocking and Rendezvous in Distributed Robotics*. Springer International Publishing.

[Freeman, 2018] Freeman, R. A. (6/27/2018 - 6/29/2018). Noncausal zames-falb multipliers for tighter estimates of exponential convergence rates. In *2018 Annual American Control Conference (ACC)*, pages 2984–2989. IEEE.

[Gonzalez et al., 2015] Gonzalez, A. M., Hoffmann, C., and Werner, H. (12/15/2015 - 12/18/2015). LPV formation control for a class of non-holonomic agents with directed and switching communication topologies. In *2015 54th IEEE Conference on Decision and Control (CDC)*, pages 2792–2797. IEEE.

[Hackbarth et al., 2015] Hackbarth, A., Kreuzer, E., and Solowjow, E. (9/28/2015 - 10/2/2015). Hippocampus: A micro underwater vehicle for swarm applications. In *2015 IEEE/RSJ International Conference on Intelligent Robots and Systems (IROS)*, pages 2258–2263. IEEE.

[Hespe, 2020] Hespe, C. (2020). *Analysis of distributed control algorithms for general non-linear mobile agents*. Master Thesis, Hamburg University of Technology.

[Hespe et al., 2020] Hespe, C., Datar, A., and Werner, H. (2020). Distributed control of mobile LTI and LPV agents using induced L2 to Linf norms. In *2020 59th IEEE Conference on Decision and Control (CDC)*, pages 4360–4365.

[Hoffmann and Werner, 2017] Hoffmann, C. and Werner, H. (2017). Convex distributed controller synthesis for interconnected heterogeneous subsystems via virtual normal interconnection matrices. *IEEE Transactions on Automatic Control*, 62(10):5337–5342.

[Holicki and Scherer, 2021] Holicki, T. and Scherer, C. W. (12/14/2021 - 12/17/2021). Algorithm design and extremum control: Convex synthesis due to plant multiplier commutation. In *2021 60th IEEE Conference on Decision and Control (CDC)*, pages 3249–3256. IEEE.

[Hu and Seiler, 2016] Hu, B. and Seiler, P. (2016). Exponential decay rate conditions for uncertain linear systems using integral quadratic constraints. *IEEE Transactions on Automatic Control*, 61(11):3631–3637.

[Hu et al., 2017] Hu, B., Seiler, P., and Rantzer, A. (2017). A unified analysis of stochastic optimization methods using jump system theory and quadratic constraints. *Conference on Learning Theory*, pages 1157–1189.

[Jeffrey Norris, 2012] Jeffrey Norris (22/03/2012). Radiation risks from fukushima are likely to be less than for chernobyl. *University of California San Francisco*.

[Jönsson, 2001] Jönsson, U. (2001). *Lecture Notes on Integral Quadratic Constraints*.

[Khong et al., 2014] Khong, S. Z., Tan, Y., Manzie, C., and Nešić, D. (2014). Multi-agent source seeking via discrete-time extremum seeking control. *Automatica*, 50(9):2312–2320.

[Krick et al., 2008] Krick, L., Broucke, M. E., and Francis, B. A. (2008). Stabilization of infinitesimally rigid formations of multi-robot networks. In *47th IEEE Conference on Decision and Control, 2008. CDC 2008*, pages 477–482. IEEE / Institute of Electrical and Electronics Engineers Incorporated.

[Lee et al., 2010] Lee, T., Leok, M., and McClamroch, N. H. (2010). Geometric tracking control of a quadrotor uav on se(3). In *49th IEEE Conference on Decision and Control (CDC)*. IEEE.

[Leonard and Fiorelli, 2001] Leonard, N. E. and Fiorelli, E. (2001). Virtual leaders, artificial potentials and coordinated control of groups. In *Proceedings of the 40th IEEE Conference on Decision and Control*, Piscataway, NJ. IEEE.

[Lessard et al., 2016] Lessard, L., Recht, B., and Packard, A. (2016). Analysis and design of optimization algorithms via integral quadratic constraints. *SIAM Journal on Optimization*, 26(1):57–95.

[Li et al., 2011] Li, T., Fu, M., Xie, L., and Zhang, J.-F. (2011). Distributed consensus with limited communication data rate. *IEEE Transactions on Automatic Control*, 56(2):279–292.

[Li et al., 2020] Li, Z., You, K., and Song, S. (2020). Cooperative source seeking via networked multi-vehicle systems. *Automatica*, 115:108853.

[Liu et al., 2011] Liu, S., Li, T., and Xie, L. (2011). Distributed consensus for multiagent systems with communication delays and limited data rate. *SIAM Journal on Control and Optimization*, 49(6):2239–2262.

[Logemann and Ryan, 2014] Logemann, H. and Ryan, E. P. (2014). *Ordinary differential equations: Analysis, qualitative theory and control / Hartmut Logemann, Eugene P. Ryan*. Springer undergraduate mathematics series, 1615-2085. Springer, London and New York.

[Magnus and Neudecker, 1979] Magnus, J. R. and Neudecker, H. (1979). The commutation matrix: Some properties and applications. *The Annals of Statistics*, 7(2):381–394.

[Mason and Papachristodoulou, 2014] Mason, R. P. and Papachristodoulou, A. (6/4/2014 - 6/6/2014). Chordal sparsity, decomposing sdps and the lyapunov equation. In *2014 American Control Conference*, pages 531–537. IEEE.

[Mastellone et al., 2008] Mastellone, S., Stipanović, D. M., Graunke, C. R., Intlekofer, K. A., and Spong, M. W. (2008). Formation control and collision avoidance for multi-agent non-holonomic systems: Theory and experiments. *The International Journal of Robotics Research*, 27(1):107–126.

[Megretski and Rantzer, 1997] Megretski, A. and Rantzer, A. (1997). System analysis via integral quadratic constraints. *IEEE Transactions on Automatic Control*, 42(6):819–830.

[Mellinger and Kumar, 2011] Mellinger, D. and Kumar, V. (2011). Minimum snap trajectory generation and control for quadrotors. In *2011 IEEE International Conference on Robotics and Automation*. IEEE.

[Mesbahi and Egerstedt, 2010] Mesbahi, M. and Egerstedt, M. (2010). *Graph theoretic methods in multiagent networks*. Princeton series in applied mathematics. Princeton University Press, Princeton.

[Michalowsky and Ebenbauer, 2016] Michalowsky, S. and Ebenbauer, C. (2016). Extremum control of linear systems based on output feedback. In *2016 IEEE 55th Conference on Decision and Control (CDC)*. IEEE.

[Moore and Canudas-de Wit, 2010] Moore, B. J. and Canudas-de Wit, C. (2010). Source seeking via collaborative measurements by a circular formation of agents. In *Proceedings of the 2010 American Control Conference*. IEEE.

[Münz et al., 2010] Münz, U., Papachristodoulou, A., and Allgöwer, F. (2010). Delay robustness in consensus problems. *Automatica*, 46(8):1252–1265.

[Nelson and Mallada, 2018] Nelson, Z. E. and Mallada, E. (2018). An integral quadratic constraint framework for real-time steady-state optimization of linear time-invariant systems. In *2018 Annual American Control Conference (ACC)*. IEEE.

[Nesterov, 2004] Nesterov, Y. (2004). *Introductory lectures on convex optimization: A basic course / by Yurii Nesterov*, volume v. 87 of *Applied optimization*. Kluwer Academic, Boston, Mass. and London.

[Ogren et al., 2004] Ogren, P., Fiorelli, E., and Leonard, N. E. (2004). Cooperative control of mobile sensor networks: Adaptive gradient climbing in a distributed environment. *IEEE Transactions on Automatic Control*, 49(8):1292–1302.

[Oh et al., 2015] Oh, K.-K., Park, M.-C., and Ahn, H.-S. (2015). A survey of multi-agent formation control. *Automatica*, 53:424–440.

[Olfati-Saber, 2006] Olfati-Saber, R. (2006). Flocking for multi-agent dynamic systems: Algorithms and theory. *IEEE Transactions on Automatic Control*, 51(3):401–420.

[Olfati-Saber et al., 2007] Olfati-Saber, R., Fax, J. A., and Murray, R. M. (2007). Consensus and cooperation in networked multi-agent systems. *Proceedings of the IEEE*, 95(1):215–233.

[Papachristodoulou and Prajna, 2005] Papachristodoulou, A. and Prajna, S. (2005). A tutorial on sum of squares techniques for systems analysis. In *2005 American control conference*, pages 2686–2700. IEEE.

[Parker et al., 2019] Parker, L., Butterworth, J., and Luo, S. (2019). *Fly Safe: Aerial Swarm Robotics using Force Field Particle Swarm Optimisation*.

[Paulsen, 2018] Paulsen, P. (2018). *Development of a software framework for implementation of co-operative control algorithms on a swarm of small quadrotors*. Project Work, Hamburg University of Technology.

[Paulsen, 2019] Paulsen, P. (2019). *Experimental Investigations into the effect of Communication Constraints on Performance of Cooperative Control Algorithms: Case Study with Quadrotors*. Master Thesis, Hamburg University of Technology.

[Pfifer and Seiler, 2015] Pfifer, H. and Seiler, P. (2015). Robustness analysis of linear parameter varying systems using integral quadratic constraints. *International Journal of Robust and Nonlinear Control*, 25(15):2843–2864.

[Pilz et al., 2011] Pilz, U., Popov, A. P., and Werner, H. (2011). An information flow filter approach to cooperative vehicle control. *IFAC Proceedings Volumes*, 44(1):7432–7437.

[Powers et al., 2015] Powers, C., Mellinger, D., and Kumar, V. (2015). *Handbook of unmanned aerial vehicles*. Springer Reference, Dordrecht.

[Rantzer, 2015] Rantzer, A. (2015). Scalable control of positive systems. *European Journal of Control*, 24:72–80.

[Rantzer and Valcher, 2018] Rantzer, A. and Valcher, M. E. (12/17/2018 - 12/19/2018). A tutorial on positive systems and large scale control. In *2018 IEEE Conference on Decision and Control (CDC)*, pages 3686–3697. IEEE.

[Ren and Beard, 2008] Ren, W. and Beard, R. W. (2008). *Distributed Consensus in Multi-vehicle Cooperative Control*. Springer London, London.

[Rotea, 1993] Rotea, M. A. (1993). The generalized h2 control problem. *Automatica*, 29(2):373–385.

[Scherer and Ebenbauer, 2021] Scherer, C. and Ebenbauer, C. (2021). Convex synthesis of accelerated gradient algorithms. *SIAM Journal on Control and Optimization*, 59(6):4615–4645.

[Scherer and Weiland, 2000] Scherer, C. and Weiland, S. (2000). *Linear matrix inequalities in control*.

[Scherer, 2022] Scherer, C. W. (2022). Dissipativity and integral quadratic constraints: Tailored computational robustness tests for complex interconnections. *IEEE Control Systems*, 42(3):115–139.

[Seiler et al., 2022] Seiler, P., Jankovic, M., and Hellstrom, E. (2022). Control barrier functions with unmodeled input dynamics using integral quadratic constraints. *IEEE Control Systems Letters*, 6:1664–1669.

[Seiler and Sengupta, 2005] Seiler, P. and Sengupta, R. (2005). An h/sub /spl infin// approach to networked control. *IEEE Transactions on Automatic Control*, 50(3):356–364.

[Senga et al., 2007] Senga, H., Kato, N., Ito, A., Niou, H., Yoshie, M., Fujita, I., Igarashi, K., and Okuyama, E. (2007). Development of spilled oil tracking autonomous buoy system. In *OCEANS 2007*. IEEE.

[Sepulchre et al., 2007] Sepulchre, R., Paley, D. A., and Leonard, N. E. (2007). Stabilization of planar collective motion: All-to-all communication. *IEEE Transactions on Automatic Control*, 52(5):811–824.

[Shamma and Cloutier, 1992] Shamma, J. S. and Cloutier, J. R. (1992). A linear parameter varying approach to gain scheduled missile autopilot design. In *1992 American Control Conference*. IEEE.

[Shu and Tadmor, 2020] Shu, R. and Tadmor, E. (2020). Flocking hydrodynamics with external potentials. *Archive for Rational Mechanics and Analysis*, 238(1):347–381.

[Su et al., 2009] Su, H., Wang, X., and Lin, Z. (2009). Flocking of multi-agents with a virtual leader. *IEEE Transactions on Automatic Control*, 54(2):293–307.

[Sundararajan et al., 2020] Sundararajan, A., van Scoy, B., and Lessard, L. (2020). Analysis and design of first-order distributed optimization algorithms over time-varying graphs. *IEEE Transactions on Control of Network Systems*, 7(4):1597–1608.

[Turgeman et al., 2019] Turgeman, A., Datar, A., and Werner, H. (7/10/2019 - 7/12/2019). Gradient free source-seeking using flocking behavior. In *2019 American Control Conference (ACC)*, pages 4647–4652. IEEE.

[van Nieuwstadt et al., 1998] van Nieuwstadt, M., Rathinam, M., and Murray, R. M. (1998). Differential flatness and absolute equivalence of nonlinear control systems. *SIAM Journal on Control and Optimization*, 36(4):1225–1239.

[Veenman et al., 2016] Veenman, J., Scherer, C. W., and Köroğlu, H. (2016). Robust stability and performance analysis based on integral quadratic constraints. *European Journal of Control*, 31:1–32.

[Wang et al., 2010] Wang, S., An, C., Sun, X.-X., and Du, X. (2010). Average consensus over communication channels with uniform packet losses. In *2010 Chinese Control and Decision Conference*. IEEE.

[Wilson et al., 2021] Wilson, A. C., Recht, B., and Jordan, M. I. (2021). A lyapunov analysis of momentum methods in optimization. *J. Mach. Learn. Res.*

[Wu and Shi, 2012] Wu, J. and Shi, Y. (2012). Average consensus in multi-agent systems with time-varying delays and packet losses. In *2012 American Control Conference (ACC)*. IEEE.

[Xia and Cao, 2017] Xia, W. and Cao, M. (2017). Analysis and applications of spectral properties of grounded laplacian matrices for directed networks. *Automatica*, 80:10–16.

[Z. Li et al., 2011] Z. Li, N. Hovakimyan, and D. Stipanović (2011). Distributed multi-agent tracking and estimation with uncertain agent dynamics. In *Proceedings of the 2011 American Control Conference*, pages 2204–2209.

[Zhang et al., 2007] Zhang, C., Siranosian, A., and Krstić, M. (2007). Extremum seeking for moderately unstable systems and for autonomous vehicle target tracking without position measurements. *Automatica*, 43(10):1832–1839.

[Zhang et al., 2019] Zhang, J., Seiler, P., and Carrasco, J. (2019). *Noncausal FIR Zames-Falb Multiplier Search for Exponential Convergence Rate*.

[Zhang et al., 2016] Zhang, Y., Makarenkov, O., and Gans, N. (2016). Extremum seeking control of a nonholonomic system with sensor constraints. *Automatica*, 70:86–93.

[Zhang and Tian, 2010] Zhang, Y. and Tian, Y.-P. (2010). Consensus of data-sampled multi-agent systems with random communication delay and packet loss. *IEEE Transactions on Automatic Control*, 55(4):939–943.

Appendix A

Crazyflie Platform for Indoor Experiments

The Crazyflie 2.1, shown in Fig. A.1, is an open-source experimental platform of a small 27gm quadrotor developed by the company Bitcraze AB, allowing modifications to the firmware of both micro-controllers of its double-MCU architecture, an nRF51 radio chip and an STM32 that runs the main firmware. An indoor positioning based on the Decawave DWM1000 chip called the Loco-positioning system also developed by Bitcraze AB is used in all experiments. At each corner of a $3m \times 4m$ area, two Loco positioning anchors are placed at different heights. This is depicted in Fig. A.2 and Fig. A.3. The anchors are configured with their positions. To determine the positions, each Crazyflie uses the method of time difference of arrival. Because the anchors are configured to send synchronous messages and based on the different times at which these messages are received, the position can be locally estimated onboard. The firmware was modified to allow peer to

Figure A.1: Crazyflie 2.1 developed by Bitcraze AB.

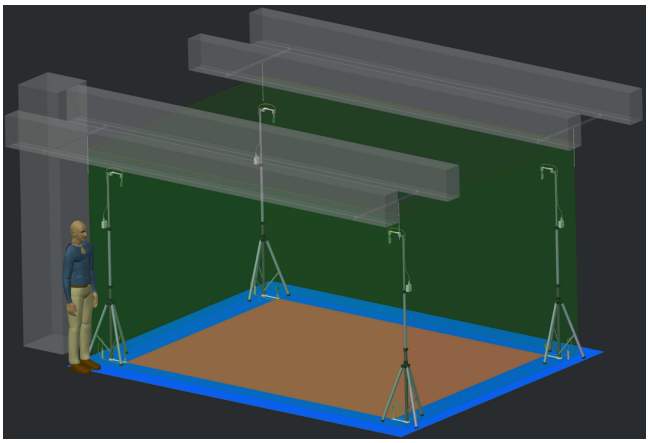

Figure A.2: Indoor positioning system setup schematic.

peer communication in a prior work [Paulsen, 2018], [Paulsen, 2019]. Each Crazyflie broadcasts its message along with an ID that identifies the sender uniquely and a time stamp. A heuristic approach of adjusting to the slowest clock is used to address the problem of clock drift [Paulsen, 2018], [Paulsen, 2019]. To avoid message collisions, time slots are used. To maintain the same time between packets it is necessary to compensate for clock drift. For this purpose the messages carry timestamps and the Crazyflie adjust to the one with the slowest clock. To identify the sender, each Crazyflie has an ID that is included in each message. Additionally, data for logging purposes is broadcast which is logged by a computer. The computer serves only to send a start command and then passively log the data for later analysis.

Figure A.3: Picture of an experiment with 7 Crazyflie.

Appendix B

Vehicle Models and Local Controllers

B.1 Quadrotor Model and LQR Control

Quadrotor dynamics have been well studied and the details on modeling aspects could be found, for example, in [Powers et al., 2015]. A very brief review is given next and the interested reader is pointed to [Powers et al., 2015]. A non-linear quadrotor model is linearized about the stable hover position to obtain a linear state space model that corresponds to the small-angle approximation, typically found in the literature. With this linearized model, the state of quadrotor can be described completely in an inertial frame by three position coordinates x_{pos}, y_{pos} and z_{pos}, respective velocities x_{vel}, y_{vel} and z_{vel}, roll, pitch and yaw angles θ, ϕ and ψ and respective angular velocities ω_θ, ω_ϕ and ω_ψ. Neglecting the fast motor dynamics in the four propellers, the angular velocities of the rotors can be assumed to be instantaneously controlled (instead of the motor torques) and using a bijective mapping [Powers et al., 2015], the control input can be considered to be $u = \begin{bmatrix} F_{\text{thrust}} & \tau_\theta & \tau_\phi & \tau_\psi \end{bmatrix}^T$, where F_{thrust} is the total thrust force in the Z direction and τ_θ, τ_ϕ and τ_ψ are the torques in the roll, pitch and yaw rotations respectively. The state space model is of the form

$$\begin{aligned} \dot{x} &= Ax + Bu, \\ y &= Cx, \end{aligned}$$

where

$$A = \begin{bmatrix} 0 & 1 & 0 & 0 & 0 & 0 & 0 & 0 & 0 & 0 & 0 & 0 \\ 0 & 0 & 0 & 0 & 0 & 0 & 0 & 0 & -g & 0 & 0 & 0 \\ 0 & 0 & 0 & 1 & 0 & 0 & 0 & 0 & 0 & 0 & 0 & 0 \\ 0 & 0 & 0 & 0 & 0 & 0 & 0 & 0 & 0 & 0 & g & 0 \\ 0 & 0 & 0 & 0 & 0 & 1 & 0 & 0 & 0 & 0 & 0 & 0 \\ 0 & 0 & 0 & 0 & 0 & 0 & 0 & 0 & 0 & 0 & 0 & 0 \\ 0 & 0 & 0 & 0 & 0 & 0 & 0 & 1 & 0 & 0 & 0 & 0 \\ 0 & 0 & 0 & 0 & 0 & 0 & 0 & 0 & 0 & 0 & 0 & 0 \\ 0 & 0 & 0 & 0 & 0 & 0 & 0 & 0 & 0 & 1 & 0 & 0 \\ 0 & 0 & 0 & 0 & 0 & 0 & 0 & 0 & 0 & 0 & 0 & 0 \\ 0 & 0 & 0 & 0 & 0 & 0 & 0 & 0 & 0 & 0 & 0 & 1 \\ 0 & 0 & 0 & 0 & 0 & 0 & 0 & 0 & 0 & 0 & 0 & 0 \end{bmatrix}, \quad B = \begin{bmatrix} 0 & 0 & 0 & 0 \\ 0 & 0 & 0 & 0 \\ 0 & 0 & 0 & 0 \\ 0 & 0 & 0 & 0 \\ 0 & 0 & 0 & 0 \\ \frac{1}{m} & 0 & 0 & 0 \\ 0 & 0 & 0 & 0 \\ 0 & 1 & 0 & 0 \\ 0 & 0 & 0 & 0 \\ 0 & 0 & 1 & 0 \\ 0 & 0 & 0 & 0 \\ 0 & 0 & 0 & 1 \end{bmatrix},$$

$$C = \begin{bmatrix} 1 & 0 & 0 & 0 & 0 & 0 & 0 & 0 & 0 & 0 & 0 & 0 \\ 0 & 0 & 1 & 0 & 0 & 0 & 0 & 0 & 0 & 0 & 0 & 0 \\ 0 & 1 & 0 & 0 & 0 & 0 & 0 & 0 & 0 & 0 & 0 & 0 \\ 0 & 0 & 0 & 1 & 0 & 0 & 0 & 0 & 0 & 0 & 0 & 0 \end{bmatrix},$$

$$x = \begin{bmatrix} x_{\text{pos}} & x_{\text{vel}} & y_{\text{pos}} & y_{\text{vel}} & z_{\text{pos}} & z_{\text{vel}} & \theta & \omega_\theta & \phi & \omega_\phi & \psi & \omega_\psi \end{bmatrix}^T,$$

$$y = \begin{bmatrix} x_{\text{pos}} & y_{\text{pos}} & x_{\text{vel}} & y_{\text{vel}} \end{bmatrix}^T,$$

the control input u is as defined above, g is the gravitational acceleration and m is the mass of the quadrotor. An LQR controller is designed with the above model and tuning parameters $Q = I$ and $R = 0.01I$. With the obtained optimal gain F_b, a feed forward gain F_f is designed such that the static gain $C(A - BF_b)^{-1}BF_f = I$.

B.2 *HippoCampus* Model and Tracking Control

Details on the modeling aspects of the *HippoCampus* underwater robot can be found at [Hackbarth et al., 2015, Section III] and a summary of the kinematic and dynamics equations is now given below for completeness following the notation exactly from [Hackbarth et al., 2015]. Let $\mathbf{p} = [N \;\; E \;\; D]^T$ denote the position (in an inertial frame) of the origin of the body frame (different from the center of gravity) represented in an inertial frame and let $\mathbf{\Theta} = [\phi \;\; \theta \;\; \psi]^T$ be the Euler angles representing the vehicle orientation. Let $\mathbf{v} = [u \;\; v \;\; w]^T$ represent the linear velocity of the origin of the body frame and $\omega = [p \;\; q \;\; r]^T$ represent the angular velocity, both represented in the

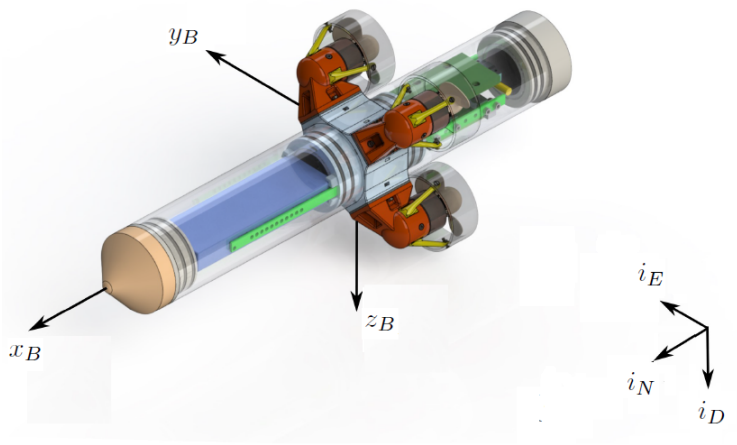

Figure B.1: *HippoCampus* with Inertial and Body coordinates [Attallah et al., 2020].

body frame. For convenience, let $\eta = \begin{bmatrix}\mathbf{p}^T & \mathbf{\Theta}^T\end{bmatrix}^T$ and $\nu = \begin{bmatrix}\mathbf{v}^T & \omega^T\end{bmatrix}^T$. The kinematics and dynamics are described by

$$\begin{aligned} \dot{\eta} &= \begin{bmatrix}\mathcal{R}(\mathbf{\Theta}) & 0 \\ 0 & T(\mathbf{\Theta})\end{bmatrix}\nu, \\ \mathbf{M}\dot{\nu} + \mathbf{C}(\nu)\nu &= \tau_{\text{hyd}} - \mathbf{g}(\eta) + \text{sat}(\tau_{\text{c}}), \end{aligned} \tag{B.1}$$

where $\mathcal{R}(\mathbf{\Theta})$ is the rotation matrix and $T(\mathbf{\Theta})$ is a matrix that transforms angular velocities from the body frame to the derivatives of Euler angles, hydrodynamic loads are modeled as $\tau_{\text{hyd}} = -\mathbf{M}_A\dot{\nu} - \mathbf{C}_A(\nu)\nu$, $\mathbf{g}(\eta)$ represents the hydrostatic load and control input is denoted by τ_{c}. Parameter values are available in [Dücker et al., 2018b] and [Attallah et al., 2020] and more details on the modeling aspects could be found in references [Hackbarth et al., 2015] and [Fossen, 2011]. Note that the control input $\tau_{\text{c}} = \begin{bmatrix}f & 0 & 0 & \tau_\phi & \tau_\theta & \tau_\psi\end{bmatrix}^T$ is passed through a saturation operation denoted here by $\text{sat}(\tau_{\text{c}})$, which transforms the control input into motor thrusts which are saturated and then transformed back to obtain the control input.

A cascaded control structure with an inner geometric attitude PD controller and an outer position PD controller is implemented. The attitude controller is described in [Dücker et al., 2018a] (and is motivated from [Mellinger and Kumar, 2011], [Lee et al., 2010]). The orientation error is described in the special orthogonal group $SO(3)$ and the intuition behind the control law is discussed next leaving the details to the cited references. Since the rota-

tion matrix $\mathcal{R}$ encodes orientation, $\mathcal{R}_{\text{ref}}$ can be used to denote the desired rotation matrix with the desired orientation and the Frobenius norm of the difference $\frac{1}{2}||\mathcal{R}-\mathcal{R}_{\text{ref}}||_F^2 = Tr(I-\mathcal{R}_{\text{ref}}^T\mathcal{R})$ represents a Lyapunov like positive-definite function (analogous to the typical Lyapunov function $\frac{1}{2}||e||^2$, where e is the error state). The derivative (appropriately defined) of this function is then defined as the orientation error e_{att}. The error in the angular velocity is defined as $e_\omega = \omega - \omega_{\text{ref}}$. The control input for the attitude dynamics is then computed as $\begin{bmatrix}\tau_\phi & \tau_\theta & \tau_\psi\end{bmatrix}^T = -K_p e_{\text{att}} - K_d e_\omega$, for positive gains K_p and K_d. Wrapped around the attitude controller is a position controller which computes the desired orientation as the one directly pointing towards the reference position and provides this to the attitude controller. Additionally, the position error e_{pos} is computed as the difference between the reference position and the position of the origin of the body frame and the forward thrust is computed as $f = K_1(||e_{\text{pos}}||) - K_2 u$ (recall that u is the forward velocity), for positive gains K_1 and K_2.

Appendix C

List of Abbreviations

IQC/ IQCs	Integral quadratic constraints
ZF	Zames-Falb
CC	Circle criterion
LTI	Linear time-invariant
LPV	Linear parameter varying
LMI	Linear matrix inequality
LQR	Linear quadratic regulator
ZOH	Zero order hold
TDOA	Time difference of arrival
PD	Proportional-derivative
SDP	Semi-definite programming